Universidade do Minho
Escola de Engenharia

Marcos Silva Martins

Ultrasonic Wireless Broadband Communication System for Underwater Applications

Setembro de 2013

Ultrasonic Wireless Broadband Communication System for Underwater Applications
Marcos Silva Martins
UMinho | 2013

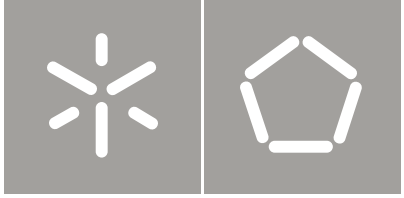

Universidade do Minho
Escola de Engenharia

Marcos Silva Martins

Ultrasonic Wireless Broadband Communication System for Underwater Applications

Tese de Doutoramento
Programa Doutoral em Engenharia Eletrónica e de Computadores

Trabalho efectuado sob a orientação de
Professor Doutor José V. Gerardo Rocha
Professor Doutor José M. Tavares Vieira Cabral
Professor Doutor Senentxu Lanceros-Mendez

Setembro de 2013

Acknowledgements

First and foremost, I want to leave a word of thanks to a group of people who directly or indirectly supported me over the last few years and let me reach the final stage of my PhD successfully.

I would like to thank my supervisor Prof. Gerardo Rocha for the opportunity and for all the support and friendship along my academic journey.

To my co-supervisor Prof José Cabral I am very grateful for all the help and patience in the difficult moments and especially for the friendship.

I am grateful to Prof. Senentxu for the opportunity of joining a research group with such amazing persons and professional scientists. Thank for friendship and support.

I am also grateful to colleagues/friends of Electroactive Smart Materials group for all the help and for the team work spirit. In particular to Vítor Correia, Silvia Reis, Helder Castro, Marco Silva, Carlos Costa and Vítor Sencadas for their support and friendship.

To IPCA I want to express my gratitude for the excellent reception and support.

I want to thank the financial support by the Foundation for Science and Technology-FCT under grant SFRH/BD/60713/2009.

To my parents and sisters I am proud and grateful for all they did for me.

Finally, to the most important person in my life, my best friend, my companion, Filipa. Thanks for all the patience, support and love which everyday enrich my life. I also thank her for the opportunity to become a father and the baby she carrying for being the inspiration of our lives.

Thank you all!

I dedicate this work to

my wife, my child and my family,

Thanks

Abstract

Underwater wireless communication systems are becoming a priority in terms of research and technological development due to the increasing demand for exploring the oceans' potential in areas such as pharmaceutical, oil, minerals, environmental and biodiversity. This demand is increasing exponentially with the need for high data rate and near-real-time communications between submerged mobile and static agents.

The existing wireless communication technologies using electromagnetic waves or lasers are not very efficient due to the large attenuation in aquatic environment. Ultrasound reveals a lower attenuation, and thus has been used in underwater long-distance communications. But the underwater acoustic medium is one of the less reliable communication channels which represent major challenges for communications. With relatively slow sound speed propagation (~1500 m/s) the delay may represent a problem for communications with real-time applications.

A theoretical model of an underwater communication system was also developed. The model allows to emulate the emitter, the hydrophone and the underwater acoustic channel, which includes attenuation, environmental noise, Doppler Effect, multipath and propagation delay. This model supported the study of wireless communications by emulating the transmission of acoustic signals using different types of digital modulations. The acoustic signal attenuation, multipath, ambient noise in several environments theoretical results were compared to those obtained experimentally. Allowing to conclude that the model represents a suitable approximation to the real subaquatic communication channel for the evaluation of digital acoustic communications.

An optimization study of ultrasound transducers for underwater communications was addressed, focusing on a piston type emitter operating in the thickness mode (d33). It was discussed how the acoustic impedance, thickness, resonance frequency and structure affect the transducer performance. This work allowed a better understanding of the emitter transducer characteristics allowing reaching the optimum point of operation for specific applications. Focusing on underwater communication, the transducer was optimized by finite element computer simulations. The results were compared with experimental tests and show that four-layer structures increase up to 16 dB in performance when compared to single-layer transducer disks.

For high data-rates and real-time applications it was necessary to develop ultrasound transducers able to work at high frequencies and wideband, with suitable responses to digital modulations. It was thus also included a comparison study that shows how the acoustic impedance influences the performance of an ultrasonic emitter when using different digital modulations and operating at frequencies between 100 kHz and 1 MHz and some tens of meters of distance. It is presented a Finite Element Method (FEM) and a MATLAB/Simulink simulation with an experimental validation to evaluate two types of piezoelectric materials: one based in ceramics (high acoustic impedance) with a resonance design and a polymer based (low acoustic impedance) system, designed to optimize the performance when using digital modulations. The transducers performance for Binary Amplitude Shift Keying (BASK), On-Off Keying (OOK), Binary Phase Shift Keying (BPSK) and Binary Frequency Shift Keying (BFSK) modulations with a 1 MHz carrier at 125 kbps baud rate were compared. The transducers materials used were the ceramics PZT-5H and the polymer PVDF. The results show that PVDF transducer has a better performance to digital modulations than PZT-5H transducer, providing the signal full demodulation for all digital modulations tested. On the other hand, the PZT-5H transducer showed a higher output, but fails to perform accurate modulated signals.

Finally, the system was validated by the implementation of a full duplex point-to-point communication at 1 Mbps using OOK modulation with a 1 MHz single carrier. The system was successfully tested in a swimming pool at a distance of 6 meters with a 1 Mbps rate, achieving a $3x10^{-3}$ Bit Error Rate (BER) using just 1.4 W of power consumption. These results represent an advance in underwater acoustic communications, being the first practical system to achieve data rates up to 1 Mbps.

Resumo

O desenvolvimento de sistemas de comunicação subaquáticos sem fios está a tornar-se uma prioridade na comunidade científica no sentido de aumentar o desenvolvimento tecnológico. Este facto deve-se à crescente necessidade de exploração do potencial dos oceanos em áreas científicas diversas como farmacêutica, petrolífera, mineral, ambiental e até do próprio estudo da biodiversidade. Essa necessidade aumenta exponencialmente com a necessidade de comunicações de alto débito e em tempo real entre agentes submersos móveis e estáticos.

As tecnologias de comunicações sem fios existentes, nomeadamente as que utilizam ondas eletromagnéticas ou lasers não são muito eficientes, devido, em grande parte, à atenuação no ambiente subaquático. Os ultrassons revelam uma menor atenuação tendo sido, por isso, utilizados em comunicações subaquáticas em longas distâncias. Contudo o canal acústico subaquático definisse como um dos mais difíceis, devido em parte as suas características únicas, o que apresenta ser um enorme desafio. Como a velocidade de propagação do som é relativamente lenta (~1500 m/s), o atraso pode representar um problema para as aplicações em tempo real.

Foi desenvolvido um modelo teórico do sistema de comunicações subaquáticos que permite emular o emissor, o hidrofone e o canal acústico subaquático. No canal acústico subaquático foi simulado o efeito da atenuação, ruído ambiente, efeito de Doppler, *multipath* e atraso de propagação. Este modelo é indicado para o estudo das comunicações subaquáticas, emulando a transmissão de sinais acústicos utilizando diferentes tipos de modulações digitais. Neste estudo foram testados, a atenuação do sinal acústico, *multipath*, ruído em diversos ambientes e os resultados teóricos foram comparados com os obtidos experimentalmente. Permitindo concluir que o modelo representa uma aproximação adequada do canal de comunicação, permitindo a avaliação das comunicações digitais acústicas.

Inclui ainda um estudo de otimização de transdutores de ultrassons para comunicações subaquáticos, tendo como base o emissor do tipo pistão, operando ao longo da espessura (d33). Foi analisada ainda a forma como a impedância, espessura, frequência de ressonância acústica e estrutura afetam o desempenho do transdutor. Este trabalho permitiu uma melhor compreensão das características do transdutor emissor que permitem atingir o ponto ótimo de operação para aplicações específicas. Tendo como base a comunicação subaquática, o transdutor foi otimizado usando os resultados de simulações pelo Método dos Elementos

Finitos. Os resultados foram comparados com os testes experimentais, onde se mostra que as estruturas de quatro camadas podem aumentar até 16dB no desempenho quando comparados com discos de transdutor de única camada.

Para aplicações em tempo real e de elevado debito, foi necessário desenvolver transdutores de ultrassons capazes de operar em banda larga a altas frequências, com resposta adequada às modulações digitais. Foi, portanto, incluído também um estudo comparativo que mostra como a impedância acústica influencia o desempenho do emissor de ultrassons quando se utilizam modulações digitais a operar com frequências entre 100 kHz e 1 MHz abrangendo distâncias de algumas dezenas de metros. São apresentadas simulações por Método de Elementos Finitos (MEF) e MATLAB/Simulink com validação experimental de modo a avaliar dois tipos de materiais piezoelétricos: um com base cerâmica PZT-5H (alta impedância acústica) com um *design* de ressonância e outro de base de polimérica PVDF (baixa impedância acústica), otimizado para modulações digitais. O desempenho dos transdutores foi comparado para as modulações: *Binary Amplitude Shift Keying* (BASK), *On-Off Keying* (OOK), *Binary Phase Shift Keying* (BPSK) e *Binary Frequency Shift Keying* (BFSK) com uma portadora de 1 MHz a 125 kbps. Os resultados mostram que o transdutor de PVDF tem um melhor desempenho do que transdutor PZT-5H, proporcionando a desmodulação completa do sinal para todas as modulações digitais testadas. Por outro lado, o transdutor de PZT-5H mostrou uma potência acústica mais elevada, embora não consiga produzir sinais modulados precisos.

Finalmente, o sistema foi validado através da implementação de uma comunicação ponto-a-ponto bidirecional de 1 Mbps utilizando uma modulação OOK com uma portadora de 1 MHz. O sistema foi testado com sucesso numa piscina a uma distância de 6 metros com uma taxa de 1 Mbps, com um BER (*Bit Error Rate*) de $3x10^{-3}$, utilizando apenas 1,4 W de consumo de potência. Estes resultados representam um avanço nas comunicações acústicas subaquáticas, sendo o primeiro sistema prático de atingir velocidades até 1 Mbps.

Contents

List of figures

List of tables

List of abbreviations

A

ACOM	Acoustic COMmunication
ADC	Analog to Digital Converter
ASCII	American Standard Code for Information Interchange
ASK	Amplitude Shift Keying

B

BASK	Binary Amplitude Shift Keying
BER	Bit Error Rate
BFSK	Binary Frequency Shift Keying
BPSK	Binary Phase Shift Keying

D

DAC	Digital to Analog Converter

E

ELF	Extreme Low Frequency
EM	Electromagnetic

F

FEM	Finite Element Method
FFT	Fast Furrier Transform
FIR	Finite Impulse Response
FM	Frequency Modulation
FPGA	Field Programmable Gate Array
FSK	Frequency Shift Keying

I

ISI	Inter Symbol Interference
ISM	Industrial, Scientific and Medical

L

LD	Laser Diode
LED	Light Emitting Diode

O

OCOM Optical COMmunication

OOK On-OFF Keying

P

P.S.D Power Spectral Density

PC Personal Computer

PMN Lead Magnesium Niobate

PPM Pulse Position Modulation

PT Lead Titanate

PVDF Poly(viylidene fluoride)

PZN Lead Zinc Niobate

PZT Lead Zirconate Titanate

Q

QAM Quadrature Amplitude Modulation

QKD Quantum Key Distribution

QPSK Quadrature Phase-Shift Keying

R

RADAR Radio Detection And Ranging

RF Radio Frequency

SNR Signal-to-Noise Ratio

SONAR SOund Navigation And Ranging

U

UAV Underwater Automatic Vehicle

V

VLF Very Low Frequency

1. Introduction

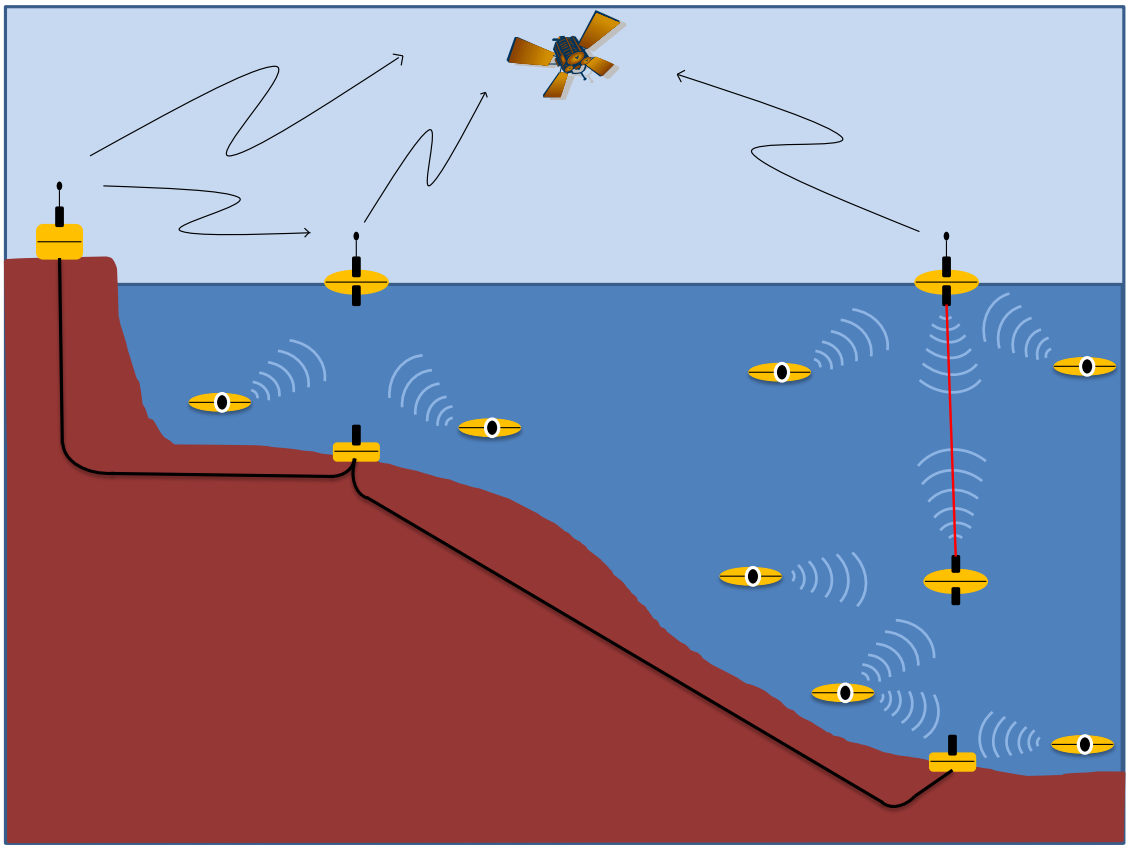

1.1. State-of-the Art

Underwater wireless communication systems have experienced a large development and increasing interest among the scientific community in the last recent decades. When compared with the advances in airborne wireless communications, this development is almost negligible. The airborne communications system fails in underwater environment and the subaquatic channel has revealed to be adverse to the propagation of different kinds of waves, namely the electromagnetic (radio frequency and optic) and acoustic waves [1]. The underwater communications development is decisive for the technology improvement in underwater sensor networks [2], divers and submarine communications [3], robotics [4] and UAV (underwater automatic vehicle) navigation and control [5], and these applications are essential to the progress in other areas, such as:

- Oceans and marine life exploration to support the biodiversity and pharmaceutics research, detecting underwater oilfields or reservoirs and assist in exploration for valuable minerals [6 – 9].
- Underwater information collection for ocean mapping [10], equipment monitoring, mine/cave reconnaissance and assisted navigation [11 – 13].
- Disaster prevention and assistance by measuring seismic activity, tsunamis scan and warning, study the effects of submarine earthquakes and to provide help in shipwrecks [14];
- Environmental protection by monitoring pollution (chemical, biological and nuclear), ocean currents and winds, water conditions (salinity and PH) and climate change to predict the effect of human activities on marine ecosystems and assist in maritime meteorology [15, 16].
- Military applications by improving the coastal surveillance, defense systems, intrusion detection systems and submarine communications [17 – 21].

Therefore, it is imperative to find a reliable solution able to fulfill all this needs. Several research teams around the world are working in this technological need. The proposed solutions are based in three distinct types of technologies: radio frequency, optical and acoustic [22].

1.1.1. Underwater Communications: Historical Notes

Radio frequency Communication System

The first attempts to send electromagnetic signals via aquatic environment occurred long before attempts to send messages through airborne communications. In 1842 Samuel Morse implemented a system that allowed communicating at a distance of approximately 1.5 km in the Susquehanna river [23]. Some years later, James Lindsay successfully implemented a telegraph system that was capable of sending signals over 3 km distance in Tay river [23]. These events inspired Sir William Preece to develop his own experiences in wireless transmissions through techniques based in induction [24]. Despite their efforts it was the Germans that were the pioneers in underwater communications using radio frequency to communicate with submarines. During World War II it was built an antenna named Goliath (Figure 1.1), in the Elbe River at northwest of Calbe in 1941 [25].

Figure 1.1: German Goliath antenna.

This antenna emitted a power of 1.8 MW and was able to send signals to submerged submarines in the Indian Ocean. Nowadays, submarines communicate with underwater electromagnetic waves of extremely low frequencies, between 76 and 82 Hz [26]. However, this is only possible because most of the transmission path is through the atmosphere.

Optical Communication (OCOM) Systems

The first optical communication system called *Photophone* was developed by Alexander Graham Bell and his assistant Charles Sumner Tainter in 1880 [27]. This device was not suitable to operate underwater. In 1950 Jerlov developed an initial classification by "types" of water color/clarity, resulting in the first generic curves for the attenuation of diffuse light as a function of wavelength [28].

The development of the first operational laser by Dr Maiman, (Figure 1.2), in the late 1950s [29 – 31] enabled the development of optical underwater communication systems.

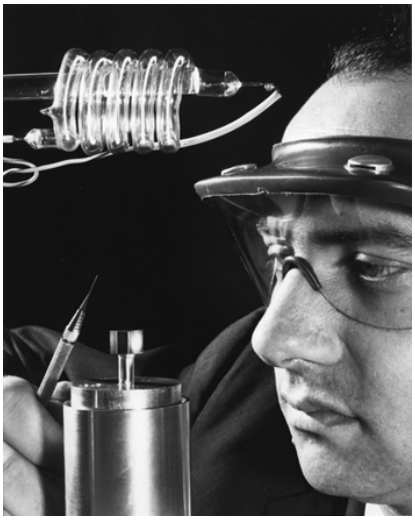

Figure 1.2: Dr. Theodore Maiman studies a ruby crystal in the shape of a cube in a laser [32].

In the 1970s appeared the first application and studies of underwater OCOM. For example, the work presented in 1969 by Burt et. al. [33], where some the optical communications characteristics and limitations were measured and analyzed. In 1975, Ferguson presented a blue-green laser for underwater applications such as optical RADAR, communications, and imaging [34]. In 1976, Karp presented an optical communication system between underwater and above surface (Satellite) Terminals [35].

Acoustic communication (ACOM) systems

ACOM is the mostly used technology for underwater communications (especially in long distance communications) [36], with a significant increase in research over the last decades. However, this area of study started many years ago, when Leonardo da Vinci in 1490 proposed detecting ships by listening to the noise they radiate into water. With this theory he demonstrated that it is possible to detect or track objects in water using sound propagation [37].

Later, in 1826 Jean Daniel Colladon, a physicist/engineer, and Charles-Francois Sturn, a mathematician realized an experiment to measure the underwater sound speed in Lake Geneva, Switzerland, (Figure 1.3) [38].

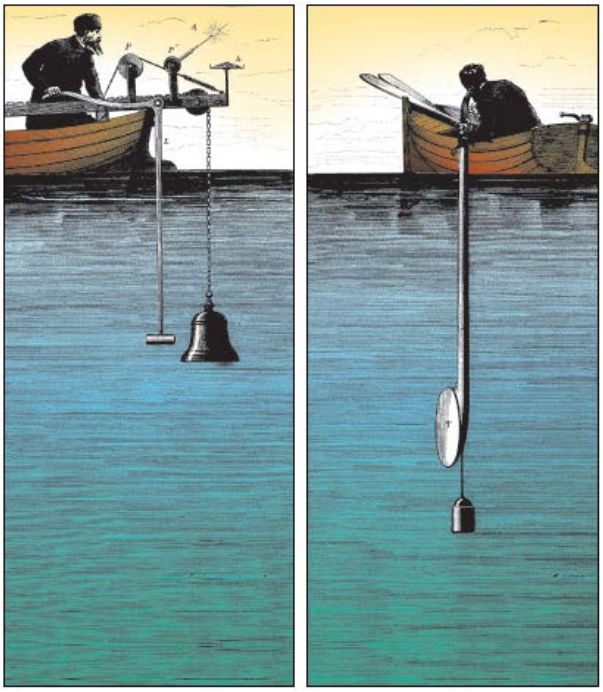

Figure 1.3: First measurement of sound speed on water in 1826 [38].

It was concluded that the velocity of sound in water was 1435 m/s. This value is not too different from currently known values.

The underwater acoustic communications and telemetry SONAR (SOund Navigation And Ranging) was born from the same roots. The beginning of this technology started in 1830, when Joseph Henry introduced the electroacoustic transducer based in a moving armature or variable reluctance transducer [39]. These developments led Alexander Graham Bell in 1876 to the telephone invention, using on both terminals moving armature transducers [39]. Between 1842 and 1847, James Joule discovered the magnetostriction [40] and in 1880 Jacques and Pierre Curie discovered the piezoelectricity in quartz and in other crystals [41]. The discovery of these two effects reveled to be an important step for underwater acoustics, since almost all nowadays ultrasonic transducers use materials with these properties. R.A Fessenden on 27 April 1914 developed a new type of transducer using a moving coil with operational frequencies of 500 and 1000 Hz [39]. This transducer was able to send signals between submarines and detect obstacles over 3 km by echo ranging. A system using this transducer was installed on United States submarines during World War I.

In 1968 it was published one of the first scientific papers of underwater acoustic communications [42]. That work showed that random signal fading has considerable effect on signal-to-noise power ratio and on the maximum information transmission rate of a communications system. In 1970, Riter presented a communication system for telemetry, with three representative modulation schemes: pulse position modulation (PPM), frequency modulation (FM) and frequency shift keying (FSK) [43]. One of the first digital modulation reports for underwater acoustic communication systems was published in 1975, where it was presented an experimental study on the high-data-rate performance limits of underwater digital data communication [44].

1.1.2. Technologies Overview and Recent Advances

Radio Frequency Communication Systems

In this technology, voice transmission is generally considered impractical at long distances, once the attenuation of radio waves through water strongly increases with frequency and distance. This technology only allows transmissions of little characters per minute. Furthermore, terrestrial repeaters are also needed due to distance limitations [45]. With this technology low frequencies are used and the propagation occurs mostly by air [46].

Radio Frequency is proven to be the most used technology in airborne wireless communication systems. It is nevertheless not suitable for application in underwater communications since electromagnetic waves experiences high attenuation. The water conductivity creates Eddy currents at the antenna periphery, which absorb much of the emitted energy. With seawater this effect is larger since it is 400 times more conductive than fresh water, being freshwater 0.01 S/m and seawater 4 S/m [47]. Beyond the high attenuation, which increases with frequency, the propagation speed also increases with frequency. For instance in sea water at 100 Hz the propagation speed is 1.77×10^4 m/s and at 1 MHz it is 1.52×10^6 m/s [48]. This propagation speed variation may represent a problem in wide band communication techniques or in modulations based on frequency shifting.

Figure 1.4 show the SeaText® by WFS that was the first commercial RF modem capable to communicate both through water and ground [49]. Using a very low frequency (VLF), the system was able to communicate in half-duplex arrangement over a range of 40 meters at a maximum depth of 3000 meters.

Figure 1.4: SeaText® by WFS, the first commercial RF modem capable to communicate through water and ground [49].

The modem used a 3 kHz single carrier with a maximum transmitting power of 16 W, reaching a maximum data rate of 100 bps. More recently WFS presented new products, namely a two-way underwater wireless RF communications operating at 100 kbps up to a distance of 10 meters for compressed video and an underwater modem that combines RF and acoustic signals: RF for high data rates at short distances and acoustic for low data rates at long distances, up to 20 km [49].

Recent projects are being developed using RF communications for very high data rates, up to 11 Mbps, at very short distances reaching a few centimeters, using 2.4 GHz frequency band. In [50] the authors described a deep underwater antenna compatible with Wi-Fi development and measurements on a prototype with a bandwidth of 70 MHz around 2.4 GHz over 15 cm distance. An underwater wireless sensor communication system in the 2.4 GHz ISM frequency band was also presented [51]. The results showed that such communication system has an optimum behavior at 16 cm, working at a frequency of 2,432 GHz, with the BPSK and QPSK modulations.

Other projects are based on lower frequencies, in the MHz range, to reach longer distances. One example is [52], where the authors presented an integrated treatment involving broadband RF antennas and digital radio systems, potentially enabling 1 Mbps underwater communications. The results show a successful communication data rate of 933 kbps over a few meters with 15 MHz bandwidth, using 15W transmitting power. In [48] the authors presented a re-evaluation of RF electromagnetic communication in underwater networks. It was presented RF-EM performance in underwater environments and it was described all key parameters of the technology. It was presented the established underwater wireless techniques, their current

limitations and finally, the potential that electromagnetic waves can offer to underwater applications.

Optical Communication (OCOM) Systems

OCOM systems became quite popular in the last years with the creation of reliable, low-cost light sources, such as Light Emitting Diodes (LEDs) [53], and Laser Diodes (LDs) [54, 55], that take advantage of the low attenuation (0.15 dB/m) of light in the 400 nm - 550 nm range (blue/green) in seawater [56]. This technology has several problems establishing a communication, due to the high beam directionality. The receptor and the transmitter must be aligned, being the communication lost with small displacements. The water conditions also affect the link quality: bubbles, particles in suspension or even daylight can interfere with the connection.

Underwater OCOM systems arise with the emerging need to provide a high-speed communication in some applications that require a real time high-data-rate communication [57]. This technology is a potential solution for high bandwidth and low latency in underwater wireless communications. Up to date optical is the technology that can achieve higher data-rates reaching up to 250 Mbps [56, 58].

As an example, in [59] it is described an optical modem that uses a transmitter based in a super bright blue LED. The results in a fresh water tank showed a successful transmission of large data files over a distance of 13 meters, with transmission rates up to 3 Mbps.

There are also commercial optical modems. For instance, the Neptune by SA Photonics (Figure 1.5) [58] is a low-power, compact, high data rate system for underwater communications and data transfer in both cost and deep ocean environments.

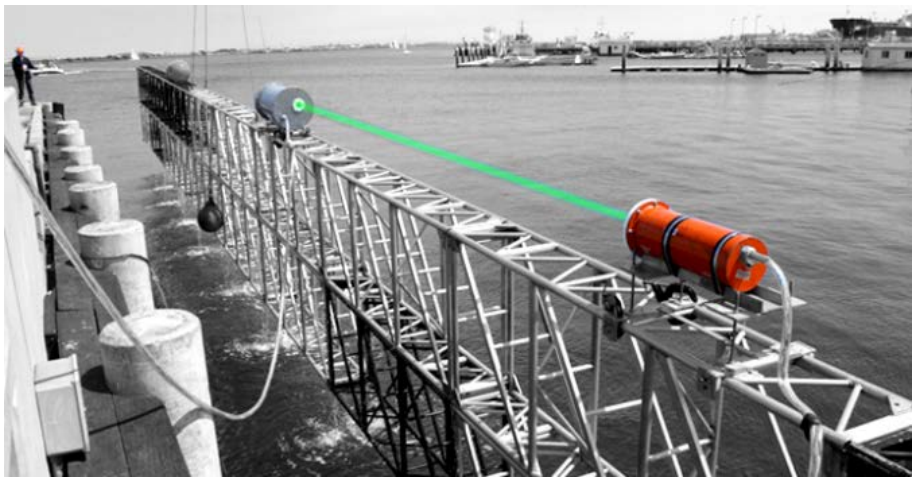

Figure 1.5: Communication test with Neptune optical modems [58].

They offer a very robust and reliable communication link with data rates up to 250 Mbps at distances up to 200 meters, depending on water quality conditions.

This high data rate characteristic of optical technology allowed the development of a communication system for remote underwater robot operation with real-time control [60]. The optical link allowed the robot to operate in cluttered environments without the need for a tether.

A more complete and thorough analysis of wireless communication systems using optical technology can be found in [61]. The author describes in detail all aspects of optical communications and addresses the recent research based on Quantum Key Distribution (QKD) [62]. This technique uses the photon quantum information to send perfectly secure keys. The information is encoded using photon lasers, where a single photon at a time, with a determined quantum state is sent [63, 64].

Acoustic communication systems

Acoustic communication systems have been widely implemented in underwater environments, once acoustic waves show low attenuation, reaching large distances. Despite the acoustic communication advantages in underwater environment, when compared to optical and radio frequencies, the propagation of sound has also significant challenges that influence the communication performance, mainly due to the slow speed of acoustic propagation in water (about 1500 m/s). When studying sound propagation in the underwater acoustic channel, some relevant phenomena must be taken into account, such as: attenuation [65 – 67], ambient noise, Doppler Effect, low and variable sound speed, multipath and sound refraction (scattering) air bubbles and particles in suspension [68 – 70]. For instance, with a 100 kHz signal, the acoustic

absorption can reach 3 dB/km. With 1 MHz signal, the absorption is up to 280 dB/km [66]. The spreading attenuation, which depends on the transducer geometry, must be added too [39].

The peculiar acoustic propagation phenomena that occur in underwater environments triggered numerous research projects around this area [71 – 73].

More recent works studied the differences between underwater acoustics and terrestrial radio, where the design of underwater acoustic network protocols by adapting or influenced by RF techniques is focused. These differences include physical propagation, energy consumption, design of medium access control, routing and topology management [74 – 77].

For a more complete notion of the current state of underwater acoustic communications, the authors presented in [78] a survey of the recent advances and future challenges in underwater acoustic communications and networking. They also introduce open problems and challenges that researchers will face in this field in the near future.

Acoustic underwater communications is a well-established technology and represents the major solution for long distances and deep water applications. This stimulated the creation of several commercial products, such as: EvoLogics R-series [79], Desert Star Systems SAM-1 [80], LinkQuest Inc. UWM Series [81], AppliedOcean Systems SAM1-Subsea Acoustic Modem [82], DSPComm AquaComm [83], Teledyne Benthos ATM [84] and JetaSonic models H-Series [85].

EvoLogics (Figure 1.6) [79] offers an acoustic modem that can reach 2000 meters deep with an operational range of 1000 meters.

Figure 1.6: EvoLogics S2C R 48/78 Underwater Acoustic Modem [79].

A maximum transmitting power of 60W can be achieved 31.2 kbps in an omnidirectional pattern, with a Bit Error Rate (BER) less than 10^{-10}.

Other interesting acoustic modem is the SAM1 by AppliedOcean System [82], that can reach 1 km distance with a maximum data rate of 100 kbps.

For long distances the better choice is the LInkQuest Inc. [81]. Their powerful modem with 40 W transmitting power consumption, offers a 10 km distance range and a 7 km maximum depth, and it can achieve 5 kbps in omnidirectional pattern with a BER less than 10^{9}.

1.2. Comparison between underwater wireless communication technologies

Considering all the information presented throughout this document, it is shown that all technologies have unique characteristics taking advantage of different propagation channels. Therefore, acoustic, optical and RF-EM wireless underwater communications are applied for different purposes with distinctive requirements. Table 1.1 shows the advantages and limitations of the different underwater communication technologies.

Table 1.1: Comparison among the different underwater communication technologies.

Technology	Advantages	Limitations
Acoustic – tens of kHz range	-Long distance coverage (up to 20 km) -Low attenuation. -Established technology. -Low power consumption.	-Low data rate (up to 100 kbps). -Impact on aquatic life. -Do not cross water/air boundary -Highly affected by turbidity, ambient noise, salinity, temperature and pressure. -Low propagation velocity. -Easily multipath occurrence in shallow water.
Optical	-Low Cost. -High data rates (up to 250 Mbps).	-Short range. -Requires an alignment between agents. -Highly affected by turbidity, particles, and marine fouling. -Need a line of sight. -Not cross water/air boundary easily.
RF – VLF and ELF	-Crosses water/air boundary easily. -Not effected by turbidity, ambient noise, salinity, temperature and pressure.	-Limited distance range through water. -Low data rate (around 300 bps). -Vulnerable to EMI.

	-Do not need alignment or line of sight. -Long distances range, mostly by air (can penetrate to a depth of approximately 20 meters).	-Almost used only in shallow waters.
RF – High Frequencies	-Crosses water/air boundary easily. -High data rates (up to 10 Mbps). -Not affected by turbidity, ambient noise, salinity, temperature and pressure. -Do not need alignment or line of sight.	-Very short range (few centimeters). -High power consumption.

By analyzing Table 1.1 it is possible to take some conclusions. For instance, acoustic is frequently used for mobile and stationary connections at very long distances, up to 20 km [86], with low data-rate. Optical technology is applied in high data rates with stationary stations, once it is necessary a thorough alignment and a line-of-sight [87]. RF is often used in communications where it is required to create a link that easily crosses air/water/seabed boundaries. In that type of applications, it is implemented a VLF or ELF with very low data rates, reaching a limited distance range [88]. Considering Table 1.1, it is notorious that there are no underwater communication technologies that can meet all the needs of a high-speed real time wireless network with mobile agents. Therefore it is necessary to study a form to improve and make a better use of the existing technologies. Using the advantage of each technology, it is possible to implement a network capable of reaching long distances at high speed connections.

1.3. Motivation

In order to render a possible implementation of the architecture presented in Figure 1.7 and Figure 1.8, it is necessary to develop a medium range (hundreds of meters) high data rate and real time communication system for mobile agents.

In Figure 1.7, a network architecture that can respond to the actual needs of wireless underwater networks to support high-speed and real time communications is presented [22, 89, 90].

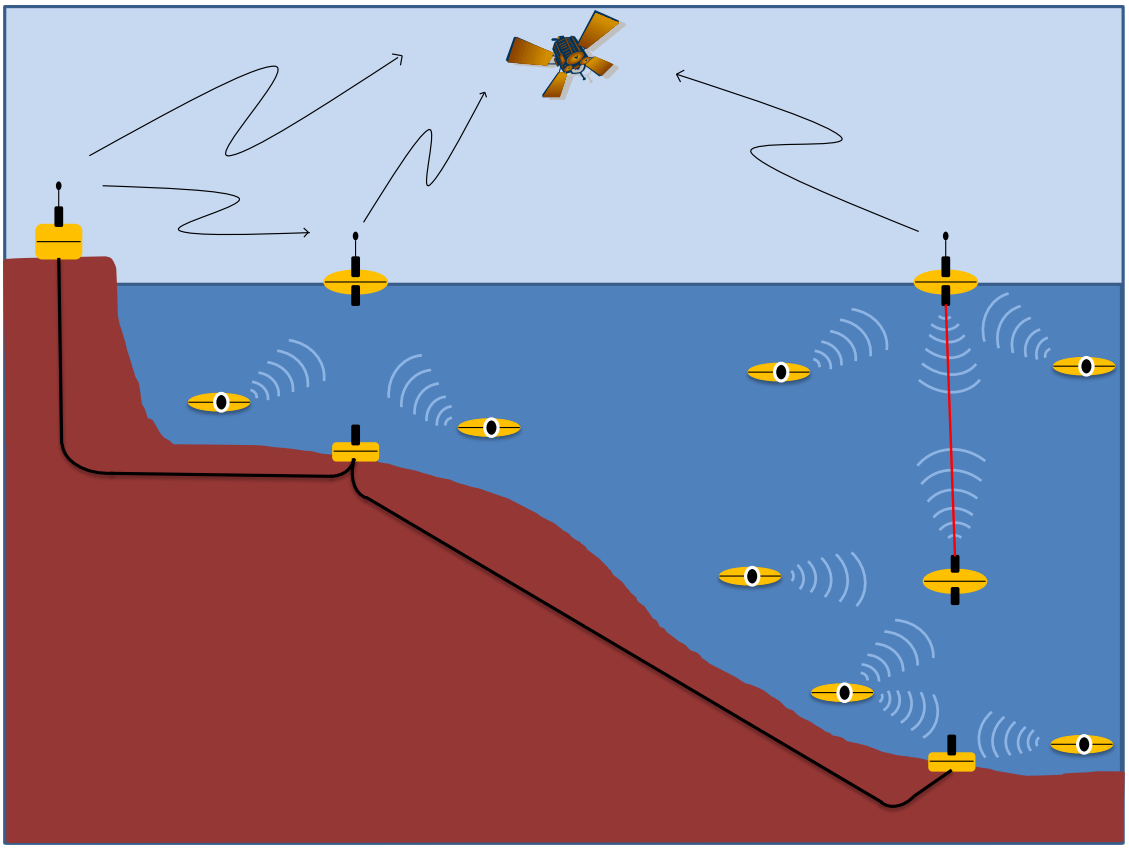

Figure 1.7: High data rate underwater network architecture.

Figure 1.7 shows that the very long distance communications can be forwarded to air links. In this way, the propagation time is reduced. In the surface there are routers to convert the acoustic or optical links in RF-EM airborne links [91]. Underwater, mobile agents communicate through high speed acoustic at a range of hundreds of meters. The static agents or routers can communicate between each other through high speed acoustic or optical links. To larger depths, multiple routers can be placed at different vertical levels that can communicate with each other via high speed acoustic or optical links [92, 93]. On the ocean floor, static agents or routers, connected to each other through electrical or optical wires can be placed, to support a high data rate network. The routers near the coast can be connected to land stations using wires too. The underwater network topology and the mobile agents are presented with more detail in Figure 1.8 [94].

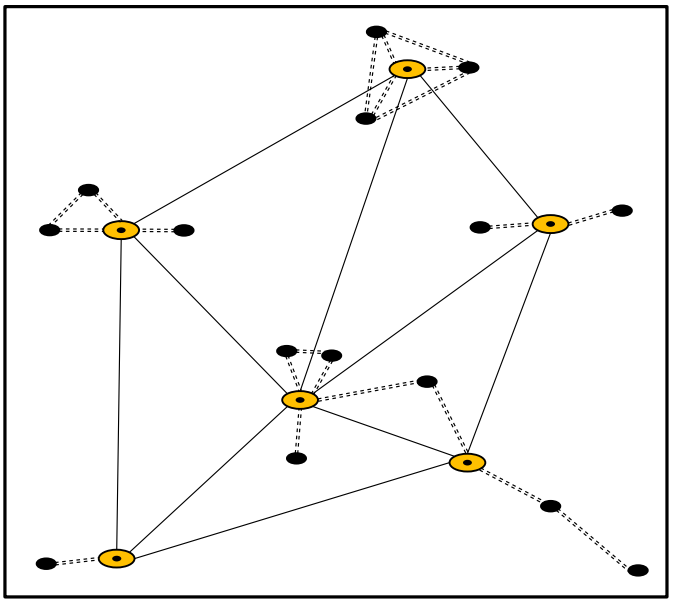

Figure 1.8: Underwater support network.

Figure 1.8 shows the top view of an underwater network placed at the bottom of the ocean. It is possible to observe that mobile agents always use the fastest route. They can communicate with a nearby mobile agent directly using acoustic communications or use a router to communicate with a more distant one.

If a mobile agent is too far to reach a router, it can use an intermediary mobile agent to reach the router.

This organization allows implementing a high speed network, covering a large underwater area and ensuring the lowest propagation delay.

Consequently, evaluating all available technologies (using Table 1.1), the most suitable for possible high data rate and real time connections between mobile agents, is the acoustic based technology. But, for this type of applications it is essential to consider two limitations of acoustic technology: the propagation delay and the data rate. Therefore, and despite the acoustic is a proven technology for long-range communications [68], in real time communications it is limited in terms of distance, once the propagation delay can reach about 10 seconds for a distance of 15 km, preventing any real time connection [95]. Therefore, the distance of an acoustic real time communication will be limited by the resulting propagation delay. Relatively to the acoustic technology at low data rates, recent works are presenting new and more efficient modulations techniques in order to increase the data rate [76, 96, 97]. There are several solutions to increase the modulation efficiency or data rate. The most frequents are: increasing the carrier frequency

[98, 99] or increasing the symbol rate per carrier period [96, 100]. For example, in [101] the authors present a high-speed acoustic modem for real-time transmission reaching a maximum data rate of 150 kbps over 100 meters in shallow-waters. The ultrasonic transducer used was developed by Jetasonic [85], which operates in a frequency band from 260 kHz to 380 kHz, using either BPSK and QPSK modulation. However, to improve acoustic communication it is necessary to understand how the ultrasonic transducers work, allowing more effective implementation of digital modulations regarding the transducer advantages and limitations.

The available ultrasonic transducers show low performance under high data rate digital communications [39, 102, 103]. Therefore, it is necessary to optimize the ultrasound transducers to perform wideband and high frequencies (from kHz to MHz range) with low power consumption. For digital modulation the transducer has to present reduced damping and a good acoustic energy transfer to the medium, allowing to minimize the signal deformation when converted from electric to acoustic.

The ultrasonic transducers used nowadays in underwater acoustic communications are adapted versions of the ones of SONAR [39]. The transducer geometry and design are directly associated to the frequency band, beam pattern, acoustic power and operation mode (projector or hydrophone) [70]. The ultrasonic transducer can be optimized to project, receive or both and the definition of the operating frequency for a hydrophone or a projector has different meanings. Projectors usually take leverage of the resonance effect, using only drive signals at the resonance frequencies, where the highest acoustic pressure if delivered to the output. Hydrophones, on the other hand, are usually used below resonance frequencies, over a much wider frequency band [104 – 105]. Hydrophones and projectors can be planar, cylindrical or spherical, mounted with only one transducer or in structures like arrays or matrixes using up to thousands of transducers [39].

The materials used show normally piezoelectric, electrostrictive or magnetostrictive properties, being the piezoelectric the most frequent [39]. There are several piezoelectric materials available for ultrasound transducers [106, 107]. The most common are Lead Zirconate Titanate (PZT), Lead Titanate (PT), Lead Magnesium Niobate (PMN) and Lead Zinc Niobate (PZN) ceramics [108, 109] and Poly(viylidene fluoride) (PVDF) polymers [110 – 112]. Single crystals of PZT, PMN and PZN can also be used [113, 114]. To better adjust transducer performance to the

application, composite materials can be used, allowing to add various capabilities of different types of materials [115 – 117].

1.4. Objectives

The main objective of this work is to develop a high speed real time link for underwater wireless communications based on acoustic technology.

The goal is to achieve frequency carriers up to 1 MHz, thus it would be necessary to develop ultrasonic transducer capable of operating at that frequencies and providing good performance response to digital modulations.

So, the main focus of the present work will be:

- Study and characterize the underwater acoustic channel.
- Design and build ultrasonic transducers for digital modulations in the MHz frequency range.
- Evaluate the performance of digital modulations in underwater environment, using high frequencies.
- Design and build a high data rate acoustic modem.

1.5. Structure and methodology

The thesis is divided into 6 chapters. Beyond introduction and conclusion chapters, each one of the chapters focuses in a specific topic of the main objectives. The chapters are organized following the sequential order of the work to better understand the research process. Chapters 2, 3, 4 and 5 are based in scientific articles.

In Chapter 2, the underwater acoustic channel is studied and characterized. It is presented a theoretical simulation model of an acoustic communication system. The simulation model emulates the underwater acoustic channel which includes attenuation, environmental noise, Doppler Effect, multipath and propagation delay. The simulation results were validated with experimental tests.

Chapter 3 describes the ultrasonic transducers optimization. It was developed a Finite Element Method (FEM) model to study the multilayer structure performance and different material families

are compared. This study is particularly focused on emitter ultrasonic transducers in order to overcome their main limitations.

Chapter 4 shows the influences of the acoustic impedance in the performance of an ultrasonic emitter, when using different digital modulations and operating at frequencies between 100 kHz and 1 MHz to a distance of tens meters. The transducers performance for Binary Amplitude Shift Keying (BASK), On-Off Keying (OOK), Binary Phase Shift Keying (BPSK) and Binary Frequency Shift Keying (BFSK) modulations are evaluated by simulation and experimental tests.

Chapter 5 describes the design and building of a high data rate acoustic modem. Experimental evaluation of a full duplex point-to-point communication link at 1 Mbps using (OOK) modulation with 1 MHz single carrier was performed.

Finally, chapter 6 presents the overall conclusions and suggestions for future work.

1.6. References

[1] U. Chakraborty, T. Tewary, and R. P. Chatterjee, “Exploiting the Loss-Frequency Relationship using RF Communication in Underwater Communication Networks,” no. 3, pp. 1–4, 2009.

[2] A. Gkikopouli, G. Nikolakopoulos, and S. Manesis, “A survey on Underwater Wireless Sensor Networks and applications,” in 2012 20th Mediterranean Conference on Control & Automation (MED), 2012, pp. 1147–1154.

[3] M. J. Brawner and S. Kurak, “Submarine Communications Modernization - Technology Insertions for Interoperability and Supportability in the 2015 Timeframe,” in MILCOM 2005 - 2005 IEEE Military Communications Conference, pp. 1–7.

[4] “The study of remotely teleoperated robotic manipulator system for underwater construction,” in Proceedings of the 2004 International Symposium on Underwater Technology (IEEE Cat. No.04EX869), pp. 269–276.

[5] O. Hegrenas, E. Berglund, and O. Hallingstad, “Model-aided inertial navigation for underwater vehicles,” in 2008 IEEE International Conference on Robotics and Automation, 2008, pp. 1069–1076.

[6] K. J. Edwards, A. T. Fisher, and C. G. Wheat, “The deep subsurface biosphere in igneous ocean crust: frontier habitats for microbiological exploration.,” Frontiers in microbiology, vol. 3, p. 8, Jan. 2012.

[7] C. R. German, E. Ramirez-Llodra, M. C. Baker, and P. A. Tyler, “Deep-water chemosynthetic ecosystem research during the census of marine life decade and beyond: a proposed deep-ocean road map.,” PloS one, vol. 6, no. 8, p. e23259, Jan. 2011.

[8] X. Zhao, Z. Bao, Z. Liu, H. Zhau, and Q. Chai, “An in-depth analysis of reservoir architecture of underwater distributary channel sand bodies in a river dominated delta: A case study of T51 Block, Fuyu Oilfield, Jilin,” Petroleum Exploration and Development, vol. 40, no. 2, pp. 194–201, Apr. 2013.

[9] C. L. Antrim, “What Was Old Is New Again: Economic Potential Of Deep Ocean Minerals The Second Time Around,” in Proceedings of OCEANS 2005 MTS/IEEE, pp. 1–8.

[10] W. H. Smith, “Global Sea Floor Topography from Satellite Altimetry and Ship Depth Soundings,” Science, vol. 277, no. 5334, pp. 1956–1962, Sep. 1997.

[11] N. Randazzo and C. Bechaz, “Scientific application of advanced underwater positioning techniques,” in Europe Oceans 2005, vol. 2, pp. 1171–1173.

[12] K.-C. Lee, J.-S. Ou, and M.-C. Huang, “Underwater acoustic localization by principal components analyses based probabilistic approach,” Applied Acoustics, vol. 70, no. 9, pp. 1168–1174, Sep. 2009.

[13] G. Marani, S. K. Choi, and J. Yuh, “Underwater autonomous manipulation for intervention missions AUVs,” Ocean Engineering, vol. 36, no. 1, pp. 15–23, Jan. 2009.

[14] T. Lay, H. Kanamori, C. J. Ammon, M. Nettles, S. N. Ward, R. C. Aster, S. L. Beck, S. L. Bilek, M. R. Brudzinski, R. Butler, H. R. DeShon, G. Ekström, K. Satake, and S. Sipkin, “The great Sumatra-Andaman earthquake of 26 December 2004.,” Science (New York, N.Y.), vol. 308, no. 5725, pp. 1127–33, May 2005.

[15] T. A. Stojanovic and C. J. Q. Farmer, “The development of world oceans & coasts and concepts of sustainability,” Marine Policy, vol. 42, pp. 157–165, Nov. 2013.

[16] C. Izaguirre, M. Menéndez, P. Camus, F. J. Méndez, R. Mínguez, and I. J. Losada, "Exploring the interannual variability of extreme wave climate in the Northeast Atlantic Ocean," Ocean Modelling, vol. 59–60, pp. 31–40, Dec. 2012.

[17] D. J. Wei, L. H. Zhang, H. W. Zhang, and F. Liu, "Finite Element Analysis of the Strength of Ladder Type Structure of the Deep-Water AUV," Advanced Materials Research, vol. 690–693, pp. 1903–1908, May 2013.

[18] A. Birk, M. Pfingsthorn, and H. Bulow, "Advances in underwater mapping and their application potential for Safety, Security, and Rescue Robotics (SSRR)," in 2012 IEEE International Symposium on Safety, Security, and Rescue Robotics (SSRR), 2012, pp. 1–3.

[19] R. H. Rahman, C. R. Benson, and M. R. Frater, "Routing challenges and solutions for underwater networks," in 2012 Military Communications and Information Systems Conference (MilCIS), 2012, pp. 1–7.

[20] F. Audo, S. Perhirin, V. Quintard, M. Guegan, A. Perennou, and Y. Auffret, "Raman amplification in an optically high-powered data link dedicated to a 10 km long extension for submarine cabled observatories," Journal of Optics, vol. 15, no. 5, p. 055703, May 2013.

[21] C. Cao, M. Zukerman, W. Wu, J. H. Manton, and B. Moran, "Survivable Topology Design of Submarine Networks," Journal of Lightwave Technology, vol. 31, no. 5, pp. 715–730, Mar. 2013.

[22] J. Partan, J. Kurose, and B. N. Levine, "A survey of practical issues in underwater networks," ACM SIGMOBILE Mobile Computing and Communications Review, vol. 11, no. 4, p. 23, Oct. 2007.

[23] J. B. Lindsay, "Mr.Lindsay's Marine Telegraph," Dundee Advertiser, 1853.

[24] W. H. Preece, "On the Maintenance and Durability of Submarine Cables in Shallow Waters," History of the Atlantic Cable & Undersea Communications, 1860.

[25] J. P. Mallmann Showell, ENIGMA U-boats. Ian Alan Publishing, pp. 14–15.

[26] S. L. Bernstein, M. L. Burrows, J. E. Evans, A. S. Griffiths, D. A. McNeill, C. W. Niessen, I. Richer, D. P. White, and D. K. Willim, "Long-range communications at extremely low frequencies," Proceedings of the IEEE, vol. 62, no. 3, pp. 292–312, 1974.

[27] A. G. Bell, “On the Production and Reproduction of Sound by Light: the Photophone,” Am. Ass. for the Advancement of Sci., vol. 29, pp. 115–136, 1880.

[28] N. K. Hojerslev, “A history of early optical oceanographic instrument design in Scandinavia,” Ocean Optics, Spinrad R.W, no. Oxford University Press, Inc., p. 118.147, 1994.

[29] W. M. Steen and J. Mazumder, Laser Materials Processing. Springer, 2010.

[30] C. H. Townes, “How the Laser Happened: Adventures of a Scientist,” 1999.

[31] C. H. Townes, “The first laser,” 2003, pp. 107–112.

[32] D. Maiman, “First Laser,” Bill McGovern. [Online]. Available: http://www.hrl.com/hrlDocs/pressreleases/2007/prsRls_071113.html.

[33] W. Burt and G. Beardsley, “Underwater Optical Measurements,” Oceanology Int, pp. 35–39, 1969.

[34] G. D. Ferguson, “Blue-Green Lasers For Underwater Applications,” SPIE Semin Proc, pp. 150–156, 1975.

[35] S. Karp, “Optical Communications Between Underwater And Above Surface (Satellite) Terminals,” IEEE Transactions on Communications, pp. 66–81, 1976.

[36] M. Stojanovic, “Recent advances in high-speed underwater acoustic communications,” IEEE Journal of Oceanic Engineering, vol. 21, no. 2, pp. 125–136, Apr. 1996.

[37] M. Stojanovic, “Underwater Acoustic Communication,” Wiley Encyclop dia of Ele e ctric al and Ele ctr onics Engine ering, vol. 22, pp. 688–698, 1999.

[38] H. Vosbein, “Introduction to Ocean Acoustics,” 2010.

[39] C. H. Sherman and J. L. Butler, Transducers and Arrays for Underwater Sound. Springer Science+Business Media, LLC, 2007, p. 610.

[40] J. . Joule, “On the Effects of Magnetism upon the Dimensions of Iron and Steel Bars,” The London, Edinburgh and Dublin philosophical magazine and journal of science, vol. 30, no. 3, pp. 76–87, 225–241, 1847.

[41] R. Mould, “Pierre Curie 1859-1906,” Current Oncology, vol. 14, no. 2, pp. 74–82, Apr. 2007.

[42] D. Marsh and R. Rowlands, “Upper Bounds On Information Rate For Underwater Acoustic Communication,” in IEEE-Nat Telemetering Conference-NTC ’68, 1968, pp. 308–313.

[43] S. Riter, “Underwater Acoustic Telemetry,” in Offshore Technol Conf, 1970, pp. 259–268.

[44] R. S. Andrews and L. F. Turner, “Investigation of The Amplitude Fluctuations Of High-Frequency Short-Duration Sound Pulses Propagated Under Short-Range Shallow-Water Conditions,” Journal of the Acoustical Society of America, vol. 58, no. 2, pp. 331–335, 1975.

[45] M. Rhodes, “Electromagnetic Propagation In Sea Water And Its Value In Military Systems,” in SEAS DTC Technical Conference, 2007.

[46] P. Smith, “Measurement and Analysis of Transmit Antenna Configurations for Underwater RF Communications,” in 3 rd SEAS DTC Technical Conference, 2008.

[47] S. Jiang, “Electromagnetic Wave Propagation into Fresh Water,” Journal of Electromagnetic Analysis and Applications, vol. 03, no. 07, pp. 261–266, 2011.

[48] X. Che, I. Wells, G. Dickers, P. Kear, and X. Gong, “Re-evaluation of RF electromagnetic communication in underwater sensor networks,” IEEE Communications Magazine, vol. 48, no. 12, pp. 143–151, Dec. 2010.

[49] WFS Techologies, “Seatooth+acoustic,” 2013. [Online]. Available: http://www.wfs-tech.com/index.php/products/seatooth/seatoothacoustic/.

[50] H. Fabian, G. Mendez, L. E. Pennec, C. Gac, C. Person, M. Geosciences, F. Lab-sticc, T. Bretagne, D. Microwave, T. B. Iroise, B. Cedex, and C. Main, “Deep Underwater Compatible Wi-Fi Antenna Development,” Wireless Personal Multimedia Communications (WPMC), 2011 14th International Symposium on, pp. 1–5, 2011.

[51] J. Lloret, S. Sendra, M. Ardid, and J. J. P. C. Rodrigues, “Underwater wireless sensor communications in the 2.4 GHz ISM frequency band.,” Sensors (Basel, Switzerland), vol. 12, no. 4, pp. 4237–64, Jan. 2012.

[52] B. Kelley and K. Naishadham, “RF multicarrier signaling and antenna systems for low SNR broadband underwater communications,” in 2013 IEEE Radio and Wireless Symposium, 2013, pp. 340–342.

[53] W. C. J. Cox, “A 1 Mbps Underwater Communication System Using a 405 nm Laser Diode and Photomultiplier Tube,” Graduate Faculty of North Carolina State University.

[54] A. Kumar and R. S. Jha, “Comparison of Underwater Laser Communication System with Underwater Acoustic Sensor Network,” vol. 3, no. 10, pp. 3–6, 2012.

[55] L. Mullen and B. Cochenour, “Communication over Lasers in Ocean Research (COLOR): Bringing Navy research to the classroom,” 2012 Oceans, pp. 1–4, Oct. 2012.

[56] W. C. Cox, J. A. Simpson, C. P. Domizioli, J. F. Muth, and B. L. Hughes, “An underwater optical communication system implementing Reed-Solomon channel coding,” in OCEANS 2008, 2008, pp. 1–6.

[57] S. Arnon, “Underwater optical wireless communication network,” Optical Engineering, vol. 49, no. 1, p. 015001, Jan. 2010.

[58] SA Photonics, “Neptune underwater optical communications,” 2013. [Online]. Available: http://www.saphotonics.com/wp-content/uploads/2012/08/Neptune-Datasheet.pdf.

[59] H. Brundage, “Designing a Wireless Underwater Optical Communication system,” Massachusetts Institute of Technology, 2010.

[60] M. Doniec, C. Detweiler, I. Vasilescu, and D. Rus, “Using optical communication for remote underwater robot operation,” in 2010 IEEE/RSJ International Conference on Intelligent Robots and Systems, 2010, pp. 4017–4022.

[61] M. Lanzagorta, “Underwater Communications,” Synthesis Lectures on Communications, vol. 5, no. 2, pp. 1–129, Oct. 2012.

[62] J. Wang, C. Luo, S. Lin, H. Zhang, K. Cui, H. Liang, G. Jin, L. Zhou, and T. Chen, “Research of hash-based secure key expansion algorithm for practical QKD,” Optik - International Journal for Light and Electron Optics, vol. 124, no. 15, pp. 2273–2276, Aug. 2013.

[63] M. Lasota, R. Demkowicz-Dobrzański, And K. Banaszek, “Quantum Key Distribution With Realistic Heralded Single-Photon Sources,” International Journal of Quantum Information, vol. 11, no. 03, p. 1350034, Apr. 2013.

[64] S. Bratzik, S. Abruzzo, H. Kampermann, and D. Bruß, “Quantum repeaters and quantum key distribution: The impact of entanglement distillation on the secret key rate,” Physical Review A, vol. 87, no. 6, p. 062335, Jun. 2013.

[65] W. H. Thorp, “Analytic Description of the Low-Frequency Attenuation Coefficient,” The Journal of the Acoustical Society of America, vol. 42, no. 1, p. 270, 1967.

[66] M. A. Ainslie and J. G. McColm, “A simplified formula for viscous and chemical absorption in sea water,” The Journal of the Acoustical Society of America, vol. 103, no. 3, p. 1671, Mar. 1998.

[67] F. H. Fisher, “Sound absorption in sea water,” The Journal of the Acoustical Society of America, vol. 62, no. 3, p. 558, 1977.

[68] M. Stojanovic and J. Preisig, “Underwater acoustic communication channels: Propagation models and statistical characterization,” IEEE Communications Magazine, vol. 47, no. 1, pp. 84–89, Jan. 2009.

[69] P. Qarabaqi and M. Stojanovic, “Small scale characterization of underwater acoustic channels,” Proceedings of the Seventh ACM International Conference on Underwater Networks and Systems - WUWNet ’12, no. 1, p. 1, 2012.

[70] D. Jackson and M. Richardson, High-Frequency Seafloor Acoustics. Springer, 2007.

[71] S. H. Huang, T. C. Yang, and C.-F. Huang, “Subspace channel tracking for correlated underwater acoustic communication channels,” Proceedings of the Seventh ACM International Conference on Underwater Networks and Systems - WUWNet ’12, p. 1, 2012.

[72] A. Sehgal, I. Tumar, and J. Schonwalder, “Variability of available capacity due to the effects of depth and temperature in the underwater acoustic communication channel,” in OCEANS 2009-EUROPE, 2009, pp. 1–6.

[73] M. C. Domingo, “Overview of channel models for underwater wireless communication networks,” Physical Communication, vol. 1, no. 3, pp. 163–182, Sep. 2008.

[74] P. Casari and M. Zorzi, “Protocol design issues in underwater acoustic networks,” Computer Communications, vol. 34, no. 17, pp. 2013–2025, Nov. 2011.

[75] S. Kim, J. Han, K. Kim, S. Baek, H. Kim, and C. Kim, “Experimental Results of Single Carrier Digital Modulation for Underwater Sensor Networks,” 2010 IEEE/IFIP International Conference on Embedded and Ubiquitous Computing, pp. 326–330, Dec. 2010.

[76] K. Ball, M. Stojanovic, L. Freitag, and P. Willett, “MIMO-OFDM for High-Rate Underwater Acoustic Communications,” IEEE Journal of Oceanic Engineering, vol. 34, no. 4, pp. 634–644, Oct. 2009.

[77] A. Patil and M. Stojanovic, “A node discovery protocol for ad hoc underwater acoustic networks,” in OCEANS 2011 IEEE - Spain, 2011, no. February 2012, pp. 1–9.

[78] M. Chitre, S. Shahabudeen, and M. Stojanovic, “Underwater Acoustic Communications and Networking: Recent Advances and Future Challenges,” Marine Technology Society Journal, vol. 42, no. 1, pp. 103–116, Mar. 2008.

[79] EvoLogics, “EvoLogics GmbH,” Underwater Acoustic Modems, 2013. [Online]. Available: http://www.evologics.de/en/products/acoustics/index.html. [Accessed: 27-May-2013].

[80] Desert Star Systems, “SAM-1 Miniature Acoustic Modem Set,” University of California, 2013. [Online]. Available: http://www.desertstar.com/Products_product.aspx?intProductID=4.

[81] LinkQuest Inc., “Underwater Acoustic Modem Models UWM-Series,” 2013. [Online]. Available: http://www.link-quest.com/html/models1.htm.

[82] Applied Ocean Systems, “Applied Ocean Systems,” SAM1 Wireless Subsea Acoustic Modem, 2013. [Online]. Available: http://www.applied-ocean.com/. [Accessed: 27-May-2013].

[83] “DSPComm,” AquaComm: Underwater wireless modem, 2013. [Online]. Available: http://www.dspcomm.com/. [Accessed: 27-May-2013].

[84] Teledyme Benthos, “Acoustic Modems,” 2013. [Online]. Available: http://www.benthos.com/index.php/product_dashboard/acoustic_modems.

[85] JetaSonic, “Underwater Communication,” 2013. [Online]. Available: http://www.jetasonic.com/underwater-communication/overview/.

[86] D. E. Lucani, M. Médard, and M. Stojanovic, “Underwater Acoustic Networks: Channel Models and Network Coding based Lower Bound to Transmission Power for Multicast,” vol. 1, no. 11, p. 12, Aug. 2008.

[87] D. Anguita, D. Brizzolara, G. Parodi, and V. O. Pia, “Optical Communication for Underwater Wireless Sensor Networks : a VHDL-implementation of a Physical Layer 802 . 15 . 4 Compatible .,” pp. 1–2.

[88] B. Kelley, K. Manoj, and M. Jamshidi, “Broadband RF communications in underwater environments using multi-carrier modulation,” 2009 IEEE International Conference on Systems, Man and Cybernetics, pp. 2303–2308, Oct. 2009.

[89] Y. Wang, Y. Liu, and Z. Guo, “Three-dimensional ocean sensor networks: A survey,” Journal of Ocean University of China, vol. 11, no. 4, pp. 436–450, Oct. 2012.

[90] I. F. Akyildiz, D. Pompili, and T. Melodia, “State of the art in protocol research for underwater acoustic sensor networks,” Proceedings of the 1st ACM international workshop on Underwater networks - WUWNet ’06, vol. 11, no. 4, p. 11, Oct. 2006.

[91] H. Yoshida, T. Hyakudome, S. Ishibashi, H. Ochi, and K. Asakawa, “Study on Land-to-Underwater communication,” Wireless Personal Multimedia Communications (WPMC), 2011 14th International Symposium on, pp. 1–5, 2011.

[92] D. Torres, “Acoustic and Optical Communication for Underwater Wireless Sensor Networks,” University of California, Los Angeles, 2010.

[93] N. Farr, A. Bowen, J. Ware, C. Pontbriand, and M. Tivey, “An integrated, underwater optical /acoustic communications system,” in OCEANS’10 IEEE SYDNEY, 2010, pp. 1–6.

[94] F. Salvá-garau, M. Stojanovic, and F. Salvi-garau, “Multi-cluster protocol for ad hoc mobile underwater acoustic networks,” in Oceans 2003. Celebrating the Past ... Teaming Toward the Future (IEEE Cat. No.03CH37492), 2003, pp. 91–98 Vol.1.

[95] D. E. Lucani, M. Stojanovic, and M. Médard, “On the Relationship between Transmission Power and Capacity of an Underwater Acoustic Communication Channel,” vol. 003, no. 2, p. 6, Jan. 2008.

[96] Z. Wang, S. Zhou, J. Catipovic, and P. Willett, “Asynchronous Multiuser Reception for OFDM in Underwater Acoustic Communications,” vol. 0704, pp. 1–7, 2011.

[97] A. C. Farrell and J. Peng, “Performance of IEEE 802.11 MAC in Underwater Wireless Channels,” Procedia Computer Science, vol. 10, pp. 62–69, Jan. 2012.

[98] N. Nowsheen, C. Benson, and M. Frater, “A high data-rate, software-defined underwater acoustic modem,” in OCEANS 2010 MTS/IEEE SEATTLE, 2010, pp. 1–5.

[99] N. Nowsheen, C. Benson, and M. Frater, “Design of a high frequency FPGA acoustic modem for underwater communication,” in OCEANS’10 IEEE SYDNEY, 2010, pp. 1–6.

[100] J. Huang, S. Zhou, and Z. Wang, “Performance Results of Two Iterative Receivers for Distributed MIMO OFDM With Large Doppler Deviations,” IEEE Journal of Oceanic Engineering, vol. 38, no. 2, pp. 347–357, Apr. 2013.

[101] P.-P. J. Beaujean, E. A. Carlson, J. Spruance, and D. Kriel, “HERMES - A high-speed acoustic modem for real-time transmission of uncompressed image and status transmission in port environment and very shallow water,” in OCEANS 2008, 2008, pp. 1–9.

[102] J. Chen, H. J. Wan, and X. W. Wang, “A Design of Underwater Acoustic Responder Based on Spread-Spectrum Communication,” Procedia Engineering, vol. 29, pp. 128–132, Jan. 2012.

[103] S. Ma, A. J. Wilkinson, and K. S. Paulson, “A phase modulation-based ultrasonic communication system using Variable Structure Control,” in 2010 IEEE 12th International Conference on Communication Technology, 2010, pp. 857–860.

[104] S. Umchid, R. Gopinath, K. Srinivasan, P. a Lewin, a S. Daryoush, L. Bansal, and M. El-Sherif, “Development of calibration techniques for ultrasonic hydrophone probes in the frequency range from 1 to 100 MHz.,” Ultrasonics, vol. 49, no. 3, pp. 306–11, Mar. 2009.

[105] P. Challande, “Optimizing ultrasonic transducers based on piezoelectric composites using a finite-element method.,” IEEE Transactions on Ultrasonics Ferroelectrics and Frequency Control, vol. 37, no. 3, pp. 135–140, 1990.

[106] T. R. Shrout, “Innovations in piezoelectric materials for ultrasound transducers,” in 2008 17th IEEE International Symposium on the Applications of Ferroelectrics, 2008, pp. 1–4.

[107] L. W. Schmerr, a Lopez-Sanchez, and R. Huang, “Complete ultrasonic transducer characterization and its use for models and measurements.,” Ultrasonics, vol. 44 Suppl 1, pp. e753–7, Dec. 2006.

[108] A. Abrar and S. Cochran, “Multilayer piezocomposite structures with piezoceramic volume fractions determined by mathematical optimisation.,” Ultrasonics, vol. 42, no. 1–9, pp. 259–65, Apr. 2004.

[109] T. Bove, W. Wolny, E. Ringgaard, and A. Pedersen, “New piezoceramic PZT–PNN material for medical diagnostics applications,” Journal of the European Ceramic Society, vol. 21, no. 10–11, pp. 1469–1472, Jan. 2001.

[110] P. A. Lewin and P. E. Bloomfield, “PVDF transducers-a performance comparison of single-layer and multilayer structures,” IEEE Transactions on Ultrasonics, Ferroelectrics and Frequency Control, vol. 44, no. 5, pp. 1148–1156, Sep. 1997.

[111] B. Granz, “PVDF hydrophone for the measurement of shock waves,” in 6th International Symposium on Electrets,(ISE 6) Proceedings., 1989, vol. 24, no. 3, pp. 223–228.

[112] F. Levassort, L. P. T. Huu Hue, G. Feuillard, and M. Lethiecq, “Characterisation of P(VDF-TrFE) material taking into account dielectric relaxation: application to modelling of high frequency transducers,” Ultrasonics, vol. 36, no. 1–5, pp. 41–45, Feb. 1998.

[113] S. Saitoh, T. Kobayashi, K. Harada, S. Shimanuki, and Y. Yamashita, “A 20 MHz single-element ultrasonic probe using 0.91Pb(Zn(1/3)Nb(2/3))O(3)-0.09PbTiO(3) single crystal.,” IEEE transactions on ultrasonics, ferroelectrics, and frequency control, vol. 45, no. 4, pp. 1071–6, Jan. 1998.

[114] J. B. Babu, G. Madeswaran, R. Dhanasekaran, K. Trinath, A. V. N. R. Rao, N. S. Prasad, and I. R. Abisekaraj, “Ferroelectric Properties and Transmission Response of PZN-PT Single Crystals for Underwater Communication,” vol. 57, no. 1, pp. 89–93, 2007.

[115] X. G. X. Geng and Q. M. Zhang, “Evaluation of piezocomposites for ultrasonic transducer applications influence of the unit cell dimensions and the properties of constituents on the performance of 2-2 piezocomposites,” IEEE Transactions on Ultrasonics Ferroelectrics and Frequency Control, vol. 44, no. 4, pp. 857–872, 1997.

[116] D. M. Mills and S. W. Smith, “Multi-layered PZT/polymer composites to increase signal-to-noise ratio and resolution for medical ultrasound transducers. II. Thick film technology,” IEEE Transactions on Ultrasonics, Ferroelectrics and Frequency Control, vol. 49, no. 7, pp. 1005–1014, Jul. 2002.

[117] M. A. B. Andrade, N. P. Alvarez, C. Negreira, and J. C. Adamowski, “Analysis of 1-3 Piezocomposite and Homogeneous Piezoelectric Rings for Power Ultrasonic Transducers,” vol. XXXI, no. 4, 2009.

2. Underwater Acoustic Channel

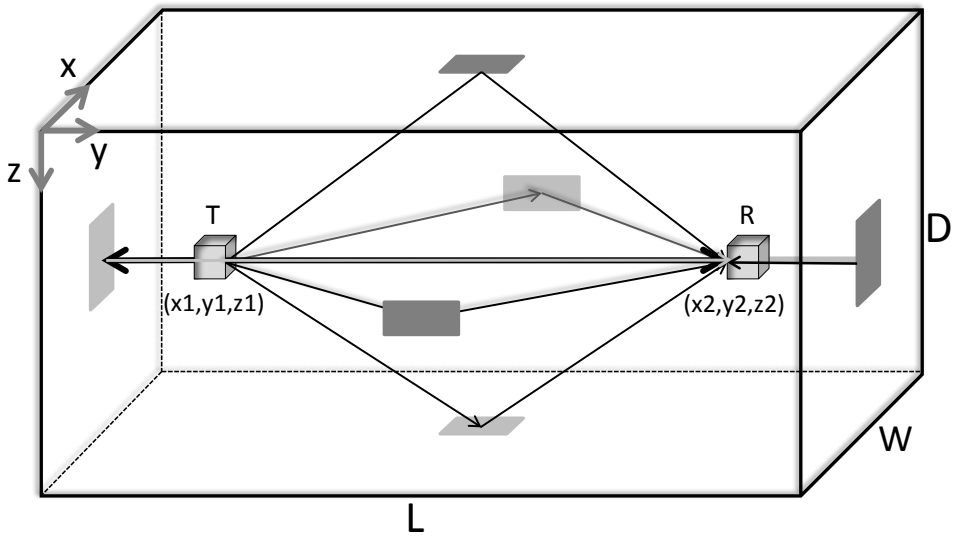

2.1. Introduction

Oceans cover over 70% of the Earth's surface and most of it remains unexplored. Due to the specificities of the underwater environment there are a wide variety of interesting aspects to be developed, including oceanographic monitoring, scientific exploration and disaster monitoring [1]. In order to make these developments/implementations possible, the underwater communication environment properties need to be understood. Since conventional wireless technology is difficult to implement in such an environment, alternative technologies must be developed.

Wireless underwater communication systems have been implemented using different technology types: acoustic and electromagnetic waves, in particular radio and optical frequencies [1]. Radio frequency is limited by the high level of absorption in water [2, 3]. Similarly, optical systems suffer from the same limitation and have further disadvantages, such as the high levels of ambient light close to the water surface, and scattering due to suspended particles [4, 5]. As a result, the implementation of these systems has also been limited. Thus, acoustic communication systems are the primary form of wireless underwater communications.

Since acoustic communication has low sound attenuation in water, this technique is considered as being preferable in this environment, especially in deep waters with stable thermal conditions [1]. Despite the advantages of acoustic communication in underwater environments, when compared to optical and radio, the propagation of sound also has significant challenges that influence the development of underwater acoustic communication systems. This is mainly due to the slow speed of acoustic propagation in water (about 1500 m/s). When studying sound propagation in the underwater acoustic channel, some relevant phenomena must be taken into account: attenuation [6 – 8], ambient noise, Doppler Effect, propagation delay and multipath [9, 10]. All these phenomena create difficulties for ultrasound communications which are aggravated with the use of digital modulations and high data-rates. With the increase of the carrier frequency, it is possible to increase the data-rate, but this also increases the attenuation, leading to a decrease in communication efficiency [11, 12].

The proposed system operates in a frequency range between 100 kHz and 1 MHz. The acoustic absorption for a 1 MHz signal achieves 280 dB/km and the spreading attenuation still has to be added, which depends on the transducer geometry. Therefore, the system was designed to communicate up to several hundred meters using a directional ultrasound emitter transducer in a point-to-point transmission. Instead of using higher frequency carriers to increase the data-rate,

it is possible to achieve the same goal by using digital modulations with higher symbol rates. But, the implementation of different types of modulations in order to evaluate their performance is an expensive and time consuming process.

Previous works have been devoted to characterizing the underwater channel [9] [13, 14], and others to comparing the results obtained via simulation, to those results obtained in real tests [15]. However, current channel models present a set of constraints [16, 17], such as: frequencies at the kHz range, multipath in a 2D model [18] propagation spreading type (cylindrical and spherical), distances at the km range, which do not normally accept modulated signals and do not simultaneously include, the most significant propagation phenomena, such as: attenuation, multipath with propagation delay and noise [19, 20]. It is therefore necessary to implement a complete system model that allows for a rapid prototyping of communication systems.

This chapter presents a MatLab/Simulink simulation model of an acoustic underwater communication system where the acoustic channel is emulated. This model will be integrated into a modulator/demodulator developed in a Xilinx FPGA with the aid of the System generator toolbox for MatLab/Simulink. With the validated model it is possible to simulate the full system. This avoids any hardware testing, and reduces the cost and time of the digital modulations' evaluation.

2.2. Acoustic propagation Background

In this section, the most relevant concepts of underwater acoustic propagation are introduced and analyzed. These concepts influence the communication system design, as they define the propagation conditions in the underwater acoustic channel.

2.2.1. Propagation Delay

Delays measured in underwater acoustic communications (approximately 0.67 s/km) are much higher than those observed in electromagnetic communication through air [13]. This is due to the fact that the nominal speed of sound in water is nearly 1500 m/s, and the velocity of electromagnetic waves in the air is 3×10^{8} m/s. This means that the propagation delay is very significant and as such affects the communication system's performance.

The speed of sound in water is influenced by properties such as temperature, salinity and depth and, therefore, the increase of any of these values leads to an increase in its speed.

There are some equations that calculate the speed of sound in water [9]. One of these is the *MacKenzie* equation:

$$c = 1448.96 + 4.591T - 5.304\times10^{-2}T^2 + 2.374\times10^{-4}T^3 + 1.340(S - 35) + 1.63\times10^{-2}D + 1.675\times10^{-7}D^2 - 1.02\times10^{-2}T(S - 35) - 7.139\times10^{-13}TD^3 \quad (2.1)$$

where c is the speed of sound, T is the water temperature, S symbolizes the salinity in parts per thousand and D is depth. This equation can display an error of approximately ±0.070 m/s [9]. In order to obtain a valid simulation, the water proprieties should be in the following ranges: the temperature assumes values from 2 C° to 30 C°, the salinity cannot be over 35 ppt, and the maximum acceptable depth is 8000 m.

2.2.2. Attenuation

During their path, between the transmitter (projector) and the receiver (hydrophone), the sound waves lose and disperse energy. This energy loss is largely due to a phenomenon called attenuation. Attenuation is one of the most important properties regarding underwater acoustic channels because it is presented in all types of underwater environments, and its value increases with an increase in distance and frequency. Attenuation is made up of three main components: spreading loss, absorption loss and scattering loss.

2.2.2.1. Spreading loss:

There are several kinds of spreading loss such as spherical, cylindrical and directional. In this work only directional spreading has been considered, since the type of projector used in the simulations and tests assumes a directional beam with lower spreading over long distances.

The energy dispersion emitted will suffer with the increasing surface area in which the signal propagates, causing spreading loss. Spreading loss (also called geometric spreading) is the term used to describe the apparent energy loss suffered by the signal. The loss is not lost, but rather spread out through a surface area that increases as the signal travels away from its source, as is shown in Figure 2.1, with an example of directional spreading loss [13].

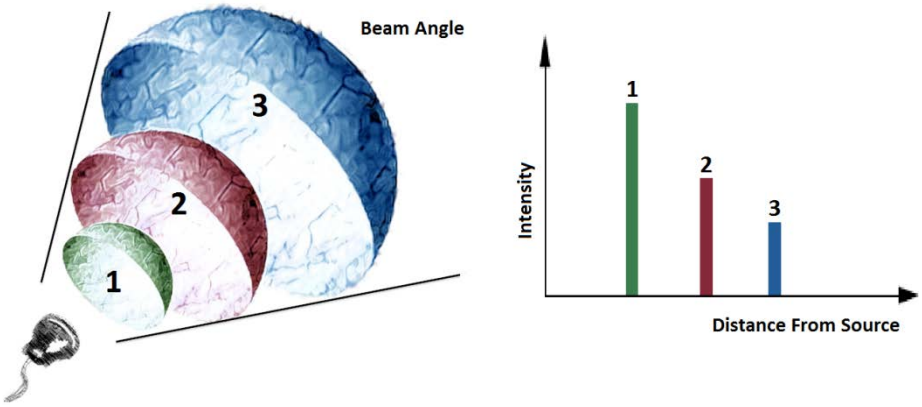

Figure 2.1: Directional spreading beam.

When directional spreading occurs in the presence of a homogenous and infinitely extended medium, the sound wave power is radiated in a sound beam with a directivity angle. The value of the beam divergence angle (δ) is given by [21]:

$$\delta = 2arcsin(\lambda/D) \tag{2.2}$$

where D is the transducer diameter and λ is the wavelength.

The directional spreading value is given by the following equation:

$$G_{directive}(r) = 10log[I_0/I] = 10log[\delta r^2/\pi r_0^2] \tag{2.3}$$

where $G_{directive}(r)$ is the directional spreading loss in dB, I_0 is the acoustic intensity at the reference distance r_0, and I is the acoustic intensity at distance r.

2.2.2.2. Absorption loss:

The partial transformation of acoustic energy into heat leads to signal energy loss. This is the definition of absorption loss. This phenomenon is strongly influenced by the signal frequency. Higher frequency signals lead to larger amounts of energy being absorbed by the water.

Absorption loss is one of the factors which contribute more to signal attenuation. Since the *Thorp* model [6], the models similar to those from *Fisher & Simmons* [8], up to the *Ainslie & McColm* model [7], have seen a constant improvement in the equations through the introduction of new parameters being taken into account. The present project takes advantage of the *Ainslie & McColm* model.

The *Ainslie & McColm* model takes into account the following factors: temperature, depth, effects caused by chemical compounds (boric acid and magnesium sulphate) and water acidity (pH). The absorption coefficient *a(f)* can be obtained from this model, in dB/km, by:

$$a(f) = \frac{0.106(f_1 f^2)e^{(pH-S/0.56)}}{f_1^2 + f^2} + \frac{0.52(1+T/43)(S/35)(f_2 f^2)e^{(-D/6)}}{f_2^2 + f^2} + 0.00049 f^2 e^{-(T/27+D/17)} \quad (2.4)$$

$$f_1 = 0.78\sqrt{(S/35)}e^{(T/26)} \text{ and } f_2 = 42e^{(T/17)}$$

where *T* represents the value of water temperature in Celsius degrees, *S* symbolizes the salinity in parts per thousand (ppt), *D* is the depth in meters, pH is the acidity of the water, *f1* and *f2* are the relaxation frequencies introduced for boric acid and magnesium sulphate, respectively.

The Ainslie & McColm model is considered the best one for calculating the absorption coefficient.

2.2.2.3. Scattering loss:

The inhomogeneity of the aquatic environment leads to the existence of anomalies in signal propagation.

Scattering loss is the loss of energy that a signal suffers when it is redirected onto a surface, or when it is due to the homogeneities of the medium. This work considers a homogeneous and infinitely extended medium and therefore, the scattering loss will not be implemented in the model.

Taking into account the above considerations, it can be concluded that the equation that allows for the attenuation calculation is the result of the sum of spreading and absorption factors. Since scattering is not considered, it is obtained as [9, 13]:

$$A(f,r) = S_L + A_L r \quad (2.5)$$

where *A(f,r)* is the attenuation suffered by a signal that is emitted with a frequency *f* at a distance *r*, S_L is the energy lost by spreading and A_L is the absorption loss.

2.2.3. Ambient Noise

Noise in an underwater acoustic channel can be classified into three types: man-made noise, site-specific noise and ambient noise [13]. Man-made noise is created by the machinery or by

shipping activity. On the other hand, site-specific noise only exists in certain places. It is compared with Gaussian noise with several non-Gaussians components [22]. Finally, ambient noise is always present, even when the sea is calm, due to turbulence, rain, breaking waves and maritime activity.

The noise in the ocean can be simulated using the four most important sources of noise: turbulence, shipping, waves and thermal noise. These noises can be described as Gaussian type and have continuous power spectral density (p.s.d.).

Turbulence Noise:

This noise is caused by the turbulence that exists in water (especially in sea water) and only influences frequencies below 10 Hz [14, 23].

$$10\log N_t(f) = 17 - 30\log(f) \tag{2.6}$$

where f is the signal frequency.

Shipping Noise:

Shipping noise is the term used to describe the noise caused by ships' hulls. This noise only affects the signals with frequencies between 10 Hz and 100 Hz [13].

$$10\log N_s(f) = 40 + 20(s - 0.5) + 26\log(f) - 60\log(f+0.03) \tag{2.7}$$

where s is the shipping factor, between 0 and 1.

Waves Noise:

In this case, the noise is caused by lapping waves. It affects the signals located at frequencies between 100 Hz and 100 kHz [12, 13].

$$10\log N_w(f) = 50 + 7.5w^{(1/2)} + 20\log(f) - 40\log(f + 0.4) \tag{2.8}$$

where w is the wind speed.

Thermal Noise:

Finally, thermal noise is caused by molecular agitation (Brownian motion) [16]. This noise affects the signals with frequencies above 100 kHz [23].

$$10\log N_{th}(f) = -15 + 20\log(f) \tag{2.9}$$

The total noise p.s.d. may be calculated by the sum of equations (2.6), (2.7), (2.8) and (2.9):

2.2.4. Doppler Effect

Despite being eventually fixed, both transmitter and receiver can be subjected to motions caused by currents, waves and other factors. This movement leads to the Doppler Effect which results in frequency shifting, and in frequency spreading. Consequently, it is important to take into account the Doppler Effect in the design of an underwater communication system [9]. The Doppler Effect is calculated by:

$$f_0 = \left(\frac{v + v_r \cos(\alpha_R)}{v + v_s \cos(\alpha_S)} \right) f_s \tag{2.10}$$

where f_0 is the frequency received by the observer, f_s is the wave frequency, v is the sound wave speed, v_r is the receiver velocity relative to the medium, v_s is the source velocity relative to the medium, α_r is the angle between the v_r and the line that connects the receiver and the transmitter and α_s is the angle between the v_s and the line that connects the receiver and the transmitter.

2.2.5. Multipath

Multipath is one of the most common problems in underwater acoustic communications [9]. This propagation phenomenon occurs when acoustic signals reach the receiving transducer from two or more paths, resulting in a collection of more than one signal being received at different times by the receiver. This phenomenon causes the *Inter Symbol Interference (ISI)* [23]. Multipath occurs most often in shallow waters, more specifically in rivers, dams, tanks and near of the shore, and the increase in the number of boundaries increases the possibility of echoes occurring.

Multiple paths can be the result of two effects: a reflection or a refraction of acoustic waves. The first case occurs when the acoustic signal collides with the surface, bottom of the sea or even with a simple object, and then arrives at the receiver. The second case usually occurs in acoustic communication systems that are present in deep waters where the sound speed varies with factors such as temperature, salinity and pressure which change according to depth and location.

The proposed model only allows for the simulation of reflected acoustic waves for scenarios containing homogenous and flat boundaries.

According to Snell's law [24] the reflected wave has a symmetric wave angle relative to the original point of collision. This wave suffers an amplitude loss, due to the fact that some of the acoustic energy is absorbed by the boundary medium, called the refracted wave. The reflected wave amplitude depends directly on the acoustic impedance mismatch between the boundary material and the medium (water).

The amplitude reflection coefficient r is the ratio between the incident and the reflected acoustic pressure amplitude, and it can be calculated by:

$$r = \left(\frac{Z_2 \sin(\alpha) - Z_1}{Z_2 \sin(\alpha) + Z_1} \right) \tag{2.11}$$

where Z_2 is the boundary material acoustic impedance and Z_1 is the medium acoustic impedance [21].

In shallow waters there are several possible scenarios for underwater communication and the most common are the tank, dam, river and the ocean. The tank is the one most affected by multipath since it has six boundaries close to each other, as shown in Figure 2.2. Dams can have four or five boundaries close to each other. The river has only four boundaries close to each other and the ocean may be considered as having three, two, or only one boundary depending on the location: near the coast, near the bottom and/or near the surface.

Since the tank scenario disables unnecessary boundaries in river and ocean scenarios, it was selected as the best medium to study the multipath effect (Figure 2.2).

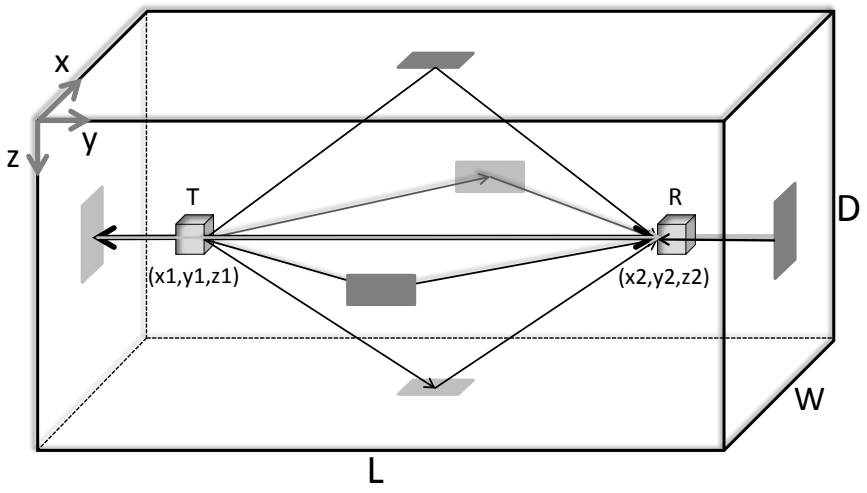

Figure 2.2: 3D tank model showing echo main paths.

Figure 2.2 illustrates the tank model, showing an ultrasound transmitter and receiver, where *L* is the length, *W* is the width and *D* is the tank depth. The transmitter assumes the position with coordinates (*x1*, *y1*, *z1*) and the receiver *(x2*, *y2*, *z2*) coordinates. Besides the direct path, the receiver will possibly obtain other signals from echoes reflected at the top, bottom and both sides. Echoes may still exist at the front and rear boundaries, and there are paths with only one echo or a combination of several echoes at different boundaries.

Equations (2.12) give the path distance for each boundary, where *n* is the number of echoes that occur along the path. The front and back echoes only occur if the path angle is perpendicular to the front and back boundaries with the following conditions: *x1=x2* and *z1=z2.*

$$
\begin{aligned}
Direct\_Echo &= \sqrt{(x_2 - x_1)^2 + (y_2 - y_1)^2 + (z_2 - z_1)^2} \\
Side_1\_Echo_n &= \sqrt{([(n+1)W - x_2] - x_1)^2 + (y_2 - y_1)^2 + (z_2 - z_1)^2} \\
Side_2\_Echo_n &= \sqrt{([(n-1)W + x_2] + x_1)^2 + (y_2 - y_1)^2 + (z_2 - z_1)^2} \\
Up\_Echo_n &= \sqrt{(x_2 - x_1)^2 + (y_2 - y_1)^2 + ([(n+1)D - z_2] - z_1)^2} \\
Down\_Echo_n &= \sqrt{(x_2 - x_1)^2 + (y_2 - y_1)^2 + ([(n-1)D + z_2] + z_1)^2}
\end{aligned}
\tag{2.12}
$$

Equations (2.13) give the distance for path with *n* number of echoes to front and back reflections.

$$
\begin{aligned}
Front\_echo_1 &= 2L - y_2 - y_1 \\
Front\_echo_{n\_odd} &= Front\_echo_{(n-1)} + 2y_2 \\
Front\_echo_{n\_even} &= Front\_echo_{(n-1)} + 2(L - y_2) \\
Back\_echo_1 &= y_2 + y_1 \\
Back\_echo_{n\_odd} &= Front\_echo_{(n-1)} + 2(L - y_2) \\
Back\_echo_{n\_even} &= Front\_echo_{(n-1)} + 2y_2
\end{aligned}
\tag{2.13}
$$

The number of echoes is limited by the transducer divergence angle. Since a directional transducer was used, there are only echoes with angles originating from the area covered by the transducer. Thus it is necessary to check whether the echoes calculated using equations (2.12)

and (2.13) show angles below the beam transducer opening angle. All the angles used to calculate the echoes are relative to the imaginary line connecting the receiver and the transmitter.

2.3. System Design

The system model was designed according to the experimental setup to perform the validation tests. Therefore, each experimental setup part has a corresponding simulation block.

2.3.1. System Setup

Figure 2.3 shows the block diagram of the communication system for the simulation and the real tests. The system can be divided in three parts. The first part is the Xilinx, which is made up of a modulator and a demodulator. The second is the electrical part and is made up of an amplifier block (emitter) and a filter (reception). The first and second part will not be addressed in this chapter. The last part is the acoustic which is made up of the transducers and the subaquatic channel.

One way to develop such systems is to build all the parts and try various settings. However, the present solution uses the second and third parts emulated on a computer, which allows for results to be obtained quicker. This method allows for rapid prototyping with the simulation of any digital modulation type by using a Xilinx FPGA platform. Then the modulator/demodulator is programed directly to a Xilinx FPGA prepared to operate in the final application.

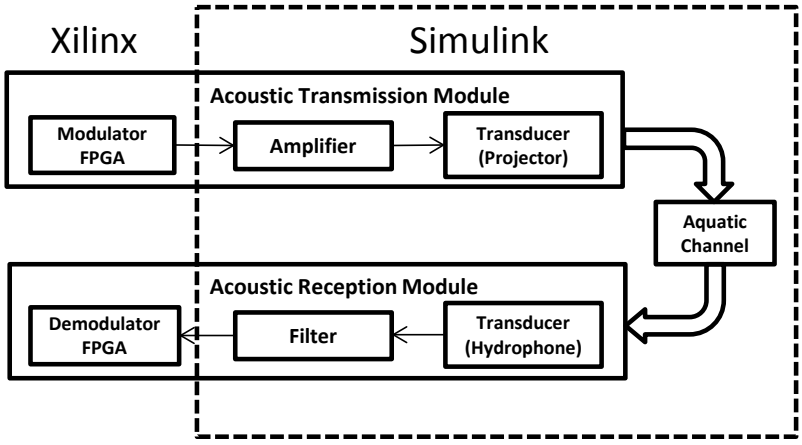

Figure 2.3: Block diagram of the complete system, including the modulator/demodulator, ultrasound projector, hydrophone and aquatic channel.

The modulator/demodulator was implemented in a Xillinx Spartan3A FPGA platform. These two blocks can be edited to test the different types of modulations being tested at the moment: Binary Phase-Shift Keying (BPSK), Binary Frequency Shift keying (BFSK) and Binary Amplitude Shift Keying (BASK) [25].

The transmitter amplifier consists of a Push-Pull symmetric voltage amplifier with 12 dB gain, implemented in the simulation by a gain block. The filter was an active band-pass between 1 and 2000 kHz, applied in Simulink with a Butterworth FIR filter with the same band-pass.

The ultrasonic projector was a PZT-5H 2 mm piston type transducer with 2 cm diameter [26]. This transducer shows a directional pattern with a divergence angle according to equation (2.2). Despite the transducer's directionality, a residual pressure wave projected in the transducer rear can achieve 15% of the main front pressure wave amplitude. The subsection 2.3.2 provides detailed information about the underwater acoustic channel.

The ultrasonic receptor used to register the pressure waves was a Cetacean Research™ C304XR hydrophone, with an effective sensibility of -181 dB, 1 V/μPa and a linear frequency range (±3dB) between 0.012 and 1000 kHz. Since the hydrophone shows a linear response, a direct conversion block using the data given by the manufacturer datasheet was implemented. A digital oscilloscope PicoScope 4227 100 MHz was used to record the results.

2.3.2. Underwater Channel Simulation

The underwater acoustic channel model was implemented in a subsystem block where 4 types of inputs and 2 types of outputs were defined. The input types are the transmitted acoustic signal, transducer characteristics (transducer diameter), medium characteristics (temperature, salinity, acidity, shipping factor and wind speed) and the scenario setup (dimensions, receiver position, transmitter position, reference distance, receiver and transmitter velocity relative to the medium). The output types are the acoustic signals (received pressure wave with and without noise) and the received signal characteristics (frequency Doppler shift, received signal propagation delay, noise factor).

The simulation core was divided into 4 main blocks: multipath, attenuation, noise and Doppler Effect. The block diagram presented in Figure 2.4 helps to better understand the relationships between the different blocks.

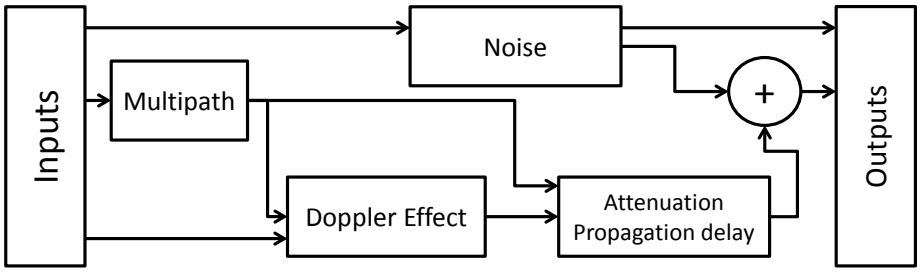

Figure 2.4: Block diagram of the aquatic channel model, including the multipath, noise, Doppler Effect, attenuation and propagation delay.

The simulation starts in the multipath block where the distances and angles for the direct path and the echo paths are calculated. The input values are the scenario dimensions (e.g. tank dimensions, length, width and depth), the maximum number of echoes that occur along a single path, and the receiver and transmitter's geographic positions. As a result, the output of this block calculates the distances and angles of each propagation path using equations (2.12) and (2.13).

The attenuation and noise blocks run in a parallel simulation, and their inputs do not depend on each other.

The noise block is responsible for generating several white noises to each ambient noise type, respecting the frequency ranges, as was presented in section 2.2.3. They are then all added together. Wind speed, shipping factor and an on/off button for each noise type are the inputs for this block. The output is a noise signal to be added to the transmitting signal.

The multipath block calculates the main signal and echo's path, distances and angles. The Doppler Effect block calculates the Doppler shift using the data from the Multipath block, and the transmitter and receiver's relative speed inputs. The attenuation block uses data from the Doppler Effect (main signal and echoes) and multipath (echoes patterns) blocks, the medium parameters and transducer characteristics, in order to calculate the attenuation and propagation delay for each propagation path. Before adding all the echo signals together, the echo path angle is verified as being inside the acoustic beam area. All the echoes outside this area are discarded.

2.4. Test conditions, Results And Discussion

This section shows the results obtained in the experimental tests in order to compare them with those obtained by simulation using the model developed in *Matla /Simulink*.

In the experimental results analysis, the Doppler Effect was discarded. This decision was justified by the great difficulty in assembling an experimental setup with moving parts in the medium.

2.4.1. Attenuation

The swimming pool is 12 m long, 4 m wide and 3m deep. Four test distances were defined: 1, 4, 8 and 12 m, where measurements were performed at 50 cm deep and in the middle of the pool (2 m either side). At each distance, several frequencies were tested: 100 kHz, 200 kHz, 300 kHz, 400 kHz, 500 kHz, 600 kHz, 700 kHz, 800 kHz, 900 kHz, 1 MHz, 1.2 MHz and 1.4 MHz.

The simulation was configured with the conditions observed in the experimental test. Fresh water at a temperature of 13 °C and 7.2 pH was used.

The projector and the hydrophone sound wave level responses are irrelevant since the considered results are relative. A reference measurement was taken at 10 cm intervals over several distances for all tested frequencies and attenuation, and calculated according to equation (2.14):

$$20\log_{10}\left(\frac{p}{p_{ref}}\right) \tag{2.14}$$

where p is the pressure wave at the receiver and the p_{ref} is the pressure wave at the reference distance. The experimental values are presented as an average of the 10 measurements, with a maximum error of 3.5%.

Figure 2.5 shows the results obtained in each experimental test and the results obtained in the corresponding simulated test.

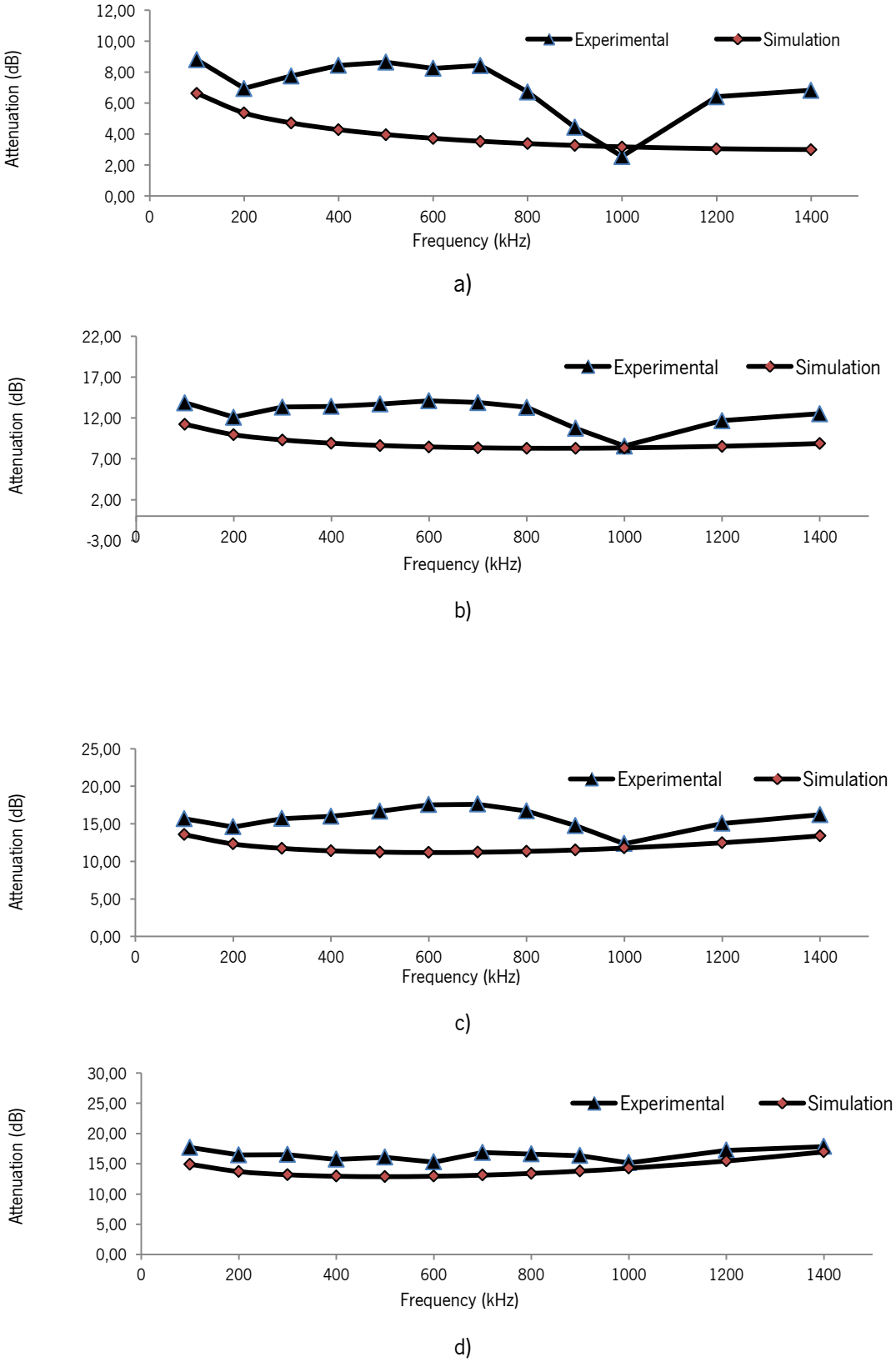

Figure 2.5: Experimental and simulated attenuation results as a function of frequency, measured at a) 1 m, b) 4 m, c) 8 m and d) 12 m.

In Figure 2.5, it is possible to observe that when the distance increases, there is an increase in the attenuation suffered by the acoustic signal. The simulation results show lower attenuations, but also a trend similar to that of the experimental results, and the resemblance between the two curves increases with distance. The difference between the experimental and the simulated results assumes an average of 3.2 dB reaching a 6 dB peak. The 1 MHz point shows a low attenuation peak in all the graphics and slowly disappears with distance. This phenomenon occurred because the emitter is operating at the optimal resonance frequency.

2.4.2. Noise

To analyze the ambient noise the FFT was calculated with a digital oscilloscope with a sampling rate of 60 MHz. The noise in the three scenarios was measured: sea, river and the pool. The sea measurements were performed in the Atlantic Ocean at 2 km away from the coast (N 41°32.075'; W 08°48.892') at 2 meters deep. The river measurements were performed in the Cávado River at approximately half the distance between the two river shores with 200 meters width at 2 meters deep (N 41°30.720'; W 08°45.550'). Finally, the pool measurements were obtained according to the conditions describe above.

Figure 2.6 shows the sound wave signal registered by the hydrophone in a spectrum window of 4.883MHz. The signals were Hamming window before FFT calculation. The values of the amplitude axis were calculated according to equation (2.14) and a p_{ref} of 1122 Pa was used because the response of 1 V in the hydrophone output requires a pressure wave of 1122 Pa.

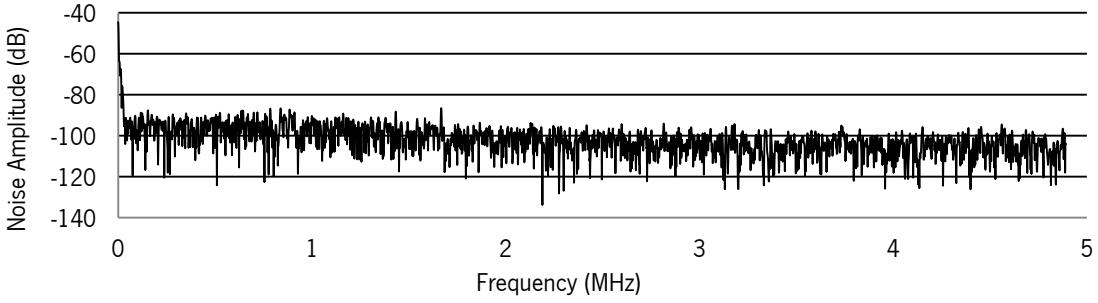

a)

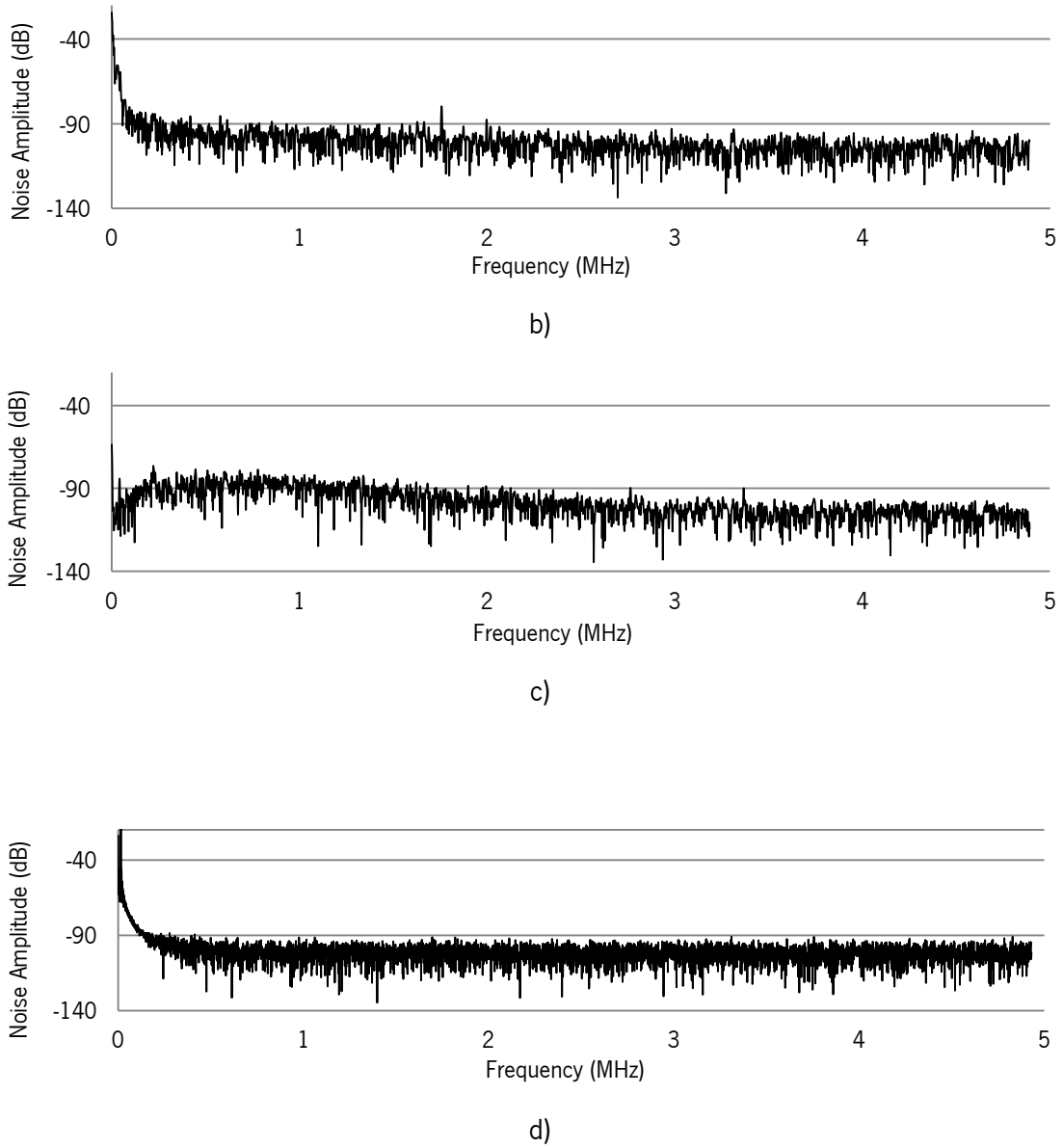

Figure 2.6: Noise signal spectrum, experimental measurements at a) Sea, b) River, c) Pool and d) Pool simulation.

Figure 2.6 shows that the underwater environment is very silent in terms of ultrasounds. This statement is no longer true for frequencies below 100 kHz, as can be seen in the three scenarios.

The measurements' results presented in Figure 2.6.a, b, c, are very similar to those presented in Figure 2.6.d. Simulation results show higher amplitudes to frequencies below 250 kHz but, for higher frequencies, the amplitudes are equivalent in both graphics (simulations and real tests). These facts allow us to conclude that the simulation model also reflects an approximation of real channel behavior in terms of noise.

2.4.3. Multipath

The scenario used to evaluate the multipath simulation performance was the pool used in the attenuation tests. Two different tests were carried out with different frequencies and distances.

In the first test a burst signal of 20 cycles at 100 kHz over a distance of 8 m was transmitted. The ultrasonic transmitter and receptor positions according to Figure 2.2 were (0.85; 1.95; 0.5) and (9.07; 1.95; 0.5) meters. With this configuration, both the transmitter and receptor operated in an omnidirectional pattern.

In the second test a burst signal of 20 cycles at 1 MHz over a distance of 12 m was transmitted. The ultrasonic transmitter and receptor positions according to Figure 2.2 were (0.03; 1.95; 0.5) and (11.61; 1.95; 0.5) meters and with this configuration both the transmitter and the receptor operated in a directional pattern.

Figure 2.7 shows the simulation and real test results for the first configuration. The direct path signal took 5.44 milliseconds from the projector to the receiver in the simulation and 5.478 milliseconds in the real test. In this results the speed of sound propagation of 1511 m/s for the simulation and 1500.5 m/s for the real test.

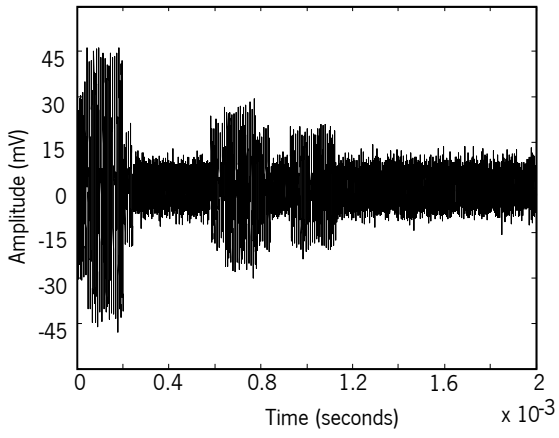

a)

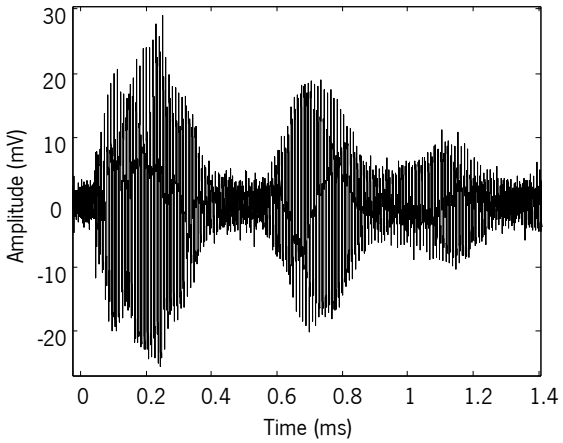

Figure 2.7: Multipath signal received from a burst signal of 20 cycles at 100 kHz over 8 meters, a) simulation and b) real test.

Both graphics present three signal sets. The first set is the result of the overlapping of the direct path signal with the surface echo, the second set is a result of the echoes from either sides, and the last set from the back and ground echoes. The front eco does not appear in the results because the propagation delay was very high: 3.87 milliseconds more than the direct path, resulting in a higher attenuation.

Figure 2.8 shows the simulation and real test results for the second configuration. The direct path signal took 7.663 milliseconds from the projector to the receiver in the simulation and 7.62 milliseconds in the real trial. This results in a speed of sound propagation of 1511 m/s to the simulation and 1519.6 m/s to the real test.

The values of the speed of sound propagation obtained in both real tests show a small difference from those obtained by simulation. The main reason for this difference is that it is very difficult to accurately place the experimental set-up in the middle of the pool. Therefore, precision in centimeters was impossible to achieve.

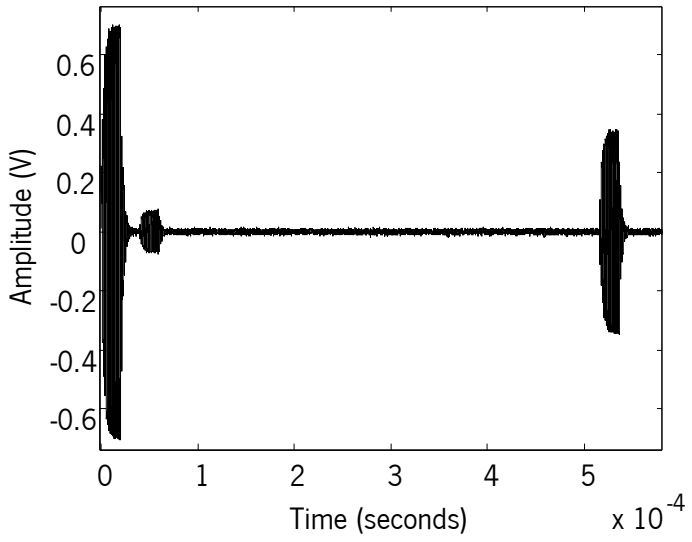

a)

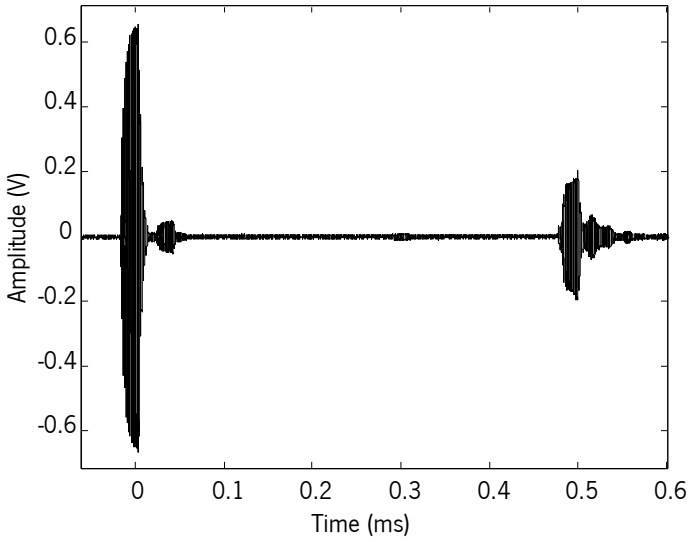

b)

Figure 2.8: Multipath signal received from a burst signal of 20 cycles at 1MHz over 12 meters, a) simulation and b) real test.

Figure 2.8 also shows three set signals, but at 1 MHz frequency the transducer was operating in a directional pattern with a divergence angle of 4.3° and therefore, only the back and front echoes appear in the results.

The first set is from the direct path, the second is from the back echo and the third is from the front echo. The back eco shows lower amplitude than the front echo, despite it travelling a shorter distance and assuming lower attenuation. This occurs because the back echo results from a residual energy loss in the transducer's back as explained in 2.3.1.

The simulation results were shown to be a good model approximation with similar timings and amplitudes, despite the simulation only including the 1st order echoes, and yielding a clear signal as shown in Figure 2.7 and Figure 2.8.

2.5. Conclusions

An acoustic communication system model for underwater applications was developed. The simulation model was designed specifically to emulate the acoustic channel and ultrasonic transducers, allowing for the communications' performance to be evaluated using digital modulations. The Xilinx System Generator toolbox allows the modulator/demodulator model to be uploaded directly into an FPGA platform for the final application.

The acoustic underwater communication channel was simulated with a Matlab/Simulink model taking into account attenuation, environment noise, Doppler Effect and propagation delay of the acoustic signal. Real tests were also implemented to validate the attenuation, noise, multipath and propagation delay.

The ambient noise simulation was compared to noise measurements obtained in sea, river and pool environments. The attenuation, multipath and propagation delay simulation models were compared to the results obtained in the pool at 8 meters distance with a 100 kHz signal, and at 12 meters distance with 1 MHz signal.

Overall, the results show that the model represents a useful approximation to the real subaquatic communication channel, being therefore an important tool to simulate the propagation of acoustic signals.

References

[1] I. F. Akyildiz, D. Pompili, and T. Melodia, "Underwater acoustic sensor networks: research challenges," Ad Hoc Networks, vol. 3, no. 3, pp. 257–279, May 2005.

[2] X. Che, I. Wells, G. Dickers, and P. Kear, "TDMA frame design for a prototype underwater RF communication network," Ad Hoc Networks, vol. 10, no. 3, pp. 317–327, May 2012.

[3] P. Mandal, S. De, and S. S. Chakraborty, “A receiver synchronized slotted Aloha for underwater wireless networks with imprecise propagation delay information,” Ad Hoc Networks, vol. 11, no. 4, pp. 1443–1455, Jun. 2013.

[4] G. Baiden, Y. Bissiri, and A. Masoti, “Paving the way for a future underwater omni-directional wireless optical communication systems,” Ocean Engineering, vol. 36, no. 9–10, pp. 633–640, Jul. 2009.

[5] Y. Liu and X. Ge, “Underwater Laser sensor network : A New Approach for Broadband Communication in the Underwater,” vol. 2006, pp. 421–425, 2006.

[6] W. H. Thorp, “Analytic Description of the Low-Frequency Attenuation Coefficient,” The Journal of the Acoustical Society of America, vol. 42, no. 1, p. 270, 1967.

[7] M. A. Ainslie and J. G. McColm, “A simplified formula for viscous and chemical absorption in sea water,” The Journal of the Acoustical Society of America, vol. 103, no. 3, p. 1671, Mar. 1998.

[8] F. H. Fisher, “Sound absorption in sea water,” The Journal of the Acoustical Society of America, vol. 62, no. 3, p. 558, 1977.

[9] M. Stojanovic and J. Preisig, “Underwater acoustic communication channels: Propagation models and statistical characterization,” IEEE Communications Magazine, vol. 47, no. 1, pp. 84–89, Jan. 2009.

[10] P. Qarabaqi and M. Stojanovic, “Small scale characterization of underwater acoustic channels,” Proceedings of the Seventh ACM International Conference on Underwater Networks and Systems - WUWNet ’12, no. 1, p. 1, 2012.

[11] T. Ebihara, K. Nishimiya, K. Mizutani, N. Wakatsuki, and K. Mizutani, “Underwater ultrasonic ranging by digital signal multiplexing with hadamard matrix,” 2009 IEEE International Ultrasonics Symposium, pp. 706–709, Sep. 2009.

[12] A. Zielinski, S. Member, Y. Yoon, and L. Wu, “Performance Analysis of Digital Acoustic Communication in a Shallow Water Channel,” vol. 20, no. 4, 1995.

[13] M. Stojanovic, “On the relationship between capacity and distance in an underwater acoustic communication channel,” in Proceedings of the 1st ACM international workshop on Underwater networks - WUWNet ’06, 2006, p. 41.

[14] S. Joshy and A. V Babu, “Capacity Of Underwater Wireless Communication Channel With Different Acoustic Propagation,” International Journal of Computer Networks & Communications, vol. 2, no. 5, pp. 192–204, 2010.

[15] A. Sehgal, I. Tumar, and J. Schönwälder, “AquaTools : An Underwater Acoustic Networking Simulation Toolkit.”

[16] D. Kraus and P. P. Kalangi, “Modelling and Simulation of an Underwater Acoustic Communication Channel,” pp. 1–3.

[17] H. Dol, M. A. Ainslie, M. Colin, and J. Janmaat, “Simulation of an underwater acoustic communication channel characterized by wind-generated surface waves and bubbles,” 2013, pp. 070054–070054.

[18] J. Wang, P. Cai, and D. Yuan, “An underwater acoustic channel simulator for UUV communication performance testing,” in The 2010 IEEE International Conference on Information and Automation, 2010, pp. 2286–2290.

[19] N. Josso, C. Ioana, C. Gervaise, and J. I. Mars, “On the consideration of motion effects in underwater geoacoustic inversion,” The Journal of the Acoustical Society of America, vol. 123, no. 5, p. 3625, 2008.

[20] A. Bouzoualegh and T. Val, “Modelling and Simulation of Underwater Acoustics Communication based on State flow and Simulink Models,” 3 rd International Conference: Science of Electronic, Techonologies of Information and Telecommunications March, 2005.

[21] C. H. Sherman and J. L. Butler, Transducers and Arrays for Underwater Sound. Springer Science+Business Media, LLC, 2007, p. 610.

[22] A. Sehgal, D. Cernea, and A. Birk, “Modeling underwater acoustic communications for multi-robot missions in a robotics simulator,” in OCEANS’10 IEEE SYDNEY, 2010, pp. 1–6.

[23] M. Stojanovic, “Underwater Acoustic Communication,” Wiley Encyclop dia of Ele e ctric al and Ele ctr onics Engine ering, vol. 22, pp. 688–698, 1999.

[24] K. B. Wolf and G. Krotzsch, “Geometry and dynamics in refracting systems,” European Journal of Physics, vol. 16, no. 1, pp. 14–20, Jan. 1995.

[25] C. Erdogan, I. Myderrizi, and S. Minaei, “FPGA Implementation of BASK-BFSK-BPSK Digital Modulators [Testing Ourselves],” IEEE Antennas and Propagation Magazine, vol. 54, no. 2, pp. 262–269, Apr. 2012.

[26] M. Martins, V. Correia, J. M. Cabral, S. Lanceros-Mendez, and J. G. Rocha, “Optimization of piezoelectric ultrasound emitter transducers for underwater communications,” Sensors and Actuators A: Physical, vol. 184, pp. 141–148, Sep. 2012.

3. Piezoelectric Ultrasound Emitters

3.1. Introduction

The piezoelectric properties of some materials are one of the key issues for underwater sound communication developments, being most of the ultrasound transducers based on piezoelectric materials. Piezoelectric properties can be found in certain types of ceramics, polymers and composites, each one of them showing different characteristics in terms of acoustic impedance, stiffness, coupling coefficient, piezoelectric and dielectric response. There are two types of ultrasound transducers: projectors, witch convert electrical energy into mechanical energy and hydrophones, which perform the opposite conversion [1, 2].

Applications of ultrasound transducers range from underwater sonars [3 – 5] to medical imaging and biomedical applications [6]. In the case of sonars, the acoustic signal has low frequency and can reach several tens of kilometers. On the other hand, medical imaging works with higher frequencies, reaching hundreds of MHz, with signals reaching just few centimeters. This technology shows an interesting and useful gap concerning underwater applications, as there are no specific transducers for wireless broadband communications [3 – 14].

This chapter is focused in projector type ultrasound transducers with piston architecture. The piston-type transducer generally projects the sound into a directional beam, whose directionality depends on the relationship between its size and the wavelength of the ultrasound signal. In this study the piston is a piezoelectric plate, which operates in the thickness mode [2].

The main goal is to develop a transducer that works at frequencies up to 1MHz, able to communicate at distances up to one hundred meters. These values were chosen considering underwater channel characteristics such as sound attenuation and propagation speed [15, 16].

3.2. Piezoelectric Transducer Considerations

Piezoelectric materials are commonly used in the fabrication of ultrasound transducers, once they show very good response at high frequencies, which can reach up to 160 MHz in the case of polymer materials [17].

Piezoelectric ultrasound transducers at high frequencies usually operate in the 33 mode, that is, the deformation along the polarization axis and the excitation electric field point into the same

direction. The free displacement of the material in direction 3, without restraining force and assuming uniform strain over the surface, is given by:

$$\xi = d_{33} v \tag{3.1}$$

where ξ is the free displacement, V is the applied voltage and d_{33} is the coupling coefficient in the thickness direction. In most of the cases, the piezoelectric deformation is not homogenous and linear as it is typically assumed [1]. In the case of a piston transducer, the largest deformation occurs at the center of the plate and smoothes away from the center in an oscillation curve as shown in Figure 3.1.

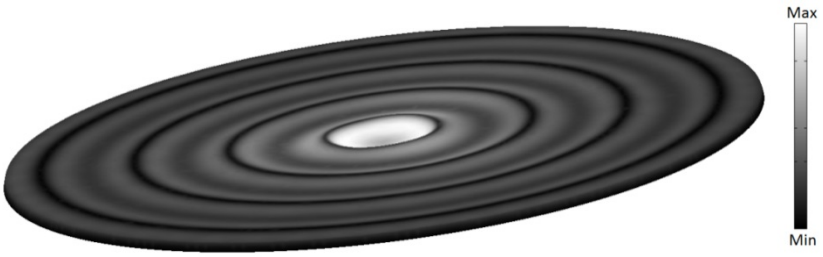

Figure 3.1: 3D representation of the active element plate deformation when excited with a sine wave signal.

Figure 3.1 is the finite element simulation result of a PZT-5H plate with 4 mm of diameter and 55 µm of thickness, excited with a 10V sine wave signal amplitude and a frequency of 10MHz. The deformation amplitude is not relevant in this case. The important information from this simulation is how the active element deforms when excited with a sine wave signal. This wavy surface do not generate a homogeneous sound wave, therefore it is essential to consider this effect to simulate the transducer behavior.

The maximum force the piezoelectric element can apply to a medium is obtained by [1]:

$$F = d_{33} \frac{A_p}{S_{33}^E t_p} v \tag{3.2}$$

where s_{33}^E is the elastic compliance coefficient, A_p is the area of the piezoelectric element and the t_p is the thickness. The deformation creates a pressure wave in the medium, whose amplitude can be obtained by [2]:

$$F = pA_p,\ p = 2\pi c \rho f \xi \tag{3.3}$$

where c is sound speed, ρ is the material density, f is the signal wave frequency and ξ is the piezoelectric material displacement. In order to increase pressure wave amplitude, several piezoelectric disks in a stack configuration can be used. This configuration allows multiplying the free displacement by the number of layers, n. In this case, the strain is given by [18]:

$$\xi = d_{33} v n \tag{3.4}$$

Despite this increase in strain, the intensity of the produced force does not change [1] [18][19]. Nevertheless, this approach reveals a problem: by increasing the number of layers, the electrical capacitance of the transducer also increases, which in turn represents a decrease of the imaginary part of the impedance and therefore an increase of the absolute value of the reactive electrical power. To ensure good acoustic signal quality, the force that the transducer can apply to the medium must be greater than the generated acoustic wave force, otherwise, the piezoelectric material displacement will be deformed, generating acoustic waves with low amplitude and noise. This condition allows for the calculation of the layer thickness and the number of layers for a specific frequency and material. Through equations (3.2) and (3.3) it is possible to obtain:

$$n t_p \leq \frac{1}{2\pi c \rho S_{33}^E f} \tag{3.5}$$

To properly design ultrasound transducers it is important to consider the acoustic impedance of materials, in order to minimize energy losses due to acoustic impedance mismatches [2].

If the acoustic impedance mismatch is very high, the wave is highly reflected. Therefore, the transducer output must have a thickness equal to half wave, as it is shown in Figure 3.2 [2]. In this way, the reflected wave will be synchronized with the next pressure wave cycle. The fundamental resonance frequency can be calculated from [2]:

$$f_r = \frac{c}{2t} \tag{3.6}$$

where t is the piezoelectric thickness and c is the sound speed. The harmonics are constituted by odd and even resonance frequencies, given by:

$$f_{odd} = (2n+1) f_r, \ n = 0, \ 1, \ 2, \ 3..... \tag{3.7}$$

$$f_{even} = (2n) f_r, \ n = 0, \ 1, \ 2, \ 3..... \tag{3.8}$$

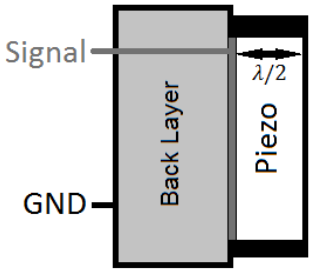

Figure 3.2: 2D representation of a piston transducer

The back layer creates a boundary to reflect most of the pressure wave and to not allow the active element layer to deform in that direction. The signal electrode is placed in the interface between layers in order to reduce electromagnetic interferences by using a shield connected to the electrical ground [2].

3.3. Selection of materials

There are several piezoelectric materials available for ultrasound transducers. The most common are the Lead Zirconate Titanate (PZT), Lead Titanate (PT), Lead Magnesium Niobate (PMN) and Lead Zinc Niobate (PZN) ceramics and Polyviylidenefluoride (PVDF) and P(VDF-TrFE) polymers. Single crystals of PZT, PMN and PZN can also be used [17] – [30].

This study will focus on PZT-5H ceramic and PVDF polymer, since these are the most interesting materials for large scale applications due to their availability and price. The results will be nevertheless representative for their respective family of materials (ceramic and polymer piezoelectrics, respectively). Table 3.1 shows the main physical properties of these materials for the proposed application:

Table 3.1: Comparison of some characteristics of PZT and PVDF

Physical Property	PZT-5H	PVDF
Acoustic Impedance Z [10^6kg/m^{2}s]	33.15	2.7
Resonance Frequency f [MHz]	<25	<160
Piezoelectric Coefficient d_{33} [10^{-12}m/V]	512	-34
Relative Dielectricic constant Ɛr	3100	12
Maximum operating temperature [°C]	365	80

The resonance frequencies and the acoustic impedance are related one another. The sound pressure variation level with frequency depends directly on the acoustic impedance mismatch between the active element and the medium (water). Over signal cycles, the reflected sound wave may be added or not to the next cycle, thus increasing the output level. Equation (3.9) gives the transmitted sound wave percentage over time.

$$S_{out}(t) = T_w\left(S_{in}(t) + LR_wS_{in}(t + D_p)\right) \tag{3.10}$$

Here, S_{out} is the sound wave output, S_{in} is the sound wave created inside the active element, T_w is the transmitted sound wave intensity percentage, R_w is the reflected sound wave intensity percentage, L is the internal energy loss and D_p is the delay of the reflected sound wave, introduced by the active element thickness.

Table 3.2 shows the reflected and transmitted sound wave percentages in water (with a water acoustic impedance of approximated $1.5 \times 10^6 kg/m^2s$), for PZT and PVDF.

Table 3.2: Reflected and transmitted sound wave percentages in water, produced by PZT and PVDF.

Material	Reflected	Transmitted
PZT-5H	91.3%	8.7%
PVDF	28.7%	71.3%

Figure 3.3 is obtained by the incorporation of Table 3.2 values in to Equation (3.9), which results in percentage level of the transmitted sound wave intensity to the medium over 7 cycles of a sine wave signal, as shown in Figure 3.4, since after these 7 cycles the sound wave output intensity begins to stabilize. It is possible to observe the resonance, resonance harmonics and anti-resonance frequencies points from 0 Hz to 6 times the resonance frequency to a certain transducer thickness and material [2].

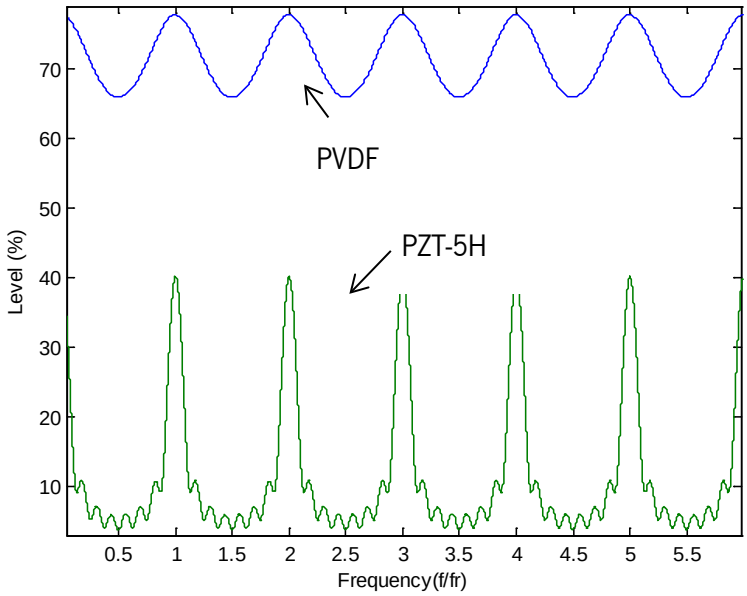

Figure 3.3: PZT-5H and PVDF responses over 7 cycles, for a frequency (f) range from 0 to 6 times the resonance frequency (fr).

As it can be seen in Figure 3.3, the percentage level of the sound power output over the frequencies shows a very low flotation to the PVDF, when compared with PZT-5H.

With the increasing of the reflected sound wave inside the transducer, increases the time necessary to reach the maximum output power at the resonance frequency and it is created a sound wave where the amplitude shows growth, therefore deforming the signal. The opposite effect happens when it is shut down the excitation signal to the transducer where the sound wave amplitude shows a decreasing; this oscillation is caused by the remaining sound wave power inside the transducer. Figure 3.4 shows the sound wave created by a sine wave signal over 20 cycles of 1MHz signal using transducers of PVDF and PZT-5H with the same dimensions and in a resonance thickness.

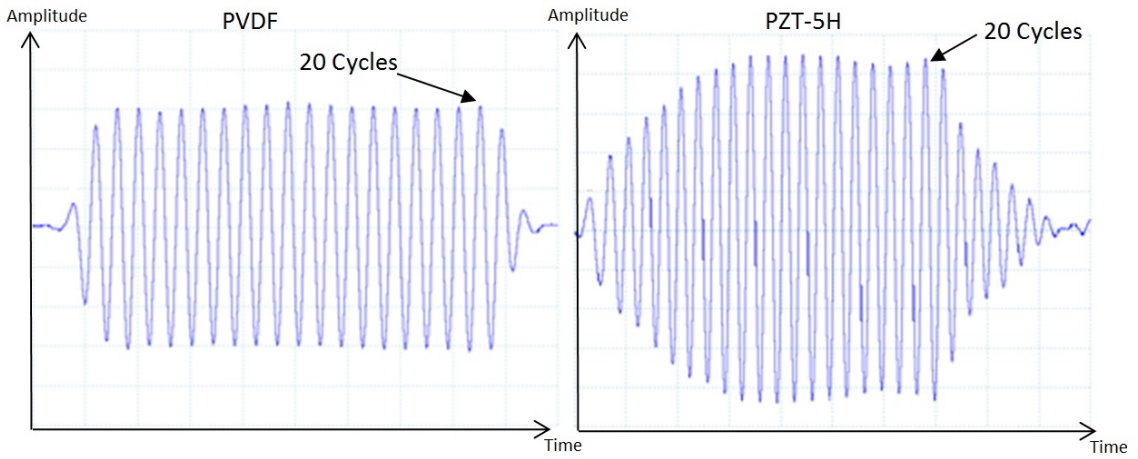

Figure 3.4: Sound wave created by PVDF and PZT-5H transducer with 1MHz sine wave signal over 20 cycles.

As it is possible to observe in Figure 3.4, the sound wave generated by the PVDF transducer has a more uniform signal than the sound wave generated by transducer PZT-5H. If we consider the results shown in Figure 3.3 and Figure 3.4, it can be conclude that, for a transducer operating in broad band of frequencies, PVDF shows more promising results. But in order to optimize other types of materials and reduce the output flotation, two solutions can be implemented. In the first solution the operating frequencies are restricted to integer multiples of the resonance frequency. The second solution it is basically a transducer designed for very high f_r, which operates with frequencies much lower than f_r. The second solution will be used to compare PVDF and PZT-5H performances. Figure 3.5 shows the transmitted coefficient percentage level of the sound power for frequencies up to $0.1fr$ in PVDF and $0.05fr$ in PZT-5H. Therefore, the sound level attenuation is below 3dB.

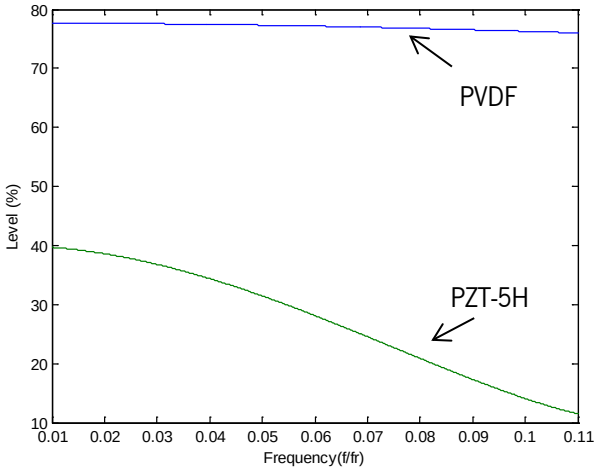

Figure 3.5: PVDF and PZT-5H sound level response over 7 cycles below $0.11fr$.

Despite the better performance of PVDF in a wider band of frequencies, its d_{33} coupling is 15 times lower than PZT-5H. This drawback can be overcome by implementing multilayer structures [1], [17 – 20].

Three different transducers were tested: PVDF and PZT-5H transducers with a single layer of 110 μm thicknesses and 1cm of diameter and a PVDF transducer with four layers of 28 μm thickness and 1cm diameter. The transducer of 110 μm thickness of PVDF has a resonance frequency of 10 MHz, the PZT-5H transducer of the same thickness has a resonance frequency of 20 MHz, and the transducer with four layers of PVDF has a resonance frequency of 10 MHz. So, if used frequencies below 1 MHz, the transmission coefficient ratio of the sound power level do not show significant flotation. The tests were performed at a frequency band from 100 KHz to 2 MHz.

3.4. Transducer Design and Fabrication

The single layer transducers have the structure represented in Figure 3.2, where the active element has 110 μm of thickness and 1 cm of diameter. The multilayer one has the structure shown in Figure 3.6, where the active element has four layers of 28 μm of thickness and 1 cm of diameter. The electrodes connections, as shown in Figure 3.6, allows removing the parasite capacitance between the electrodes and the glue. By bonding reversed polarization layers, the electrodes between the glue have the same electrical potential, and there is no current between them and consequently reduce the power consumption once the parasite capacitance was disabled.

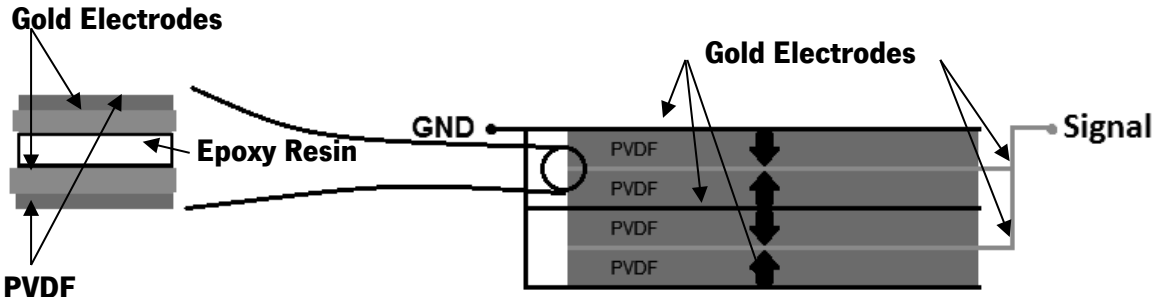

Figure 3.6: 2D representation of the active element multilayer structure.

The Gold electrodes with 10 mm circular shape were deposited by sputtering in both sides of the film, with a Polaron SC502 sputter coater. The four layers of the transducer were then glued with

an epoxy resin Devcon 5 minute©, in a compression press. Finally, the active element was glued to a stainless steel mass and the active element outside surface was isolated with a thin silicone layer to protect it from water. Figure 3.7 shows a picture of the final device.

Figure 3.7: Final transducer set up.

3.5. Simulation and Experimental Setup

In order to compare the behavior of PZT-5H with PVDF single and multiple layers, the mechanical and electrical proprieties of each transducer were theoretically calculated; a computational simulation was performed and, finally, experiments in a water tank were conducted.

To a better understanding of the comparative performance between the single-layer PZT, four-layer PVDF and the single-layer PVDF (reference), the relative performance graphics between two transducers and the reference are obtained from the equation (2.14).

3.6. Simulations

The transducers performance for the PZT-5H with PVDF single and multiple layers were previous simulated. The finite element platform used was the Comsol Multiphysics in a 2D symmetric plane with the models Piezo Strain Plane for the active element actuation and the model Pressure Acoustic for the pressure waves. The simulations setup is the same for all transducers, where only the active element is replaced. The outside boundaries of the medium were configured as *match boundaries* to work as absorbers, removing all the echoes. The selected

mesh has particles with triangular shape and a size of 10% of the wavelength. With this *mesh* the results of all simulations have 10 samples for each wavelength regardless the frequency of simulation signal.

The simulations were performed with the following settings: fresh water as propagation medium, 20 C° of temperature and sine wave excitation signal with 10V of amplitude. The measurements were taken 3 cm away from the transducer in order to ensure that the measurement is not taking place inside the near field of the sound beam where there is some turbulence.

3.6.1. Experimental

The real trails were implemented with the same conditions as the simulations: fresh water as propagation medium, 20 C° of temperature, 10 V sine wave excitation signal and a distance of 3 cm. The experimental setup consisted in a water tank with 1.2x0.5x0.4 m (length, width, height). With these dimensions echoes occurs very easily and the hydrophone surface work as sound reflector. It was not suitable the elimination of echoes, but it was possible to ensure the same settings for the three transducers tested.

The ultrasonic receptor, used to register the pressure waves, was the Cetacean Research™ C304XR hydrophone, with an effective sensibility of 181 dB, re 1V/µPa and a usable range of 0.005 to 2000 KHz.

3.7. Simulations and Experimental Tests

Before the simulations and experimental tests were carried out, it was necessary to analyze the potential transducers behavior. An ideal system was considered using the equations referred above, where the active element has a homogeneous displacement. Table 3.3 shows the materials features and output response analysis of the three transducers (PZT-5H 110 µm, PVDF 110 µm and PVDF 4x28 µm).

Table 3.3: PZT-5H 110µm, PVDF 110µm and PVDF 4x28µm analysis considering homogeneous displacements.

Feature	PZT 110µm	PVDF 110µm	PVDF 4x28µm
Thickness (m)	1.10E-04	1.10E-04	2.80E-05
Resonance frequency (Hz)	2.00E+07	1.02E+07	1.00E+07
Sound speed (m/s)	4.40E+03	2.25E+03	2.25E+03
Density (kg/m^3)	7.50E+03	1.47E+03	1.47E+03
d_{33} (C/N)	5.12E-10	3.40E-11	3.40E-11
S^{E}_{33} (1/Pa)	2.07E-11	4.72E-10	4.72E-10
Number of Layers	1	1	4
Electrical Potential (V)	10	10	10
Free displacement (m)	5.12E-09	3.40E-10	1.36E-09
Max applied force (N)	1.77E+02	5.14E-01	2.02E+00
Max frequency (Hz)	4.66E+07	2.04E+06	2.01E+06
Test frequency (Hz)	1.00E+06	1.00E+06	1.00E+06
Transmitted wave percentage at 1MHz (%)	32%	76%	78%
Expected Performance (vs PVDF single layer) (dB)	21.92	-	12.19

It is important to notice that, by dividing the active element into layers without changing its final thickness, the maximum frequency does not change, but the equivalent excitation voltage, free displacement and maximum applied force are multiplied by the number of layers. If the active element thickness is not divided according the number of layers, the multi structure transducer was not able to achieve the same single layer maximum frequency, once the maximum applied force remains the same but the free displacement is multiplied by the number of layers. In the four-layer case, the expected performance increases 12.04 dB, for PZT the expected increase in performance is 23.56 dB.

3.7.1. Simulations

A transducer 2D model was designed and simulated for each topologies described in sections 3.4 and 3.5.

To better understand the difference of performance among the three topologies, Figure 3.8 shows the simulated relative performance according equation (2.14) between single-layer PZT versus single-layer PVDF, four-layer PVDF versus single-layer PVDF and expected values, respectively.

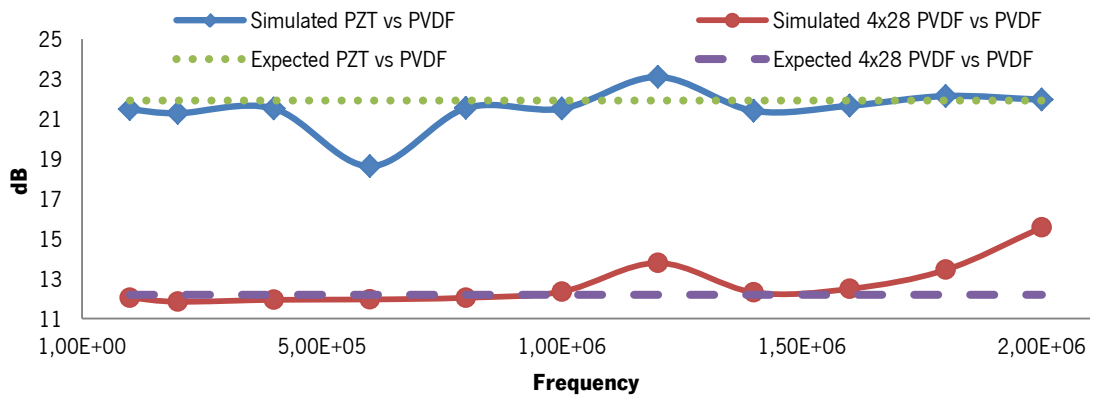

Figure 3.8: Simulations performance improvement results of PZT versus single-layer PVDF, four-layers PVDF versus single-layer PVDF and expected values, respectively.

Analyzing Figure 3.8 it was possible to observe that the ratio of PZT versus PVDF performance is slightly below than the expected value and the four-layer PVDF versus single-layer PVDF performance match the expected values with the exception of values to frequencies above 1.6MHz where the graphic shows a performance growth. This growth results from the fact that multilayer structures with thinner layers will have different mechanical, morphological and structural characteristics [17 – 30].

3.7.2. Experimental

Figure 3.9 shows the experimental pressure wave measurements, where it is possible to observe the behavior of the three transducers over frequency.

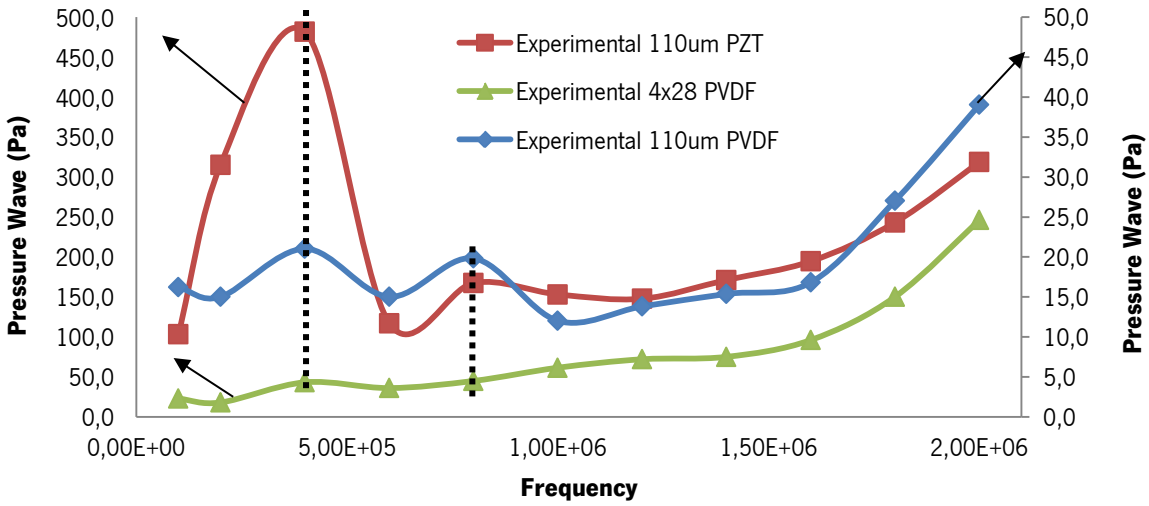

Figure 3.9: Pressure wave responses over frequency of single layer PZT (left axis), four layer PVDF (left axis) and single layer PVDF (right axis).

In Figure 3.9 it is possible to observe two peaks in the three transducer measurements: one at 400 kHz and the other at 800 kHz. These peaks are due to a set of features of the experimental setup. By considering the equation (2.2) it is possible to understand that, at low frequencies, the emitter presents a pattern with a wide divergence angle and, to these frequencies, the signal is emitted to the sides, where it is rebound back to the receiver. At higher frequencies the signal has a more directional pattern which prevents side echoes. Considering all these facts together, the peaks are the result of the tank resonance signal. Another fact that helps to conclude that these peaks do not result from the transducer but from the experimental setup is the graphics shown in Figure 3.11, where it is possible to observe that the electric current consumption over frequencies does not show any type of flotation, typical of the resonance harmonics and anti-resonance points.

Figure 3.10 shows the relative performance results from the tank experiments according to equation (2.14) among single-layer PZT versus single-layer PVDF, four-layer PVDF versus single-layer PVDF and expected values, respectively.

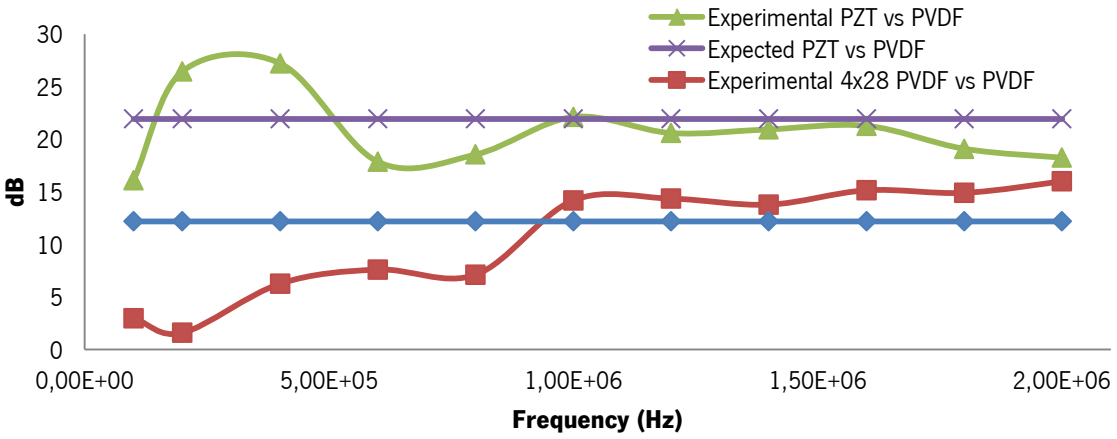

Figure 3.10: Performance results of four-layers PVDF versus single-layer.

In the PZT results shown in Figure 3.10, not considering the initial peak, the results are very similar to the simulations results and shown an average performance of 20 dB versus single layer PVDF. However, in the four-layer PVDF case, the results are more interesting and can be divided in two parts. In the first part, between 100 kHz and 1 MHz, the results are far below of the expected values, although show a continuous growth beginning at 100kHz with 3dB and reaching the 14.2 dB at 1MHz. In the second part, between 1 MHz and 2 MHz, the growth rate slows down and, at 2MHz, shows a performance improvement of 16dB.

It is possible to increase the transducer performance using multilayers, but this optimization has increases energy consumption as shown in Figure 3.11.

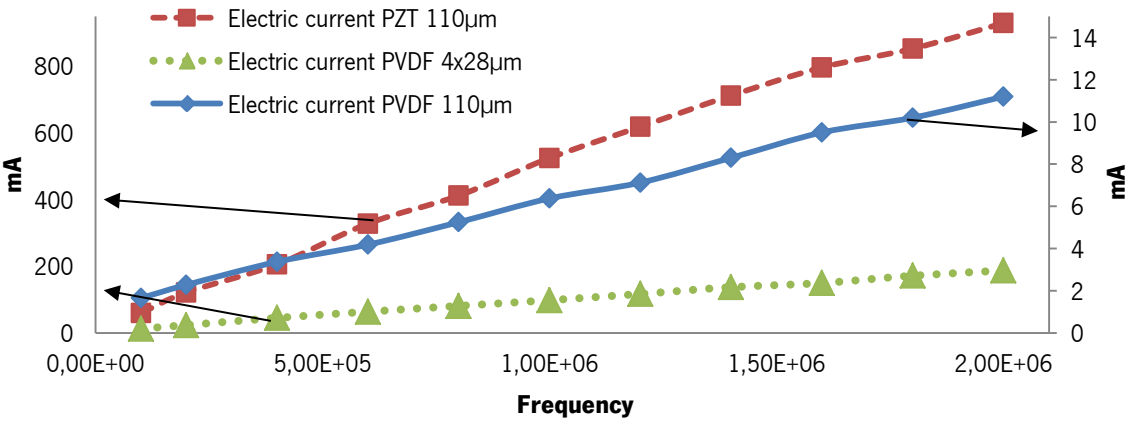

Figure 3.11: Electric current consumption over frequency to PZT 110 µm (left scale), PVDF 4x28 µm (left scale) and PVDF 110 µm (right scale).

The results shown in Figure 3.11 allow visualizing the electric current consumption and they are according to theoretical analysis where the electrical current is directly proportional to the frequency. The PZT electric current consumption is 87 times higher than single-layer PVDF duo to the high values of PZT relative dielectric constant. However the four-layer PVDF only shows 16.7 times more electric current consumption than single-layer PVDF and this occurs due to two factors: there is 4 times more effective area in the four-layer transducer and the distance between electrodes it is 4 times lower. It is possible to reduce the electric current consumption by increasing the film thickness but it is important to consider the effect that this change will introduce in the transducer performance. According to equation (3.2), the resultant force decline with increasing thickness. Another way to reduce the electric current consumption is to reduce the transducer area but this change will affect the sound beam wide and divergence angle.

Figure 3.12 shows the electric current consumption per Pascal of the three topologies single-layer PZT-5H, four-layer PVDF and single-layer PVDF.

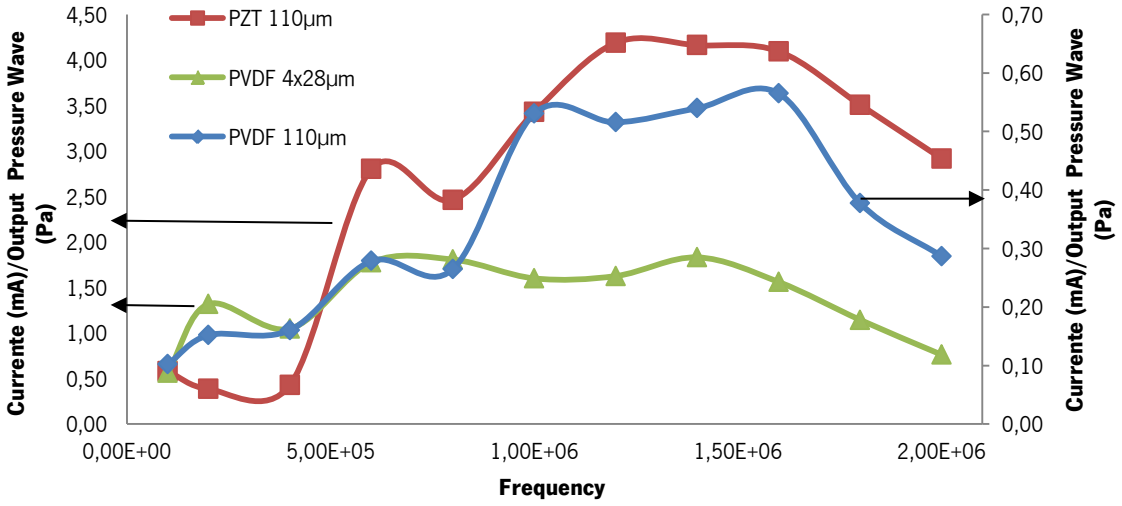

Figure 3.12: Electric current consumption per Pascal of single layer PZT (left axis), four-layer PVDF (left axis) and single layer PVDF (right axis).

Figure 3.12 helps to understand the efficiency level of each transducer. Despite the low outcome of single-layer, PVDF shows to be the most efficient concerning electric current consumption per Pascal, followed by the four-layer PVDF and the less efficient the single-layer PZT. By ignoring the peaks related to experimental constrains, the average electric current consumption of the tree topologies are 3.5 mA/Pa for the single-layer PZT, 1mA/Pa for the four-layer PVDF and 0.3mA/Pa for the single-layer PVDF.

3.8. Conclusions

An optimization study for ultrasonic transducers for underwater communications was performed. Three different designs with piston topology were compared, namely PZT-5H single-layer, PVDF single-layer and PVDF four-layer.

The study includes calculations, finite element simulation and experimental tests.

From the three studied topologies studied, the PZT transducer achieves higher output sound pressure, but the four-layer PVDF demonstrates to be the best for this kind of applications, due to its higher bandwidth and lower power consumption.

In this study, the single-layer PZT output sound pressure shows to be in average 7dB higher than four-layer PVDF, but also shows an average power consumption of 3.5 times higher.

References

[1] Donald J. Leo, "Engineering Analysis of Smart Material Systems", John Wiley & Sons, Inc, ISBN 978-0-471-68477-0, 2007.

[2] Charles H. Sherman, John L. Butler, "Transducers and Arrays for Underwater Sound", Springer Science Business Media, LLC, ISBN-10: 0-387-32940-4, 2007.

[3] John J. Leonard, Bradley A. Moran, Ingemar J. Cox and Matthew L. Miller, "Underwater Sonar Data Fusion Using an Efficient Multiple Hypothesis Algorithm", IEEE International Conference on Robotics and Automation, 1995.

[4] P.G. Auran and O. Silven, "Underwater Sonar Range Sensing and 3d Image Formation", Control Eng. Practice, Vol. 4, No. 3, Pages 393-400, Elsevier Science, 1996.

[5] David F. Waechter, S. Eswar Prasad , Richard G. Blacow and Bin Yan, "Internally biased PZT materials for high-power sonar transducers", 11th CF/DRDC International Meeting on Naval Applications of Materials Technology.

[6] D.A. Hughes, J.M. Girkin, S. Poland, C. Longbottom, T.W. Button, J. Elgoyhen, H. Hughes, C. Meggs, S. Cochran, "Investigation of dental samples using a 35MHz focussed ultrasound piezocomposite transducer", Ultrasonics, Elsevier Science, Volume 49, Issue 2, February 2009, Pages 212-218, ISSN 0041-624X.

[7] M.Stojanovic, “On the relationship between capacity and distance in an underwater acoustic communication channel”, ACM SIGMOBILE Mobile Computing and Communications Review (MC2R), Vol.11, Issue 4, Pages 34–43, October 2007.

[8] I. A.Sehgal and J.Schonwalder, “Aquatools: An underwater acoustic networking simulation toolkit”, IEEE Oceans, Sydney, Australia, May 2010.

[9] M.Stojanovic and J.Presig, “Underwater acoustic communication channels: Propagation models and statistical characterization”, IEEE Communications Magazine, Pages 84–89, January 2009.

[10] M.Stojanovic, “Underwater acoustic communications: Design considerations on the physical layer”, IEEE / IFIP Fifth Annual Conference on Wireless On demand Network Systems and Services (WONS 2008), January 2008.

[12] J.Preisig, “Acoustic propagation considerations for underwater acoustic communications network development”, Underwater Networks (WUWNet’06), Pages 1–5, September 2006.

[13] I. A.Sehgal and J.Schonwalder, “Variability of available capacity due to the effects of depth and temperature in the underwater acoustic communication channel”, OCEANS 2009 - EUROPE, Pages 1–6, May 2009.

[14] Francois R. E., Garrison G. R., "Sound absorption based on ocean measurements: Part I: Pure water and magnesium sulfate contributions", Journal of the Acoustical Society of America, 72(3), 896-907, 1982.

[15] Malcolm J. W. Pavey, “Ultrasonic Techniques for Fluids Characterization”, Academic Press, ISBN-13: 978-0-12-563730-5 ISBN-IO: 0-12-563730-6, 1997.

[16] Ainslie M. A., McColm J. G., "A simplified formula for viscous and chemical absorption in sea water", Journal of the Acoustical Society of America, 103(3), Pages 1671-1672, 1998.

[17] Thomas R. Shrout, “Innovations in Piezoelectric Materials for Ultrasound Transducers”, Applications of Ferroelectrics, ISAF, 17th IEEE International Symposium, 2008.

[18] A. Abrar, S. Cochran, “Multilayer piezocomposite structures with piezoceramic volume fractions determined by mathematical optimization”, Ultrasonics, Elsevier Science, Volume 42, Issues 1–9, April 2004, Pages 259-265, ISSN 0041-624X.

[19] Qian Zhang, Peter A. Lewin, Philip E. Bloomfield, “PVDF Transducers-A Performance comparison of Single-Layer and multilayer Structures”, IEEE Transactions On Ultrasonics, Ferroelectrics And Frequency Control, Vol. 44, No. 5, September 1997.

[20] Raúl A. Reyes-Villagrana, Gerardo Gutiérrez-Juárez and Rumen Ivanov Tsonchev, “Characterization of Simulated Mechanical – Electrical Properties of PVDF and PZT Piezoelectric Material for Use in the Pulsed Optoacoustic Spectroscopy”, International Journal of Pure and Applied Sciences and Technology, Pages 26-45, 2011.

[21] L.W. Schmerr, A. Lopez-Sanchez, R. Huang, “Complete ultrasonic transducer characterization and its use for models and measurements”, Ultrasonics, Elsevier Science, Volume 44, Supplement, 22 December 2006, Pages e753-e757, ISSN 0041-624X.

[22] Torsten Bove, Wanda Wolny, Erling Ringgaard and Annette Pedersen, “New piezoceramic PZT–PNN material for medical diagnostics applications”, Journal of the European Ceramic Society, Volume 21, Issues 10–11, Pages 1469-1472, 2001.

[23] S. Saitoh, T. Kobayashi, K. Harada, S. Shimanuki and Y. Yamashita, "A 20 MHz Single-element ultrasonic probe using 0.91Pb(Zn1/3Nb2/3)O3-0.09PbTiO3 single crystal", IEEE Transactions On Ultrasonics, Ferroelectrics And Frequency Control, Vol. 45, Pages 1071-1076, 1998.

[24] T. Ritter, K.K. Shung, X. Geng, P.D. Lopath, S.E. Park and T.R. Shrout, "Single crystal PZN-Tpolymer composites for ultrasound transducer applications", IEEE Transactions On Ultrasonics, Ferroelectrics And Frequency Control, Vol. 47, Pages 792-800, 2000.

[25] S. Saitoh, T. Takeuchi, T. Kobayashi, K. Harada, S. Shimanuki and Y. Yamashita, "Fortychannel phased array ultrasonic probe using 0.91Pb(Zn1/3Nb2/3)O3-0.09PbTiO3 single crystal", IEEE Transactions On Ultrasonics, Ferroelectrics And Frequency Control, Vol. 46, Pages 152-157, 1999.

[26] Linxiang Wang, M. Willatzen, “Modelling of nonlinear dynamics for reciprocal multi-layer piezoceramic transducer systems”, Applied Mathematical Modelling, Elsevier Science, Volume 33, Issue 5, May 2009, Pages 2263-2273, ISSN 0307-904X.

[27] F. Levassort, L.P. Tran-Huu-Hue, G. Feuillard and M. Lethiecq, “Characterisation of P(VDFTrFE) material taking into account dielectric relaxation : application to modelling of high frequency transducers”, Ultrasonics, Vol. 36(1-5), Pages 41-45, 1998.

[28] K.A. Snook, J.-Z Zhao, C.H.F. alves, J.M. Cannata, W-H.Chen, R.J. Meyer, T.A. Ritter and K.K. Shung, “Design, fabrication, and evaluation of high frequency, single-element transducers incorporating different materials”, IEEE Transactions On Ultrasonics, Ferroelectrics And Frequency Control, Vol. 49, Pages 169-176, 2002.

[29] Yongrae Roh, Vasundara V. Varadan and Vijay K. Varadan, “Characterization of All the Elastic, Dielectric, and Piezoelectric Constants of Uniaxially Oriented Poled PVDF Films”, IEEE Transactions On Ultrasonics, Ferroelectrics And Frequency Control, Vol. 49, No. 6, JUNE 2002.

[30] Bloomfield, P.E., "Dielectric and piezoelectric properties of stacked and plated PVDF, P(VDF/TeFe), P(VDF/TrFE) and ceramic/rubber composite thick films", Applications of Ferroelectrics, 1994.ISAF '94., Proceedings of the Ninth IEEE International Symposium, Pages 287-290, 7 Aug 1991.

4. Response of Transducers to Digital Modulations

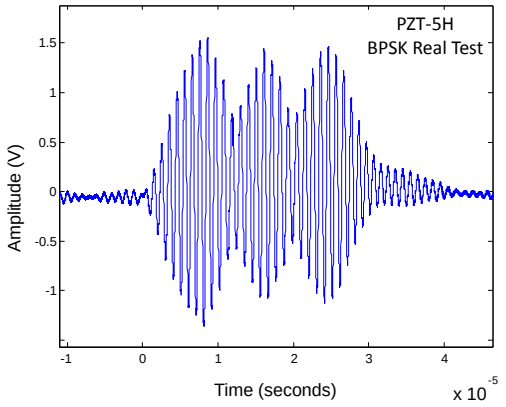

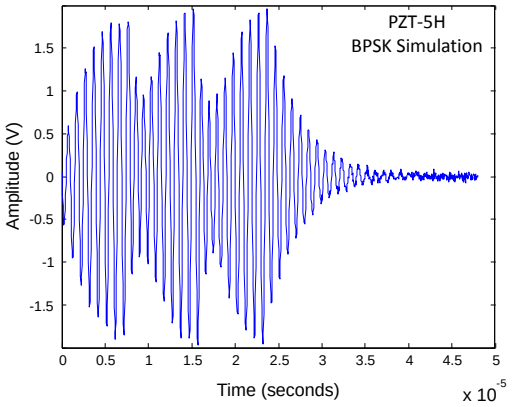

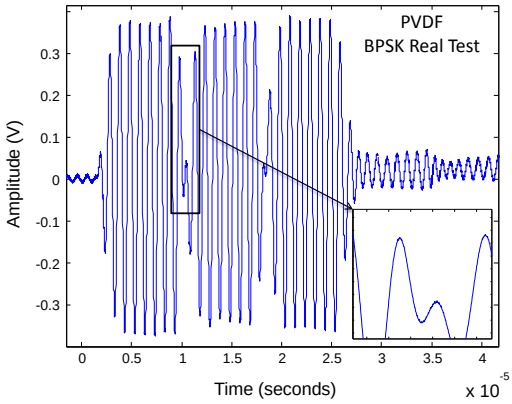

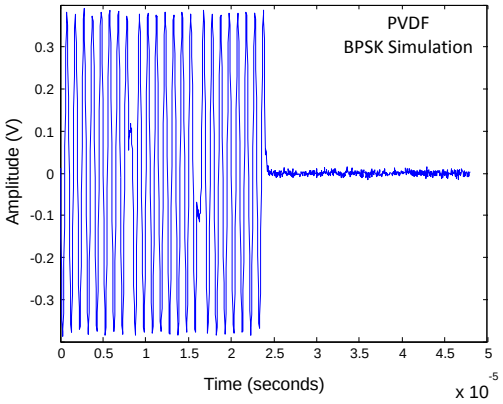

4.1. Introduction

To develop high data-rate wireless communication systems in underwater environments it is important to incorporate the state of the art of conventional digital modulation techniques. Therefore, there are several projects under development [1 - 8], such as the work presented in [7] which presents an underwater communication system with modulations as Amplitude Shift Keying (ASK), Binary Frequency Shift Keying (BFSK), Quadrature Phase Shift Keying (QPSK) and 16 Quadrature Amplitude Modulation (16QAM) to transmit an image over a distance of 15 m, reaching a bit-rate of 3 kbps with carriers from 17 kHz to 23 kHz. Another project is the commercial product presented by "Evo Logics", with different underwater acoustic modem models, with a maximum data rate of 31.2 kbps, with a frequency band from 48 kHz to 78 kHz [8]. The project described in [1] presents a high data-rate underwater acoustic modem FPGA based, where it was implemented a BPSK with 800 kHz carrier, reaching 80 kbps rate.

Nonetheless, ultrasound communication systems are still very limited [1, 7, 8], with very low data rates and high delays, mostly due to the physical characteristics of the subaquatic channel. Using carriers with upper frequencies, the attenuation increases leading to a decrease of the distance range. For a 1 MHz signal, the acoustic absorption achieves 280dB/km and to this effect also the spreading attenuation has to be added, which depends on the transducer geometry.

Ultrasound transducers are usually manufactured with piezoelectric materials and, to maximize the output pressure level with low consumption, the transducer must operate at the resonance frequency [9].

There are several factors that influence the signal quality: structural damping, electrical damping and acoustic impedance mismatch. Structural damping is due to the energy dissipation in geometrical deformations of the transducer when the electrical field is applied. Electrical damping is due to transducer capacitor effects which result in a time lag between the application of the electrical signal and the transducer response. However, to the 1 MHz limit range, the most significant factor is the acoustic impedance mismatch, since the structural and electrical damping only affects the signal quality above tens of MHz in piezoelectric ceramic transducers and hundreds of MHz in piezoelectric polymer transducers [10]. The acoustic impedance mismatch between the transducer and the medium causes acoustic waves to be reflected back to transducer. The resonance transducers are designed to overcome this fact, since the internal

acoustic waves are synchronized with the electrical drive signal, causing an addition of the two signals and therefore increasing the output. On the other hand, to communicate using digital modulations it is not advisable to operate with resonance transducers, as for the modulated signal the synchronization is not possible due to the lack of periodicity.

This chapter is focused in the study of the influence of the acoustic impedance on the ultrasonic transducer performance operating with high and wideband frequencies (100 kHz to 1MHz range) using digital modulations, being also addressed how to improve the signal quality.

The projector used in this study was a piston type with a piezoelectric disk, which operates in the thickness mode. The piston-type transducer was selected because it is easy to be manufactured and low-cost. The study presented in this work is not exclusive to the used transducers and it can be applied to other types of piezoelectric transducers. Two types of piezoelectric materials were used: the ceramic Lead Zirconate Titanate (PZT) (high acoustic impedance) [11, 12] and the polymer Polyvinylidenefluoride (PVDF) (low acoustic impedance) [11 - 14].

With the objective of evaluating the performance of ultrasound transducers using digital modulations, such as: Phase-Shift Keying (PSK), Frequency Shift keying (FSK) and Amplitude Shift Keying (ASK). A Matlab/Simulink Model was developed to estimate the transducer performance to guide transducer construction and test evaluation, since it allows for the most suitable design to be selected. Using Field Programmable Gate Arrays (FPGAs), a reconfigurable platform to develop all the necessary building blocks to implement different types of digital modulations was developed. Two experimental set-ups were developed: a small water tank, where digital modulations measurements were carried out to perform signal analysis and to validate the simulation model; and a swimming pool where the difference of linearity of both types of piezoelectric materials was studied for a wideband frequency range.

4.2. Materials Selection and Transducer Fabrication

Before carry out the experimental validation, piezoelectric materials and transducer dimensions needed to be selected. This section will describe the materials selection and the transducer manufacture.

Among all the piezoelectric materials, the most common to these types of applications are the ceramics: Lead Zirconate Titanate (PZT), Lead Titanate (PT), Lead Magnesium Niobate (PMN)

and Lead Zinc Niobate (PZN) [12 - 17]. However, other materials often used are the polymers Polyviylidenefluoride (PVDF) and P(VDF-TrFE) [12 – 14, 18, 19] and single crystals of PZT, PMN and PZN [20 - 22].

This study focus on PZT-5H since this is the most interesting material for large scale applications due to its availability and price [11 - 13]. For comparison, the PVDF polymer will be used, since it is an interesting material due to the low acoustic impedance ($3.3x10^6 kg/m^2s$) and price [11]-[12]. With values near to the medium acoustic impedance (proximally $1.5x10^6 kg/m^2s$), it is possible to minimize the acoustic signal distortions and allow a better acoustic energy transference from the transducer to the medium, resulting in a reduction of the acoustic energy accumulated inside the transducer.

For a better understanding on how the acoustic impedance mismatch influences the ultrasonic transducer performance, Figure 4.1 shows the acoustic pressure wave along the transducer thickness and the medium when positioned at the center of the acoustic pattern. The transducer dimensions were defined to operate at 1 MHz resonance frequency, resulting in a 2.05 mm thickness for PZT-5H and 1.125 mm for PVDF, and a diameter with 2.5 times the wavelengths.

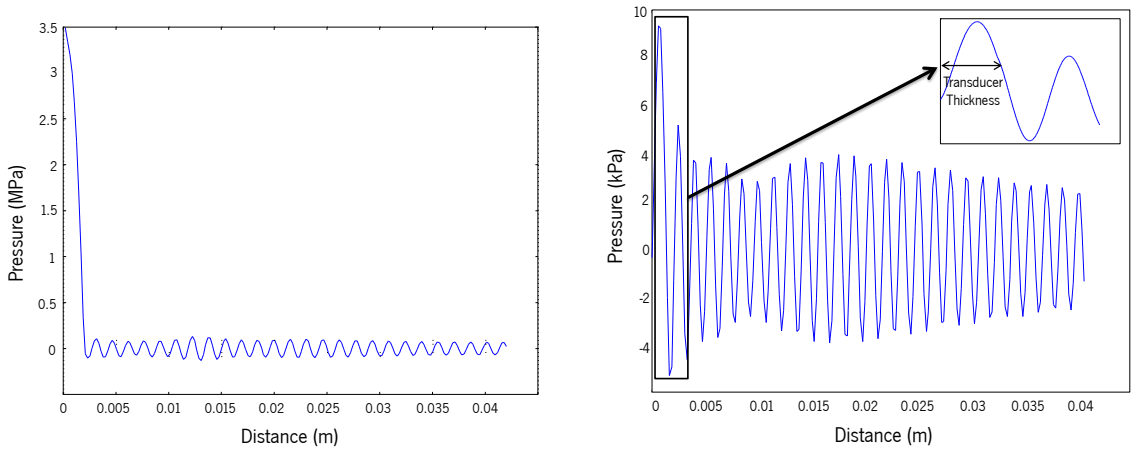

a) b)

Figure 4.1: FEM simulation of two piston transducer, PZT-5H (a) and PVDF (b).

Figure 4.1.a shows that the pressure wave inside the PZT-5H transducer has a much higher level than the acoustic pressure transferred to the medium, the boundary between the two materials holds back most of the acoustic energy. In Figure 4.1.b this effect is reduced, with the acoustic energy having a better transference form the transducer to the medium.

The utilization of a matching layer in this case would not be useful since the frequency of the digital modulation signal would be unknown leading to unknown matching layer thickness. With electronic control it is possible to improve the signals quality by overcoming the internal energy, but this means high power consumption and cost.

These signals were obtained from a FEM simulations using Comsol Multiphysics platform in a 2D symmetric plane with the Piezo Strain Plane models for the active element actuation and the Pressure Acoustic model for the pressure waves. The simulations setups are the same for all transducers, where only the active element is replaced. The outside boundaries of the medium were configured as *match boundaries* to work as absorbers, removing all the echoes. The selected *mesh* is divided in areas with triangular shape and a size of 10% of the wavelength. The simulations were performed with the following settings: fresh water as propagation medium, 20 C° of temperature and sine wave excitation signal with 12V of amplitude.

Further, the results will be representative for their respective family of materials: ceramic, polymer and piezoelectric, respectively.

The transducer design specifications must be exclusive for each material, ensuring the best performance. The PZT-5H transducer dimensions were defined to operate at the resonance frequency to replicate the conventional commercial transducers. Else, the PVDF transducer dimensions were defined to operate at the optimal conditions for 1 MHz range, generating non periodic signals.

Before defining the transducer dimensions, it is necessary to verify if the piezoelectric material has the required strength to produce vibrations at 1 MHz frequency in underwater environments. Table 4.1 shows the main physical properties and the project considerations of these materials for the proposed application, according to equations (3.1) to (3.5):

Table 4.1: Comparison of some characteristics of PZT-5H and PVDF [23].

Physical Property	PZT-5H 2mm	PVDF 8x28
Thickness(m)	2,00E-3	2,80E-5
Resonance Frequency (Hz)	1,05E+6	5,02E+6
Sound Speed (m/s)	4,20E+3	2,25E+3
Density (kg/m^3)	7,50E+3	1,47E+3
Acoustic Impedance Z [10^6kg/m^{2}s]	33	3.3075

Relative Dielectricic constant Ɛr	3100	12
Piezoelectric Coefficient d_{33} (C/N)	5,12E-10	3,40E-11
Elastic compliance coefficient S_{33}^{E} (1/Pa)	2,07E-11	4,72E-10
Layers	1	8
Max Applied Force/Excitation Tension (N/V)	3,88	8,08E-1
Applied Force at 1MHz/Excitation Tension (N/V)	1,49	7.92E-1
Max Operating Frequency Underwater (Hz)	2,61E+6	1,02E+6
Transmitted wave percentage at 1MHz (%)	32%	78%

In order to operate at 1 MHz resonance frequency, the PZT-5H disk must have a thickness of 2 mm.

From Table 4.1, PZT-5H shows that a larger force than necessary can be applied to the medium without sacrificing the piezoelectric material full displacement. However, PVDF has a higher S^{E}_{33} than PZT-5H, and therefore it cannot be applied the displacement to the medium at the same vibration frequencies with the same material thickness.

Therefore, the solution for the lack of force and for the acoustic energy retained inside the active element is the use of thin films. From equation (3.5), by reducing the active element thickness it is possible to increase the force applied to the medium, and by equation (3.9), reducing the active element thickness results in a decrease of the internal reflected wave propagation delay. This will minimize the signal distortion since the transmitted and reflected waves will be almost synchronized.

For the PVDF, a multilayer topology to increase the acoustic performance [13, 23] was selected and, at 1 MHz operational frequency, the thickness of the PVDF transducer was limited by the piezoelectric strength (equation (3.2)). In this case, the total thickness could not exceed 225 μm. According to [23], 8 layers with 28 μm of thickness are enough to achieve approximately the same PZT-5H acoustic pressure levels. With 225 μm the PVDF transducer has a resonance frequency of 5MHz, but in underwater environment it just shows the necessary strength to reach 1MHz.

The eight layers of the transducer were then glued with silicone in a compression press. Finally, the active element was glued to a stainless steel mass and the active element outside surface was isolated with a thin silicone layer to protect it from water. Each layer was connected with a

parallel drive excitation circuit. As the number of layers increases the performance is also improved, but manufacturing complexity and power consumption also increases.

Therefore, the multilayer transducer was manufactured. In [23] it is possible to find more details about the assembling methods used in transducers described above.

4.3. Simulations and Experimental Setup

4.3.1. Sceneries' Setup

The swimming pool scenario was 12 m long, 4 m wide and 3m deep. Two test distances were defined: 10 cm and 12 m, where measurements were performed at 50 cm deep and in the middle of the pool (2 m either side). It was used fresh water at a temperature of 13 °C and 7.2 pH. The drive signal was a sine wave 100 cycles burst with 16 V amplitude and at each distance, several frequencies were measured: 100 kHz, 200 kHz, 300 kHz, 400 kHz, 500 kHz, 600 kHz, 700 kHz, 800 kHz, 900 kHz, 1 MHz, 1.2 MHz and 1.4 MHz.

The second scenario used for the digital modulations evaluation, both in real tests and simulations, was a small water tank with 1.2×0.5×0.4 meters (length, width, height). The ultrasonic transmitter and receptor position coordinates were (22.5; 23; 11) and (87.5; 23; 11) centimeters. With these dimensions, echoes occur very easily and therefore a matching boundary (foam) at the boundary in front of the projector was used. The foam did not completely eliminate all the echoes but it was still possible to ensure the same settings for the two transducers tested.

Different tests with different modulations were performed: ASK, FSK and PSK were selected. All the modulations were defined as binary with just 1 bit per symbol. Accordingly, two types of modulations were defined from the ASK, BASK and OOK.

Figure 4.2 shows the drive signals used in both simulations and real experiments.

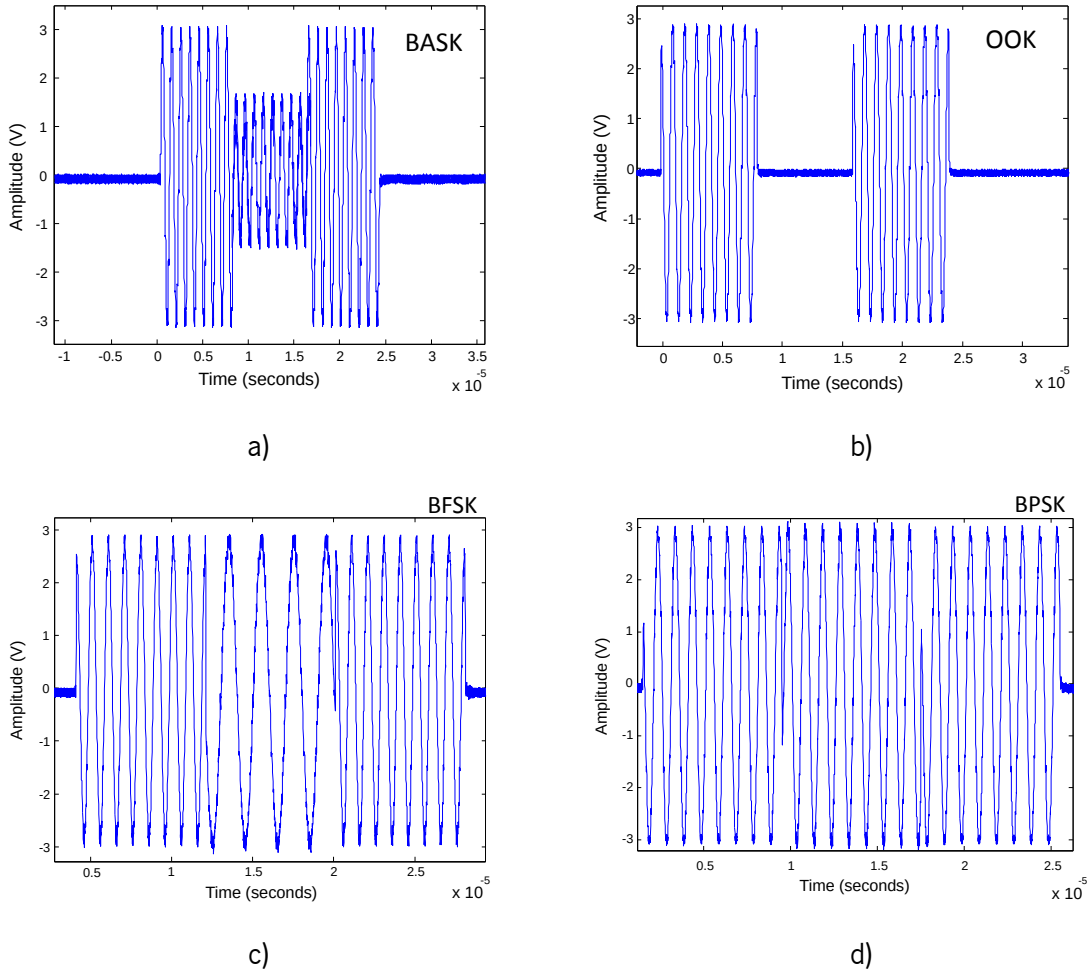

Figure 4.2: Drive signal of digital modulations, a) BASK, b) OOK, c) BFSK and d) BPSK.

Figure 4.2.a, .b, .c and .d display the drive signals at the transmission module output for BASK, OOK, BFSK and BPSK, respectively. The signals were generated at 25 Mega samples per second with 14 bit. Since the highest carrier has a frequency of 1 MHz, it is possible to ensure a very good signal quality with 25 samples per period. Before being sent to the transducer, these signals were amplified 4 times, resulting in a 12 V excitation voltage.

In the BASK modulation (Figure 4.2.a), the low logic level was set to half of the high logic level amplitude, and in OOK (Figure 4.2.b) the high level was the same as BASK, but with no signal at the low level. In the BFSK (Figure 4.2.c) the high logic level was set at 1 MHz and the low logic level at 500 kHz. This high difference between frequencies allows for an easy analysis of the results, since close frequencies would be masked by the resonance effect. But this difference will be limited by the Doppler Effect and will depend on the underwater environmental conditions, since it is necessary to ensure that the Doppler shift does not exceed the difference between the

frequencies of different levels. In the BPSK modulation (Figure 4.2.d) the logic level transition is made by a 180° phase shift.

The bit streaming selected for the tests was a sequence of '101', being therefore possible to analyze the transducer reactions to a '0' to '1' and '1' to '0' transition. The bit period selected for these tests was 8 μs, corresponding to 8 cycles at 1MHz. For a better understanding of this decision, Figure 4.3 shows the PZT-5H transducer response for a signal burst with 4, 8 and 16 μs periods.

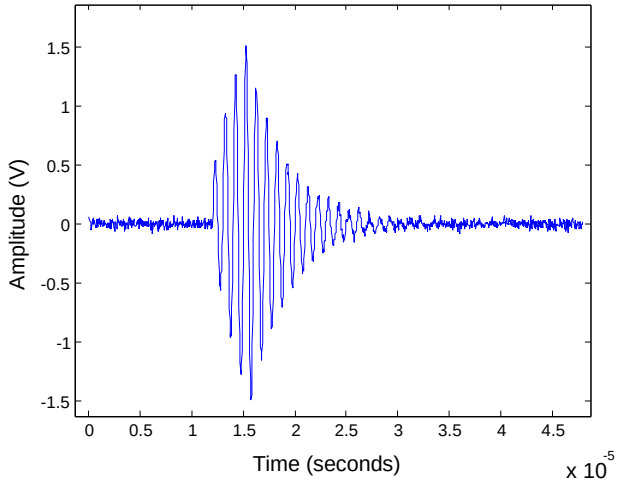

a)

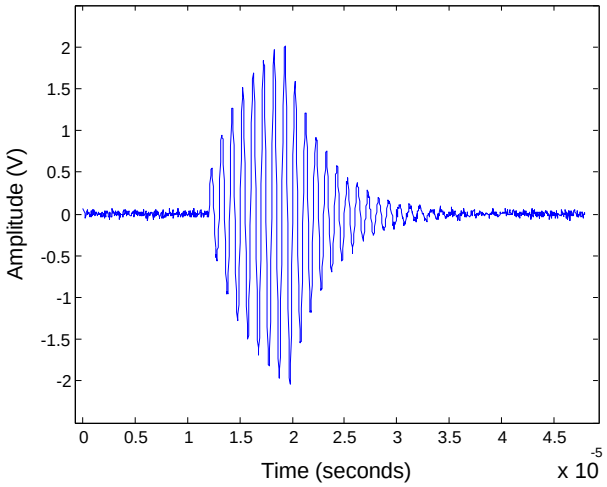

b)

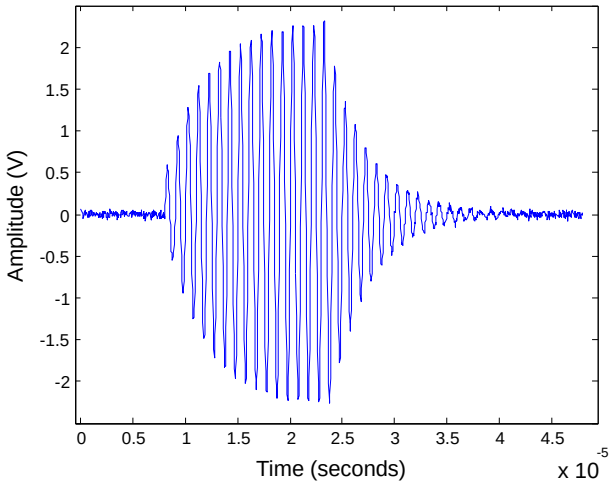

c)

Figure 4.3: PZT-5H transducer response for a signal burst with 4,8 and 16 μs periods at 1 MHz.

Figure 4.3 shows that the minimum time necessary for the signal start to stabilize is around 8 μs. Then, to increase the probability of sending a good quality signal, it was decided not to use bit periods much below 8 μs. With 8 μs bit period and 1 MHz carrier, the baud rate is 125 kbps.

4.3.2. Simulations

A Matlab/Simulink model was developed to simulate the ultrasonic transducers performance for different piezoelectric materials. The Simulink block was defined with 8 inputs and 1 output. The inputs are the excitation electrical signal, the water acoustic impedance and the piezoelectric material proprieties: density, sound speed, piezoelectric coefficient, elastic compliance coefficient, thickness and the number of layers. The output is the acoustic wave signal generated by the transducer. The block diagram presented in Figure 4.4 represents a simplified view of the model and helps to understand the relationships between the different sub-blocks.

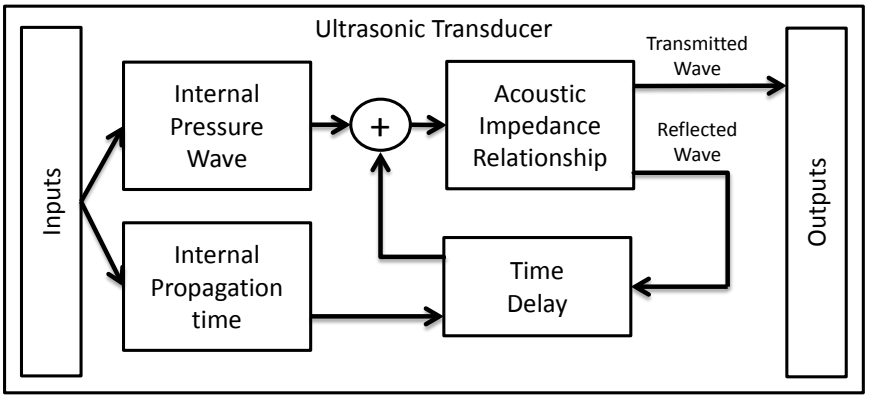

Figure 4.4: Block diagram of the MatLab/Simulink simulation.

The block diagram is based on equation (3.9). The model begins by calculating the pressure wave generated inside the transducer. Based on the transducer acoustic impedances and on the medium parameters, the transmitted and reflected pressure wave amplitudes are calculated. The reflected wave suffers a time delay, corresponding to the internal propagation time and, in a closed loop system it is added to the current internal pressure wave. The model was implemented as a discrete model with a sampling time of 40 ns, corresponding to a frequency sample of 25 Mega samples per second.

4.3.3. Experimental test system

In order to evaluate the results of the subaquatic channel model, experiments were carried out in a test tank. The system configuration is shown in Figure 4.5.

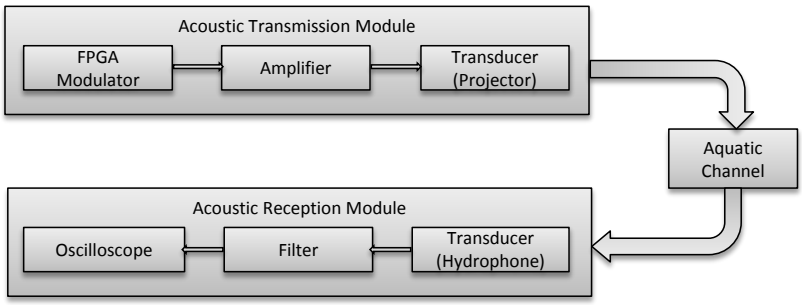

Figure 4.5: Block diagram of the test system.

The acoustic transmitter module is made up of a Xilinx Spartan-3A FPGA starter kit that it is responsible for modulating a bit stream into an electrical signal. Then drive signals from the FPGA modulator are amplified by a Push-Pull symmetric voltage amplifier with a gain of 12 dB.

The ultrasonic receptor used to register the pressure waves was the Cetacean ResearchTM C304XR hydrophone, with a transducer sensibility of -201 dB, re 1 V/µPa and a linear Frequency Range (±3dB) of 0.012–1000 kHz. The filter consists of a 2nd order active band-pass from 1 to 2000 kHz with 6dB gain. The digital oscilloscope used to record the measurements was a PicoScope 4227 100 MHz.

4.4. Results and Discussion

As was referred before, two materials types were evaluated: PVDF and PZT-5H. The results include an analysis of the frequency range linearity and the digital modulation performance.

4.4.1. Frequency Range response

Figure 4.6 shows the amplitude response of the two transducers over a wide range of frequencies: 100 kHz to 1.4MHz to different distances: 10 cm (Figure 4.6.a) and 12 m (Figure 4.6.b).

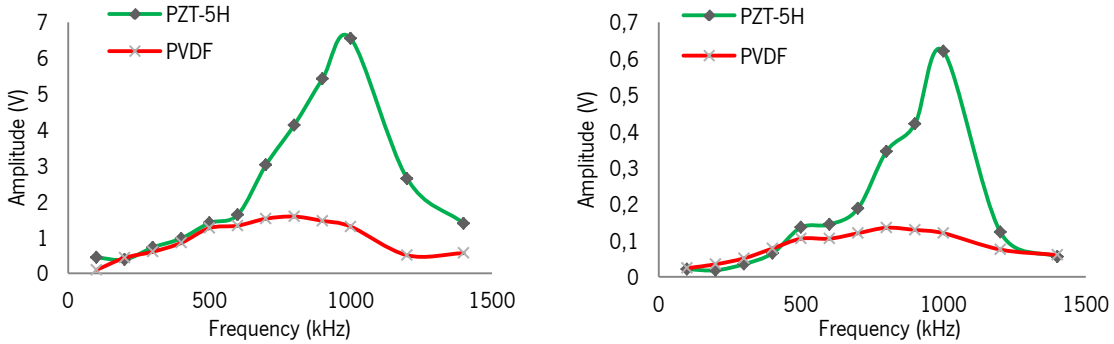

a) b)

Figure 4.6: Transducer acoustic pressure response from 100 kHz to 1 MHz, for 10 cm (a) and 12 m (b) distance.

It is observed that PZT-5H has a higher acoustic pressure output, but the response is not linear, with the highest level at resonance frequency point 1MHz. Both materials in Figure 4.6 show an acoustic output with a growing tendency between 100 kHz and 1 MHz. At 10 cm (Figure 4.6.a) the PZT-5H displays a growth of 13.7 dB between 100 kHz and 500 kHz, but if the range between 500 kHz and 1 MHz was considered the growth reaches 16.6dB. Conversely, the PVDF

displays a growth of 14.8 dB between 100 kHz and 500 kHz range, but to a frequency range between 500 kHz and 1 MHz only reach 3.6dB.

In Figure 4.6.b, the results for a 12 m distance shows the same tendency: the PZT-5H displays a growth of 16.2 dB between 100 kHz and 500 kHz and 19.6 dB between 500 kHz and 1 MHz. The PVDF has a lower growth: 7.4 dB to the first interval and 3.7 dB to the second interval.

However, PVDF showed a much lower amplitude, it was capable to maintain the output pressure almost linear to frequencies between 500 kHz and 1 MHz. Increasing the number of layers it is possible to increase the response without compromising the linearity.

4.4.2. Digital Modulations

The two materials were simulated than measured with real tests for 4 modulation types: BASK, OOK, BFSK and BPSK.

Figure 4.7 represents the PZT-5H transducer responses to the BASK and OOK amplitude modulations, respectively.

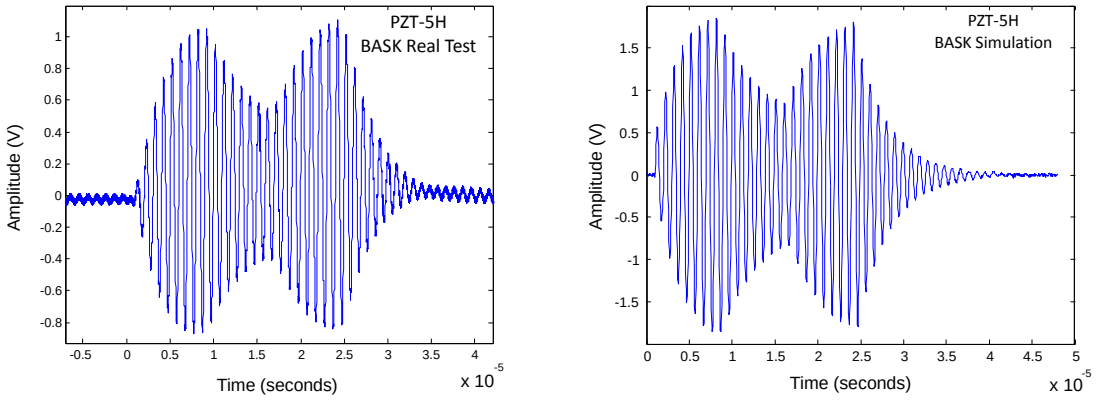

a) b)

Figure 4.7: PZT-5H response to BASK and OOK modulations, real measurement and simulation.

In both amplitude modulations, the results are very similar, being only a difference in relation to the low logic level. Due to the slower characteristics of PZT-5H, when comparing the amplitude variations, the low logic level in OOK results still display a low amplitude level signal. Nonetheless, real tests (Figure 4.7.a and .c) and simulation results (Figure 4.7.b and .d) show

that information can still be recovered, but the signal displays a high level of degradation. Consequently, in adverse conditions such as turbulence, moving agents or by increasing the bitrate information, loss can occur.

In comparison, the PVDF transducers responses to BASK and OOK modulations are shown in Figure 4.8.

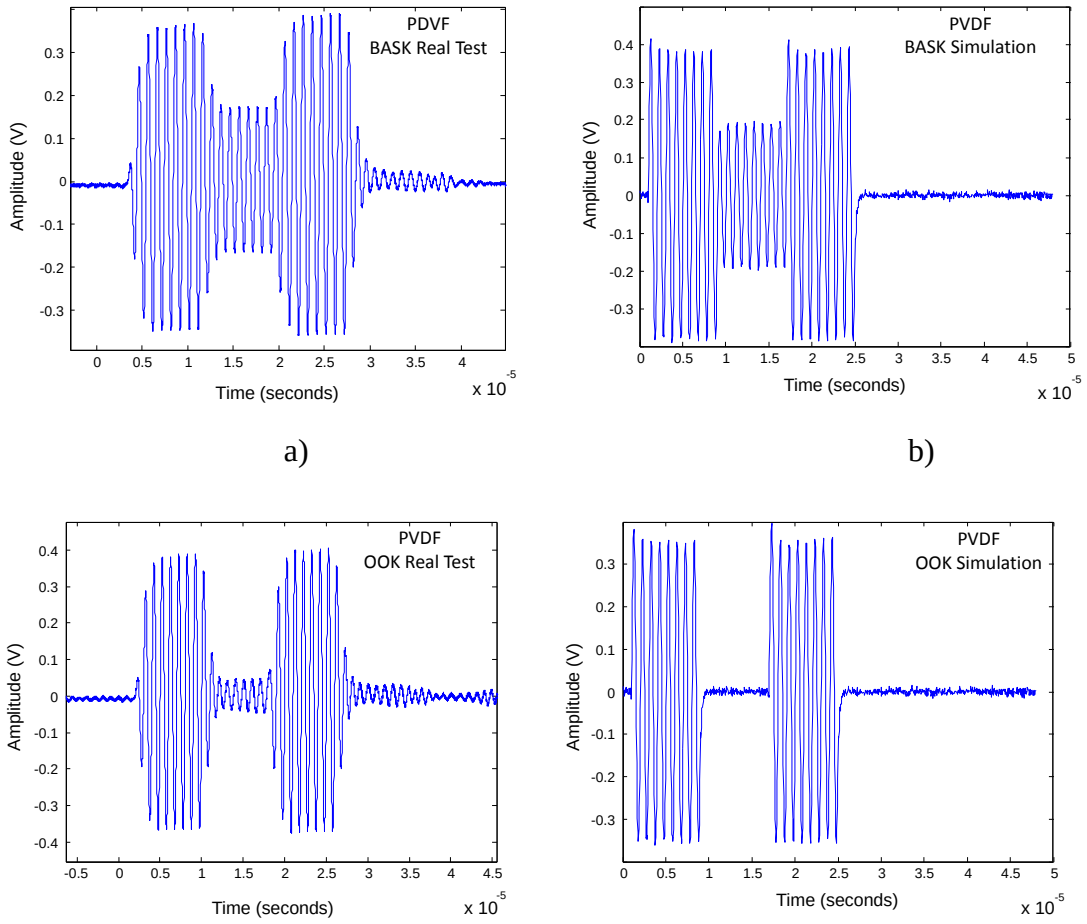

Figure 4.8: PVDF response to BASK and OOK modulation, real measurement and simulation.

Real tests (Figure 4.8.a and .c) are slightly slower in sudden amplitude transitions than in simulations (Figure 4.8.b and .d) for BASK and OOK modulations, and much of the signal deformations are due to echoes that overlap the signal. In fact, the remaining echoes that appear at the end of each signal (Figure 4.8.c) imply that there is an intermediate signal. In general the signals show a high quality, resulting in easy information retrieval.

Figure 4.9 show the PZT-5H and PVDF transducers' response to a BFSK modulation.

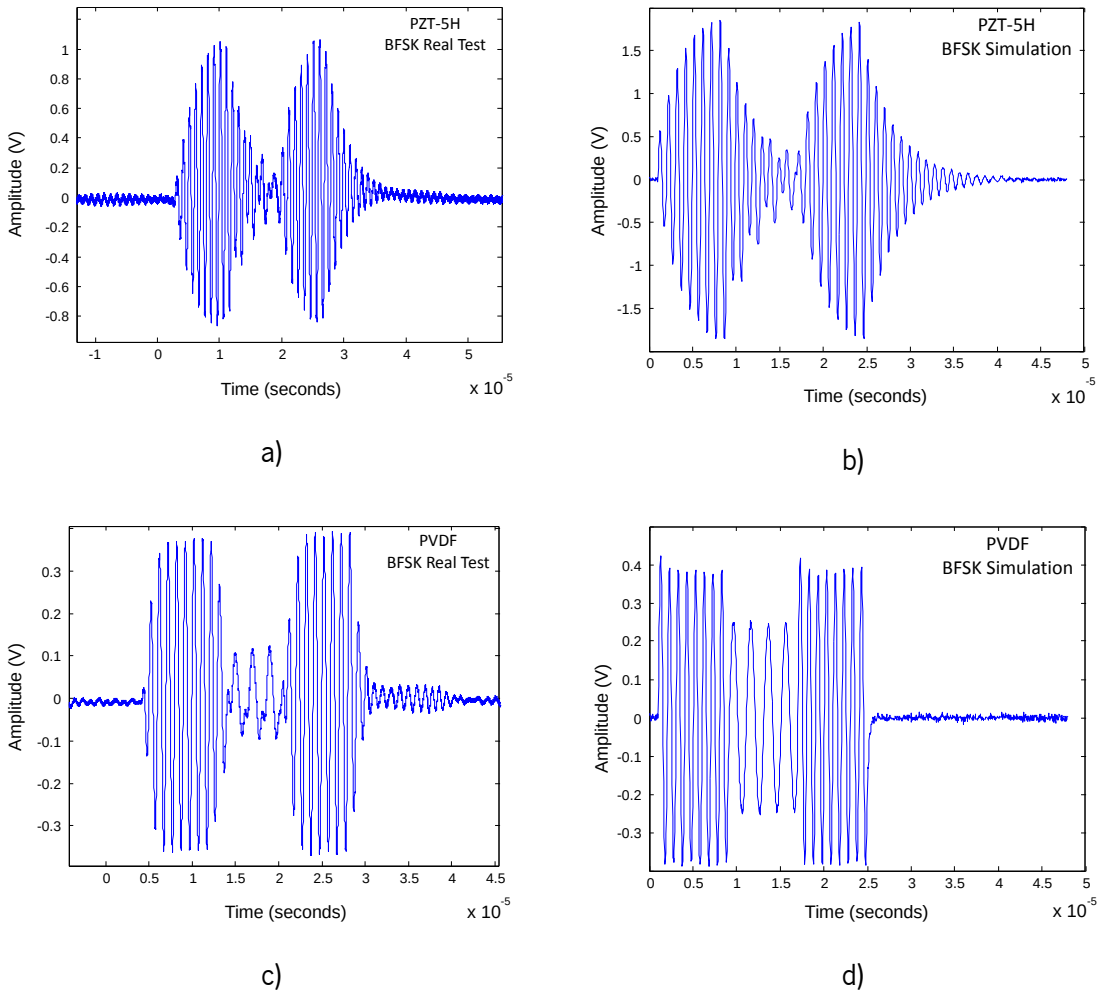

Figure 4.9: PZT-5H and PVDF response to BFSK modulation, real measurement and simulation.

Figure 4.9.a and .b show that the recovery of information in the 500 kHz signal is very difficult due to the high level of deformation. This is because the acoustic pressure is proportional to the frequency, resulting in a 500 kHz signal with half of the 1 MHz signal amplitude and also that of the most of the acoustic pressure generated is retained inside the active material. This fact results in an overlapping of signals and a deformation on the 500 kHz signal. However, simulation results (Figure 4.9.b) are shown to be very similar with the real tests (Figure 4.9.a), despite the remaining echoes that appeared in the real tests.

Figure 4.9.c and .d present the PVDF transducer response to the BFSK modulation. This signal shows a higher quality than the PZT-5H, where the small deformations presented in real tests (Figure 4.9.c) are due to the effect of remaining echoes.

Figure 4.10 shows the PZT-5H and PVDF transducers' response to a BPSK modulation. BPSK was expected to be the worst of all the modulations due to their characteristics, since the stored energy has an opposite sign of the drive signal.

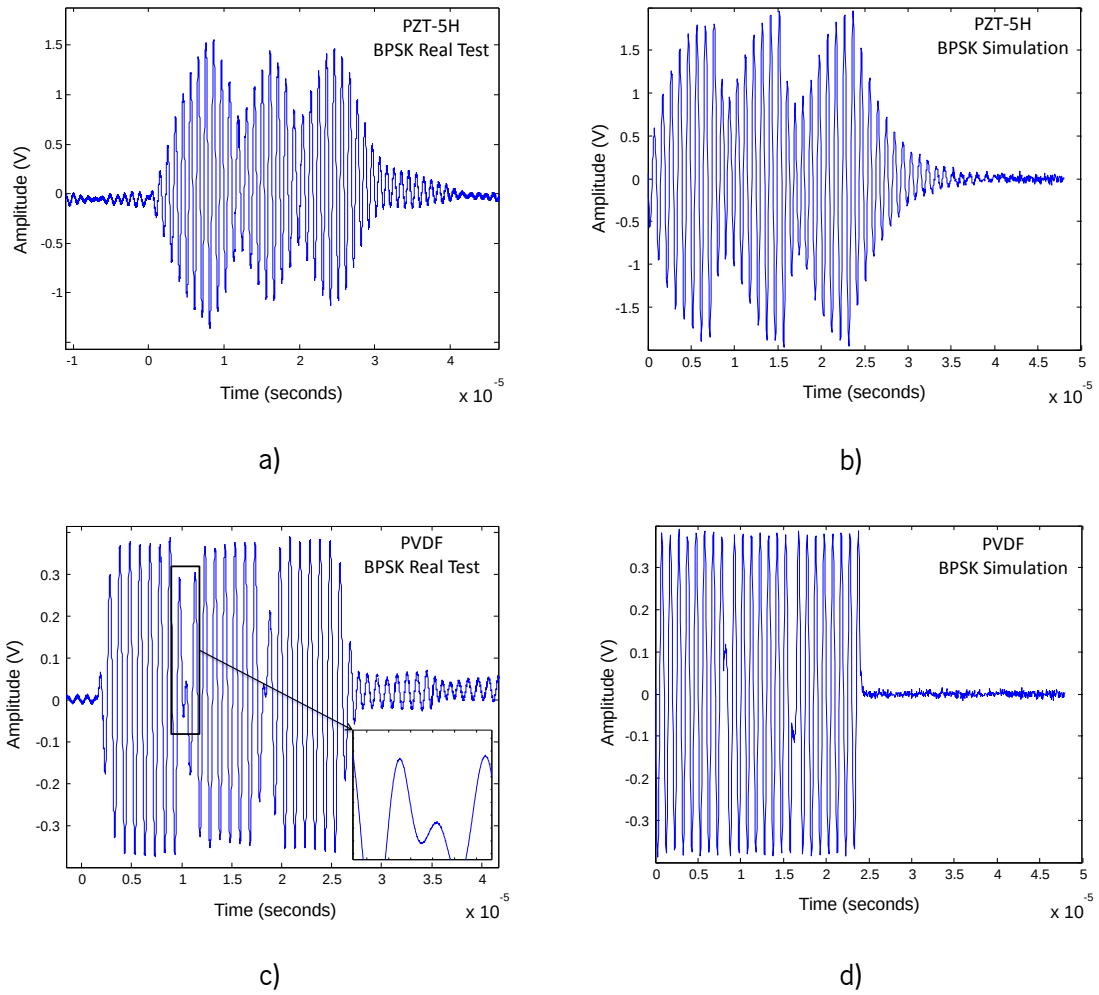

Figure 4.10: PZT-5H and PVDF response to BPSK modulation, real measurement and simulation.

As it is possible to observe in Figure 4.10.a and .b, the 180° phase shift is absorbed by the accumulated internal acoustic pressure, since both signals have opposite signs, masking the phase transition smoothly. But, in PVDF (Figure 4.10.c), the case is sorely different.

For the PVDF real measurements (Figure 4.10.c), the signal amplitude is highly reduced in the 180° phase shift. The main reasons to this fact is that, when the 180° phase shift is applied, the resulting signal in the transducer has double the frequency with half amplitude and offset. The transducer tends therefore to produce an acoustic pressure with twice the frequency but without the necessary force. So it generates a stunted and deformed acoustic pressure wave. In

simulation (Figure 4.10.d) this effect is reduced, being an ideal model and without echoes. The signal is cleaner and therefore it will be easier to recover the information.

In a general way, PVDF shows better performance. Low acoustic impedance plays an important role in the non-periodic signals when using digital modulations. Real tests results are shown to be slightly slower in the sudden amplitude transitions than in the simulations results for all the modulations and much of the signals' deformations are due to echoes that overlap the signal, a fact which is ascribed to the reduced dimensions of the water tank.

4.5. Conclusion

A signal quality evaluation of ultrasonic transducers was carried out using Digital Modulations. Two types of transducers were tested based on PZT-5H ceramic based transducers and on PVDF polymers.

The study includes MATLAB/Simulink simulations and experimental validations for BASK, OOK, BFSK and BPSK modulations with a 1 MHz carrier at 125 kbps baud rate.

Both materials show a non-linear acoustic output, but in a frequency range between 500 kHz and 1 MHz, PVDF shows an almost linear output with a 3.7 dB growth at 12 m. In contrast, PZT-5H shows a 19.6 dB growth.

It was concluded that PZT-5H resonance transducers are not suitable to be used with non-periodic high frequency signals. Signal deformation prevents a proper recovery of the information.

On the other hand, a PVDF transducer, with much lower acoustic impedance than PZT-5H, displays a better signal quality and, therefore, provides the signal full demodulation. On the other hand, the PZT-5H transducer has a higher output, but fails to perform accurate modulated signals.

References

[1] Nowsheen, N.; Benson, C.; Frater, M., "A high data-rate, software-defined underwater acoustic modem," OCEANS 2010 , vol., no., pp.1,5, 20-23 Sept. 2010, doi: 10.1109/OCEANS.2010.5664474.

[2] I. A.Sehgal and J.Schonwalder, “Aquatools: An underwater acoustic networking simulation toolkit”, IEEE Oceans, Sydney, Australia, May 2010.

[3] M.Stojanovic and J.Presig, “Underwater acoustic communication channels: Propagation models and statistical characterization”, IEEE Communications Magazine, Pages 84–89, January 2009.

[4] M.Stojanovic, “Underwater acoustic communications: Design considerations on the physical layer”, IEEE / IFIP Fifth Annual Conference on Wireless On demand Network Systems and Services (WONS 2008), January 2008.

[5] J.Preisig, “Acoustic propagation considerations for underwater acoustic communications network development”, Underwater Networks (WUWNet’06), Pages 1–5, September 2006.

[6] Chitre, M.; Shahabudeen, S.; Freitag, L.; Stojanovic, M., "Recent advances in underwater acoustic communications & networking," OCEANS 2008, vol., no., pp.1-10, 15-18 Sept. 2008.

[7] Se-Young Kim; Jeong-Woo Han; Ki-Man Kim; Sang-Hoon Baek; Hyung-chul Kim; Chang-Hwa Kim, "Experimental Results of Single Carrier Digital Modulation for Underwater Sensor Networks," Embedded and Ubiquitous Computing (EUC), 2010 IEEE/IFIP 8th International Conference on , vol., no., pp.326-330, 11-13 Dec. 2010.

[8] “EvoLogics GmbH”, Underwater Acoustic Modems, http://www.evologics.de/en/products/index.html, 20-03-2012.

[9] Charles H. Sherman, John L. Butler, “Transducers and Arrays for Underwater Sound”, Springer Science Business Media, LLC, ISBN-10: 0-387-32940-4, 2007.

[10] M.S. Martins, V. Correia, S. Lanceros-Mendez, J.M. Cabral, J.G. Rocha, “Comparative finite element analyses of piezoelectric ceramics and polymers at high frequency for underwater wireless communications”, Procedia Engineering, Volume 5, 2010, Pages 99-102, ISSN 1877-7058.

[11] Raúl A. Reyes-Villagrana, Gerardo Gutiérrez-Juárez and Rumen Ivanov Tsonchev, “Characterization of Simulated Mechanical – Electrical Properties of PVDF and PZT Piezoelectric Material for Use in the Pulsed Optoacoustic Spectroscopy”, International Journal of Pure and Applied Sciences and Technology, Pages 26-45, 2011.

[12] Thomas R. Shrout, “Innovations in Piezoelectric Materials for Ultrasound Transducers”, Applications of Ferroelectrics, ISAF, 17th IEEE International Symposium, 2008.

[13] A. Abrar, S. Cochran, “Multilayer piezocomposite structures with piezoceramic volume fractions determined by mathematical optimization”, Ultrasonics, Elsevier Science, Volume 42, Issues 1–9, April 2004, Pages 259-265, ISSN 0041-624X.

[14] Qian Zhang, Peter A. Lewin, Philip E. Bloomfield, “PVDF Transducers-A Performance comparison of Single-Layer and multilayer Structures”, IEEE Transactions On Ultrasonics, Ferroelectrics And Frequency Control, Vol. 44, No. 5, September 1997.

[15] Donald J. Leo, “Engineering Analysis of Smart Material Systems”, John Wiley & Sons, Inc, ISBN 978-0-471-68477-0, 2007.

[16] L.W. Schmerr, A. Lopez-Sanchez, R. Huang, “Complete ultrasonic transducer characterization and its use for models and measurements”, Ultrasonics, Elsevier Science, Volume 44, Supplement, 22 December 2006, Pages e753-e757, ISSN 0041-624X.

[17] Torsten Bove, Wanda Wolny, Erling Ringgaard and Annette Pedersen, “New piezoceramic PZT–PNN material for medical diagnostics applications”, Journal of the European Ceramic Society, Volume 21, Issues 10–11, Pages 1469-1472, 2001.

[18] F. Levassort, L.P. Tran-Huu-Hue, G. Feuillard and M. Lethiecq, “Characterisation of P(VDFTrFE) material taking into account dielectric relaxation : application to modelling of high frequency transducers”, Ultrasonics, Vol. 36(1-5), Pages 41-45, 1998.

[19] K.A. Snook, J.-Z Zhao, C.H.F. alves, J.M. Cannata, W-H.Chen, R.J. Meyer, T.A. Ritter and K.K. Shung, “Design, fabrication, and evaluation of high frequency, single-element transducers incorporating different materials”, IEEE Transactions On Ultrasonics, Ferroelectrics And Frequency Control, Vol. 49, Pages 169-176, 2002.

[20] S. Saitoh, T. Kobayashi, K. Harada, S. Shimanuki and Y. Yamashita, "A 20 MHz Single-element ultrasonic probe using 0.91Pb(Zn1/3Nb2/3)O3-0.09PbTiO3 single crystal", IEEE Transactions On Ultrasonics, Ferroelectrics And Frequency Control, Vol. 45, Pages 1071-1076, 1998.

[21] T. Ritter, K.K. Shung, X. Geng, P.D. Lopath, S.E. Park and T.R. Shrout, "Single crystal PZN-Tpolymer composites for ultrasound transducer applications", IEEE Transactions On Ultrasonics, Ferroelectrics And Frequency Control, Vol. 47, Pages 792-800, 2000.

[22] S. Saitoh, T. Takeuchi, T. Kobayashi, K. Harada, S. Shimanuki and Y. Yamashita, "Fortychannel phased array ultrasonic probe using 0.91Pb(Zn1/3Nb2/3)O3-0.09PbTiO3 single crystal", IEEE Transactions On Ultrasonics, Ferroelectrics And Frequency Control, Vol. 46, Pages 152-157, 1999.

[23] M. Martins, V. Correia, J.M. Cabral, S. Lanceros-Mendez, J.G. Rocha, Optimization of piezoelectric ultrasound emitter transducers for underwater communications, Sensors and Actuators A: Physical, Volume 184, September 2012, Pages 141-148, ISSN 0924-4247.

5. Acoustic Modem

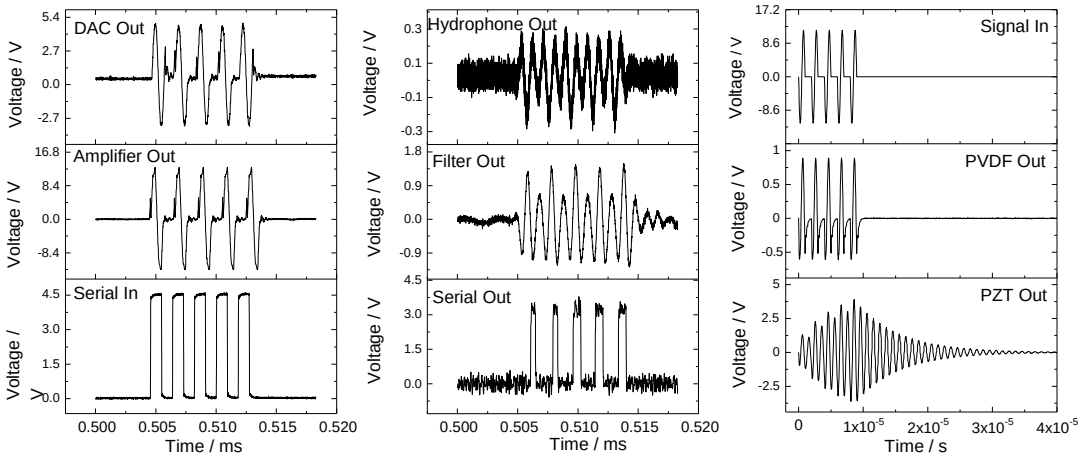

5.1. Introduction

Acoustic communications have been used for long distance communications, up to 20 km, and in deep waters with stable thermal conditions. But, despite underwater wireless communications having shown strong advances in recent years, there are still many limitations concerning data rates and robustness for real-time applications [1].

There are works showing that it is possible to use frequencies up to 1 MHz to achieve high data rate acoustic communications [2, 3]. For example, in [3] the authors presented an acoustic FPGA based modem operating at frequencies between 100 kHz and 1 MHz for distances ranging between 50 m and 100 m. Using a BPSK modulation with a 800 kHz carrier frequency, the system archived a 80 kbps data rate.

High communication frequencies also raise strong problems related to attenuation. Being directly related to the frequency, the acoustic absorption at 1 MHz can reach 280 dB/km [4, 5]. Consequently, the maximum communication range decreases dramatically to a few hundred meters or less with increasing frequency. On the other hand, real time acoustic communications are not supported at long distances, since acoustic waves propagate at around 1500 m/s, resulting in high propagation delays and disabling, therefore, any real time connection [4]. Summarizing, a high data rate and real time acoustic communication only can be applied at medium range, meeting therefore the needs of applications such as costal sensor networks, underwater unmanned vehicle control, equipment monitoring on offshore platforms and docks, among others [6, 7].

There are also several commercial acoustic modems available [8 – 10], which are not reliable solutions for data rates above 100kbps. For instance, EvoLogics [9] offers acoustic modems that can reach 2000 meters deep with an operational range of 1000 meters that can reach up to 2000 meters under specific water conditions. A maximum transmitting power of 60W can achieve 31.2 kbps in an omnidirectional pattern with a BER less than 10^{-10}. Another very interesting acoustic modem is the SAM1 by AppliedOcean System [8] that can reach 1 km in distance with a maximum data rate of 100 kbps.

The best choice for long distances is the LinkQuest Inc. [10], their powerful modem with a 40W transmitting power consumption offers a 10 km distance range and a 7 km maximum depth, and can achieve 5 Kbps in a omnidirectional pattern with a BER less than 10^{9}.

In this chapter an underwater acoustic modem that allows communications over several meters, achieving a maximum data rate of 1 Mbps, using 1.4 W of power consumption with a 1 MHz carrier is presented. This solution allows for reprogramming the digital signal processing block and the implementation of different types of digital modulations in order to improve the modem's performance. The system is based on a poly(vinylidene fluoride) PVDF ultrasonic emitter transducer which is capable of sending high quality and clean signals needed for digital modulations with high symbol rates per carrier period, as presented in detail in [11]. However, the PVDF transducer cannot reach the same acoustic pressure level as other such as piezoelectric ceramic transducers [12, 13], reducing the effective distance range of the acoustic waves.

5.2. Modem design

In order to design an acoustic modem capable of performing several types of digital modulations, a highly adaptable system was developed. Figure 5.1 shows the block diagram of the hardware of the system.

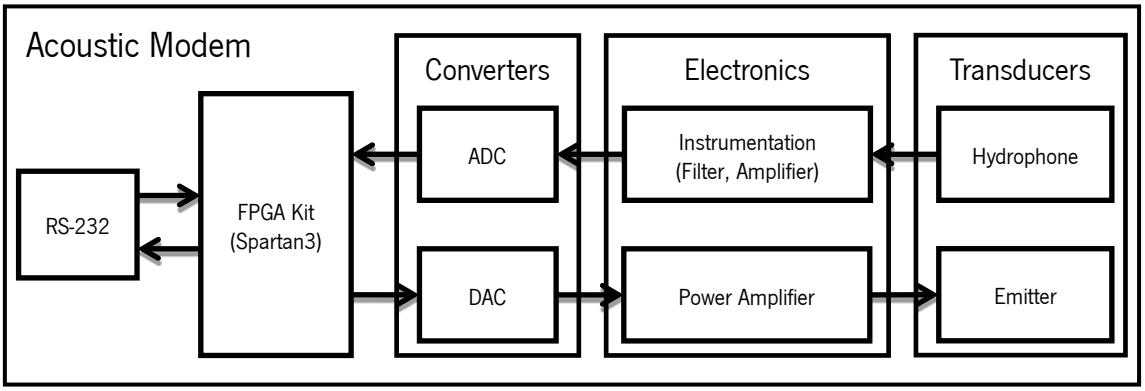

Figure 5.1: Block diagram of the acoustic modem system.

The FPGA Spartan3 is responsible for the modem processing and control functions. The main task is to process digital signals by implementing the modulator and demodulator. It is also responsible for controlling the electronic circuits, the analog to digital converter (ADC) and the digital to analog converter (DAC). In section 3 the details of the modulator/demodulator process

are presented. The selected A/D converter is an AD9244 capable of converting 65 Mega samples per second with 14 bits [14], and the D/A converter is a DAC904 with a current output and 14 bit resolution that supports update rates in excess of 165 Mega samples per second [15].

To carry out the A/D conversion it is necessary to handle the electrical signal from the hydrophone. For this purpose a filter, an amplifier and a signal conditioning system were implemented. The filter is an active 2nd order band-pass between 1 and 2000 kHz with a 12 dB gain. After amplification the signal cannot overcome the 3.3 V (peak-to-peak) because in order to obtain accurate measurements in the ADC input the signal must have a voltage between 1.65 V and 4.95 V centered at 3.3 V.

The DAC has a current output so it was necessary to implement a current to voltage converter using an operational amplifier, resulting in a 3 V peak-to-peak voltage output. The Power Amplifier block amplifies the modulated signal before being sent to the ultrasound transducer and consists of a Push-Pull symmetric amplifier with a 12 dB gain.

The ultrasound transducers are the most important part of the acoustic modem since at high frequencies and high symbol rate per carrier period, the transducer must project and receive accurate modulated signals. At 1 Mbps communications with 1 MHz carrier frequency, the most used ceramic piezoelectric transducers operating at the resonance frequency [16, 17] are not a suitable solution since the acoustic energy within the transducer creates a deformation on the modulated signal. Therefore, an emitter transducer based on the piezopolymer PVDF was developed [13]. This material has a much lower piezoelectric coefficient d_{33} ~ 3.40×10^{-11} C/N [18] than the most used piezoceramics such as Lead Zirconate Titanate, PZT, ~ 5.10×10^{-10} C/N [19], leading to a weaker acoustic signal. On the other hand, the acoustic impedance (~3.3×10^{6} kg/m^{2}s) is close to the acoustic impedance of water (~1.5×10^{6}kg/m^{2}s) when compared to the acoustic impedance of piezoceramics (~34×10^{6}kg/m^{2}s) [13]. The acoustic impedances matching between transducer and communication medium allows for an improved acoustic energy transfer from the transducer to the medium, reducing energy losses within the transducer and resulting in a more perfect acoustic signal [11]. The ultrasonic projector active element was constructed with two layers of PVDF with a thickness of 110 μm each in a piston configuration with 2 cm diameter. Specific details on the transducer construction and characteristics can be found in Chapter 3 [13].

The ultrasonic receptor was a Cetacean ResearchTM C304XR hydrophone with an effective sensibility of -181 dB, 1 V/µPa, a linear frequency range (±3dB) between 0.012 and 1000 kHz and a frequency range (+3/-12dB) between 0.005 and 2000 kHz.

5.3. Digital signal processing

An OOK modulator and demodulator was implemented in the Xillinx Spartan3A using the Xillinx System Generator Toolbox for MatLab. The modulator and demodulator logic circuits were optimized to reduce the consumption of resources in order to be able to include more functions in the future.

The modulator and demodulator logic circuits were implemented in parallel without any interconnection between each other. In this way it is possible to ensure the optimal functioning for full-duplex communication without any interference and/or delays.

5.3.1. Modulator

Using a DDS Compiler block it is possible to generate a 1 MHz sine wave for the carrier frequency. The signal from the RS232 port controls the sine wave generator, sending the sine wave in the case of a logic level '1 ' or a null value in the case of a logic level '0'. At the beginning of each transmission the reset of the DDS Compiler block is carried out, restoring the sine wave phase to 0° in order to synchronize the data stream with the carrier frequency. The DDS Compiler block was set to generate a sine wave with amplitude values between 0 and 16384 with an 8192 offset. These values have a direct current output correspondence in the DAC [15]. After the current/voltage converter the signal shows an amplitude between 3 and -3 V. A clock output of 25 MHz was also implemented to the DAC with 25 samples per period. In this way, it is possible to ensure the best quality of the 1 MHz modulated signal avoiding the early deformation.

5.3.2. Demodulator

The amplitude ranges of the signals received from the ADC range between -8192 and 8192 which corresponds to an input voltage between -1 and 1 Volt. Since digital filters require too many resources, it was necessary to reduce the sampling frequency to 6.25 MHz. Before filtering the signal an absolute value function, converting all samples into positive values was

implemented. Thus, the signal appears to have twice the frequency and an offset. Then, the filter allows for the lower frequency to be isolated which corresponds to the digital information. The filter consists of a FIR Equiripple with an order of 90 and a density factor of 16. The filter was configured to a 6.25 MHz frequency sample, a pass frequency of 250 kHz and a stop frequency of 500 kHz. After filtering it is necessary to select what is a '1' and what is a '0'. Therefore, an adaptive threshold function where the signal amplitude is measured each 20 milliseconds was implemented. Then the optimal threshold function measures the filtered signal amplitude and sets the threshold with half of the measured value only if the period is higher than 1 bit, in order to avoid narrow noise peaks. Finally, the resulting signal is a bit stream sent to the RS232 port.

5.4. Experimental Results

The performance of the communication system was evaluated by implementing an experimental set-up for the measurement and recording of the acoustic signals with several baud-rates. With the collected data it was possible to measure the transmission BER.

5.4.1. Experimental setup

The experimental tests were performed in a swimming pool with 10 meters in length, 5 meters width and 1.5 meters deep. The receiver and emitter transducers were placed in the swimming pool 6 meters away from each other, with 2.5 meters from each side wall, 2 meters from the back wall and 50 centimeters deep. The distances were selected in order to avoid sidewall echo interferences.

Results

The initial test consisted in sending the ASCII char 'U' in a continuous mode. The code bits of this character has the particularity to toggle between '1' and '0', resulting in a '01010101' binary sequence. This is one of the most difficult sets of bits to demodulate, due to the constant change of state. Figure 5.2 shows the signals from the emitter and receiver acoustic modem as well as the transducer simulations.

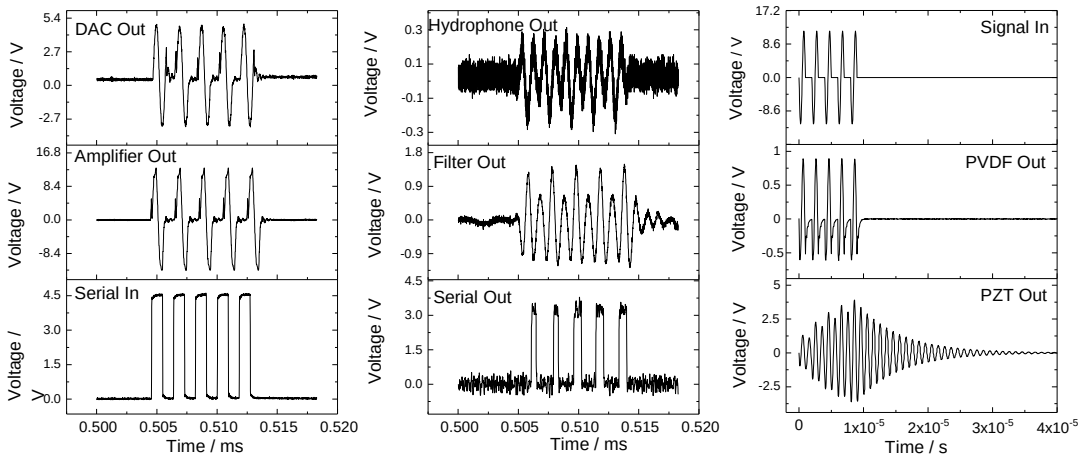

Figure 5.2: a) Signals from the emitter; b), signals from the receiver; c) PVDF and piezoceramic PZT transducer performance simulation [13].

The emitter side shows (Figure 5.2.a) the input serial stream bits from the PC, the modulated signal in the DAC output and the signal sent to the emitter transducer. In the receiver side (Figure 5.2.b) it is shown the signal coming from the hydrophone, the signal at the filter output and the serial stream bits at the modem output. In Figure 5.2.c a simulation of the expected performance of the PVDF and PZT transducers is shown [11, 13].

This test was performed using an OOK 1 Mbps transmission with a 1 MHz single carrier, resulting in a sine period to each bit length. In the emitter side it is possible to observe that each high logic state is converted to a 1 MHz sine wave. It is noteworthy that the serial port is operating with inverted logic, meaning that a high logic state corresponds to a '0' bit and low logic state to a '1' bit.

The simulation was obtained through a transducer simulation model developed in Matlab Simulink [11]. The simulation was carried out under the same swimming pool setup conditions, the PVDF characteristics being the same as the one used in the experimental measurements and the PZT transducer being a 1 MHz resonator piston type with 2 mm thickness and 2 cm diameter [13].

The simulation results show a large difference between the PZT and PVDF signal amplitude. The PZT shows amplitude ~ 4 times higher than PVDF, however the PZT transducer shows high levels of signal deformation, disabling any attempt to recover the digital information.

The PVDF transducer simulations are consistent with the results obtained experimentally. Analyzing the signals at the receiver modem it can be observed that the signal never reaches the zero value, having residual signal at the end of each sine wave. This is due to part of the acoustic energy that is retained and dissipated within the transducer. Despite this setback, it is still possible to clearly distinguish the high logic level with higher amplitude, enabling the signal demodulation. The signal at the hydrophone presents a SNR of 7 dB. Since the distance between emitter and receiver could not be increased due to experimental restrictions, experimental tests using lower transmission powers were also performed the signal demodulation under a minimum SNR of -1.74 dB still possible. Interpolating these values leads to the conclusion that the system will be operational up to the 16 meters range. Another aspect regarding the maximum distance range was the low excitation voltage tension (12 V) applied to the transduced. This value can be increased by at least an order of 10 times limited only by the piezoelectric material maximum operating voltage [20], enabling the system to reach further distances.

The BER was also measured for the baud rates of 1 Mbps, 512 kbps and 256 kbps. The measurements were performed at two RS232 ports, allowing for sending and receiving the file on the same computer for comparison. The file size is 2 MB and no type of error detection or correction mechanisms were implemented. The results registered were $3x10^{-3}$ BER with 1 Mbps, $2.3x10^{-5}$ with 512 kbps and $1x10^{-8}$ with 256 kbps.

Most of the errors were caused by a false start bit that initialized the demodulation process. These false start bits were caused by noise peaks. When the baud rate is reduced the noise peaks were no longer detected by the receiver modem. However, there are several ways to reduce this occurrence by improving the filter quality or implementing a function that detects and distinguish a real data transmission from a demodulated peak noise. Subsequently, an error control coding can be also implemented to reduce the BER.

Consequently, it is possible to conclude that the developed solution achieves data rate speeds 10 times higher than one of the fastest acoustic modems available, the SAM1 by AppliedOcean System [8], but in proper water conditions and with external power supply this system can reach over 160 times further. When compared to the EvoLogics [9] the developed system is 32 times faster in terms of data rate and consumes 1370 times less energy to send 1 MB. On the other hand, their solution is able to communicate over 300 times further. Nevertheless, it is important

to take into account that the present prototype still has room for improvement and optimization before the development of a commercial product.

5.5. Conclusions

A Low Power Acoustic Modem for underwater wireless communications capable of reaching a maximum data rate of 1 Mbps was presented.

The measured BER using an OOK 1 MHz single carrier modulation was $3x10^{-3}$ BER at 1 Mbps, $2.3x10^{-5}$ at 512 kbps and $1x10^{-8}$ in 256 kbps. These results mean that it overcomes 2G broadcast speeds and reaches almost half of the UMTS 3G maximum data rate [21]. These characteristics allow for the implementation of unmanned underwater vehicles (UUV) in real time remote control with compressed video and sound or access to internet from a submarine.

Future work will consist of increasing emitter transducer power output to reach long distances, implement other digital modulations with higher bit rates per symbol and optimizing the corresponding electronic circuits and digital filters.

References

[1] R. Frank Busby, "Underwater inspection/testing/ monitoring of offshore structures," Ocean Engineering, vol. 6, no. 4, pp. 355–491, Jan. 1979.

[2] F. Wang, L. Gu, and Y. Chen, "An energy conversion system based on deep-sea pressure," Ocean Engineering, vol. 35, no. 1, pp. 53–62, Jan. 2008.

[3] A. Elibol, R. Garcia, and N. Gracias, "A new global alignment approach for underwater optical mapping," Ocean Engineering, vol. 38, no. 10, pp. 1207–1219, Jul. 2011.

[4] I. F. Akyildiz, D. Pompili, and T. Melodia, "Underwater acoustic sensor networks: research challenges," Ad Hoc Networks, vol. 3, no. 3, pp. 257–279, May 2005.

[5] X. Che, I. Wells, G. Dickers, P. Kear, and X. Gong, "Re-evaluation of RF electromagnetic communication in underwater sensor networks," IEEE Communications Magazine, vol. 48, no. 12, pp. 143–151, Dec. 2010.

[6] G. Baiden, Y. Bissiri, and A. Masoti, “Paving the way for a future underwater omni-directional wireless optical communication systems,” Ocean Engineering, vol. 36, no. 9–10, pp. 633–640, Jul. 2009.

[7] M. Stojanovic and J. Preisig, “Underwater acoustic communication channels: Propagation models and statistical characterization,” IEEE Communications Magazine, vol. 47, no. 1, pp. 84–89, Jan. 2009.

[8] H.-P. Tan, R. Diamant, W. K. G. Seah, and M. Waldmeyer, “A survey of techniques and challenges in underwater localization,” Ocean Engineering, vol. 38, no. 14–15, pp. 1663–1676, Oct. 2011.

[9] M. Chitre, S. Shahabudeen, and M. Stojanovic, “Underwater Acoustic Communications and Networking: Recent Advances and Future Challenges,” Marine Technology Society Journal, vol. 42, no. 1, pp. 103–116, Mar. 2008.

[10] N. Nowsheen, C. Benson, and M. Frater, “Design of a high frequency FPGA acoustic modem for underwater communication,” in OCEANS’10 IEEE SYDNEY, 2010, pp. 1–6.

[11] N. Nowsheen, C. Benson, and M. Frater, “A high data-rate, software-defined underwater acoustic modem,” in OCEANS 2010 MTS/IEEE SEATTLE, 2010, pp. 1–5.

[12] M. Martins, J. Cabral, G. Rocha, and S. Lanceros-Mendez, “Theoretical Modeling and Experimental Validation of an Underwater Acoustic Communication System,” Submitted in IEEE Journal of Oceanic EngineeringOceanic Engineering,, 2013.

[13] J.-H. Li, B.-H. Jun, P.-M. Lee, and S.-W. Hong, “A hierarchical real-time control architecture for a semi-autonomous underwater vehicle,” Ocean Engineering, vol. 32, no. 13, pp. 1631–1641, Sep. 2005.

[14] Applied Ocean Systems, “Applied Ocean Systems,” SAM1 Wireless Subsea Acoustic Modem, 2013. [Online]. Available: http://www.applied-ocean.com/. [Accessed: 27-May-2013].

[15] EvoLogics, “EvoLogics GmbH,” Underwater Acoustic Modems, 2013. [Online]. Available: http://www.evologics.de/en/products/acoustics/index.html. [Accessed: 27-May-2013].

[16] LinkQuest Inc., “Underwater Acoustic Modem Models UWM-Series,” 2013. [Online]. Available: http://www.link-quest.com/html/models1.htm.

[17] M. Martins, J. Cabral, S. Lanceros-Mendez, and G. Rocha, “Effect of the Acoustic Impedance in Ultrasonic Emitter Transducers using Digital Modulations,” Submited Elsevier Ocean Engineering , April 2013., 2013.

[18] K. W. Kwok, H. L. W. Chan, and C. L. Choy, “Multifrequency transducers fabricated using PZT/P(VDF-TrFE) 1-3 composite,” Ferroelectrics, vol. 201, no. 1, pp. 75–82, Sep. 1997.

[19] M. Martins, V. Correia, J. M. Cabral, S. Lanceros-Mendez, and J. G. Rocha, “Optimization of piezoelectric ultrasound emitter transducers for underwater communications,” Sensors and Actuators A: Physical, vol. 184, pp. 141–148, Sep. 2012.

[20] A. Devices, “AD9244.” 2013.

[21] T. Instrument, “DAC904.” 2013.

[22] C. H. Sherman and J. L. Butler, Transducers and Arrays for Underwater Sound. Springer Science+Business Media, LLC, 2007, p. 610.

[23] a Abrar, D. Zhang, B. Su, T. W. Button, K. J. Kirk, and S. Cochran, “1-3 Connectivity Piezoelectric Ceramic-Polymer Composite Transducers Made With Viscous Polymer Processing for High Frequency Ultrasound.,” Ultrasonics, vol. 42, no. 1–9, pp. 479–484, Apr. 2004.

[24] V. Sencadas, R. Gregorio, and S. Lanceros-Mendez, “ α to β Phase Transformation and Microestructural Changes of PVDF Films Induced by Uniaxial Stretch,” Journal of Macromolecular Science, Part B, vol. 48, no. 3, pp. 514–525, May 2009.

[25] R. Ramesh, H. Kara, and C. R. Bowen, “Characteristics of piezoceramic and 3–3 piezocomposite hydrophones evaluated by finite element modelling,” Computational Materials Science, vol. 30, no. 3–4, pp. 397–403, Aug. 2004.

[26] M. Specialties, “Piezo Film Sensors Technical Manual,” 2013. [Online]. Available: http://www.meas-spec.com/product/t_product.aspx?id=2488.

[27] J. Lloret, S. Sendra, M. Ardid, and J. J. P. C. Rodrigues, “Underwater wireless sensor communications in the 2.4 GHz ISM frequency band.,” Sensors (Basel, Switzerland), vol. 12, no. 4, pp. 4237–64, Jan. 2012.

6. Conclusions and future work

The main objective of this project was to develop a high speed real time link for underwater wireless communications based on acoustic technology.

To meet the final goal it was necessary to develop the following tasks:

- Develop a simulation model of the underwater communication system.
- Design and build ultrasonic transducers for digital modulations in the MHz frequency range.
- Evaluate the performance of digital modulations in underwater environment, using high frequencies.
- Design and build a high data rate acoustic modem.
- Test and evaluate the modem performance in a swimming pool.

The acoustic underwater communication channel was simulated with a Matlab/Simulink model taking into account attenuation, environment noise, Doppler Effect and propagation delay of the acoustic signal. Real tests were also implemented to validate the attenuation, noise, multipath and propagation delay. The ambient noise simulation was compared to noise measurements obtained in sea, river and pool environments. The attenuation, multipath and propagation delay simulation models were compared to the results obtained in the pool at 8 meters distance with a 100 kHz signal, and at 12 meters distance with 1 MHz signal.

An acoustic communication system model for underwater applications was developed. The simulation model was designed specifically to emulate the acoustic channel and ultrasonic transducers, allowing for the communications' performance to be evaluated using digital modulations. The Xilinx System Generator toolbox allows the modulator/demodulator model to be uploaded directly into an FPGA platform for the final application. Overall, the results show that the model represents a useful approximation to the real subaquatic communication channel, allowing to simulate the performance of the acoustic modem before their construction.

The ultrasonic transducers were optimized specifically for underwater communications. Three different designs with piston topology were compared, namely PZT-5H single-layer, PVDF single-layer and PVDF four-layer. The study included calculations, finite element simulation and experimental tests. The results show that the PZT transducer achieved a higher output sound

pressure, but the four-layer PVDF demonstrated to be the best for this kind of applications, due to its higher bandwidth and lower power consumption. In this study, the single-layer PZT output sound pressure shows to be in average 7 dB higher than four-layer PVDF, but also shows an average power consumption of 3.5 times higher.

Two types of transducers based on PZT-5H ceramic based transducers and on PVDF polymers were evaluated to Digital Modulations. The study includes MATLAB/Simulink simulations and experimental validations for BASK, OOK, BFSK and BPSK modulations with a 1 MHz carrier at 125 kbps baud rate.

Both materials show a non-linear acoustic output, but in a frequency range between 500 kHz and 1 MHz PVDF shows an almost linear output with a 3.7 dB growth at 12 m. In contrast, PZT-5H shows a 19.6 dB growth. It was concluded that PZT-5H resonance transducers are not suitable to be used with non-periodic high frequency signals. Signal deformation prevents a proper recovery of the information. On the other hand, a PVDF transducer, with much lower acoustic impedance than PZT-5H, displays a better signal quality and, therefore, provides the signal full demodulation. The PZT-5H transducer has a higher output but fails to perform accurate modulated signals.

The Low Power Acoustic Modem for underwater wireless communications was capable of reaching a maximum data rate of 1 Mbps in swimming pool tests. It was obtained a $3x10^{-3}$ BER at 1 Mbps, $2.3x10^{-5}$ at 512 kbps and $1x10^{-8}$ in 256 kbps. The BER was measured using an OOK 1 MHz single carrier modulation. The modem was capable of perform a full demodulation under an SNR of -1.74 dB using just 1.4 W of power consumption.

6.1. Future work

This project demonstrates that it is possible to implement a real time high data rate communication system in underwater environment. The system showed a large potential and can be improved in order to achieve data rates up to 3 Mbps (or even more) for distances up to 100 meters.

To achieve this goal it will be necessary to develop the following tasks:

- Design and build more powerful ultrasonic transducers for digital modulations in the MHz frequency range with electronic beam pattern control.
- Evaluate the performance of digital multi-carrier modulations with higher bit rates per symbol in underwater environment using frequencies up to 1MHz.
- Optimize the corresponding electronic circuits and digital filters.
- Improve the final prototype with proper water sealing to depths of thousands of meters.

With a robust prototype the major goal will be to implement a real time high data rate underwater sensor network. This network may be installed in a river, dam or even the ocean to collect environmental data or to support underwater exploration.

In parallel with these objectives, the development of partnerships with industry to foment the technology transference will be a priority.